The Institute of Paper Chemistry

Appleton, Wisconsin

Doctor's Dissertation

A Study of the Porous Structure of Fibrous Sheets Using Permeability Techniques

William Clark Bliesner

June, 1963

A STUDY OF THE POROUS STRUCTURE OF FIBROUS SHEETS USING PERMEABILITY TECHNIQUES

A thesis submitted by

William Clark Bliesner
B.S. (Ch. E.) 1957, University of Idaho
M.S. 1961, Lawrence College

in partial fulfillment of the requirements
of The Institute of Paper Chemistry
for the degree of Doctor of Philosophy
from Lawrence College,
Appleton, Wisconsin

June, 1963

ERRATA

In the study concerning the effect of fiber shape on the Kozeny factor it was necessary, in the case of fibers of noncircular cross section, to correct the geometric fiber surface area for the finite areas of contact between fibers. In this development it was assumed that the total area of contact in a fibrous bed was given by the expression:

$$\text{total area of contact} = N_c A_c \tag{1E}$$

where N_c is the total number of contact points and A_c is the average area of contact between fibers. It is apparent, however, since two fibers participate in each fiber-to-fiber contact, the area which is not effective in offering resistance to fluid flow is twice that given by the above expression or

$$\text{total area of contact} = 2 N_c A_c \tag{2E}.$$

The value of N_c in this relationship was assumed to be equal to the total length of fiber in the bed divided by the average distance between contact points. The average distance between contact points (or fiber segment length), b', is defined by Equation (80) of the thesis. The resulting expression for N_c was

$$N_c = 16 W^2/(\pi^3 D A_f \rho_s^{2?} AL) \tag{81E}$$

where the symbols are as defined on page 116 of the thesis.

That this expression for N_c is incorrect can be shown by the following argument. Consider, for the moment, that the entire fibrous bed is composed of a single, continuous fiber which is doubled and folded back on itself so as to form N_c contact points. It is apparent that the total number of fiber segments (of average length, b') in the bed is represented by $2N_c - 1$, or, assuming N_c to be very large, by $2N_c$. This result can be seen more clearly by reference to the

simplified diagram below.

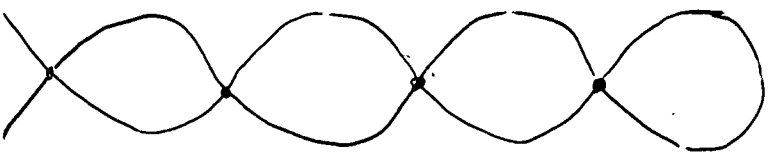

Figure 1E. Simplified Diagram of Fiber Contacts

In this sketch there are 4 contact points (i.e., $\underline{N_c} = 4$) while the total number of segments between contacts is equal to 7 (i.e., $2\underline{N_c} - 1$). If the ends of the fiber are ignored and $\underline{N_c}$ is very large (as is actually the case), the number of segments is equal to $2\underline{N_c}$ or 8. While this step may be questionable in this simplified situation, in the actual case no significant error will result.

From the above argument, it is easily seen that the total fiber length $\underline{L_f}$, in the bed is given by

$$2 N_c b' = L_f$$

or
$$N_c = \frac{L_f}{2b'}, \qquad (3E).$$

Applying this correction, Equation (81E) becomes

$$N_c = 8 W^2/(\pi^3 D A_f \rho_s^2 AL) \qquad (4E).$$

Combining this result with Equation (82) of the thesis and Equation (2E) above yields

$$\text{total area of contact} = 8 W^2 U^2/(\pi^2 D A_f \rho_s^2 AL) \qquad (83E)$$

which is identical with Equation (83) given on page 117 of the thesis.

Thus, the calculated values of the Kozeny factor listed in Tables XIV and XV of the thesis and the results plotted in Fig. 21 remain unchanged. However, it is felt that the above-mentioned conceptual errors are of theoretical

significance and warrant the publication of this errata. In spite of the difficulties encountered in estimating the correct surface area exposed to flow in fibrous beds, it is felt that the results obtained do indicate a possible effect of fiber shape on the Kozeny factor and that certainly this subject is of sufficient significance to warrant further investigation.

It should also be pointed out that there are two typographical errors in the thesis. In Equation (81), page 116, π in the denominator should be raised to the third power and in Equation (85) the value of π should be squared.

TABLE OF CONTENTS

SUMMARY

The major objectives of this thesis were: (1) to determine the permeability and pore size distribution properties of carefully prepared handsheets of paper, (2) to relate the permeability of these sheets to the hydrodynamic specific surface area and porosity of the sheet, and (3) to determine the effect of pore size distribution on the permeability properties of paper. All of the specimens tested in this study were prepared from an unrefined, bleached sulfite pulp. This pulp was classified to remove fines with only the fraction held on a 20-mesh screen being retained.

A number of experiments were conducted on thick mats (basis weight of about 2300 g./sq. m.) in which the air permeability properties of the dry, bonded specimens were determined as a function of the compacting pressure on the mat. The specific objective of these studies was to establish the relationship between the hydrodynamic specific volume of the fibers and the apparent density of the mats. The apparent density of the thick mats was varied by changing the applied wet pressure. It was noted that the calculated hydrodynamic specific surface area of the mats increased as the wet pressure applied to the mat was increased. This increase was shown to be due, in part, to a progressive collapse of the fiber into a flatter, more ribbonlike structure. In permeability studies on synthetic fiber beds, it was demonstrated that at a given level of porosity the resistance to fluid flow increased as the fibers became flatter. These changes were manifested in a higher value of the Kozeny factor for the flattened fibers.

In the experiments conducted on thin handsheets, both the air permeability and pore size distribution properties were measured. It was found that while the permeability properties were unaffected by basis weight, the pore size distribution of these sheets became narrower and shifted to smaller pore sizes as the basis weight was increased. As a result of this observation, it was concluded

that changes in the pore size distribution (as measured by the gas-drive technique) have relatively little effect on the permeability properties of paper over the range of pore size distribution studied. These results also indicated that the pore size distribution of the thick mats must have been relatively narrow.

In the study of the effect of wet pressure on the porous structure of paper, it was found that the mean of the pore size distribution decreased rapidly, while the standard deviation of the pore size distribution decreased slightly, as the wet pressure applied to the sheet was increased. These changes were attributed to a rearrangement of the fibers in the structure when the sheet was wet pressed.

An attempt was made to calculate the hydrodynamic specific surface area of the handsheets using the modified hydraulic radius theory developed in this thesis. While this theory represented a significant improvement over the usual form of the Kozeny-Carman equation, several anomalies were found in applying the modified hydraulic radius theory to the data. These discrepancies were attributed to the effects of pore branching and pore constrictions. It was not possible to account for the branching and interconnecting of pores in the modified hydraulic radius theory. The errors introduced by pore constrictions are inherent in the gas-drive method for measuring pore size distribution.

INTRODUCTION

The physical properties of paper may be divided, in a general way, into mechanical, optical, and porous properties. While the mechanical and optical properties of paper have been investigated extensively in recent years, the study of the porous structure of paper appears to have been largely neglected. Yet, in the utilization of paper, the porous structure of the sheet has a prominent role. Many of the applications of paper, such as filter papers, blotting papers, and sanitary tissues, are related directly to the porous nature of the sheet. In other cases, the usefulness of paper is limited by its porous nature. For example, paper is laminated or impregnated with waxes to lower its permeability to moisture vapor; paper is sized to prevent excessive spreading of inks, and paper is laminated with a variety of plastics to produce a sheet which is resistant to the penetration of water and other solvents. In addition, in many converting operations where liquids are forced into the sheet by the action of a nip, the porous structure of the base sheet is undoubtedly of importance.

Early studies on the porous structure of paper were concerned primarily with the air and liquid permeability properties of the sheet. Only in recent years have attempts been made to characterize the distribution of pore sizes in a sheet of paper. In only a few studies have any attempts been made to relate the pore size distribution to the permeability properties of the sheet. In addition, relatively little work has been done to relate the permeability of paper to the more fundamental properties of the surface area exposed to flow and the fractional volume of voids in the sheet.

Because of the extremely complex nature of the porous structure of fibrous sheets, a rather complete review of the pertinent literature is presented. For the purposes of this review, the methods which have been used to describe the structure of porous media have been divided into three broad categories. These include: (1) the phenomenological approaches such as the hydraulic radius theories, (2) the analytical approaches as exemplified by the various drag theories, and (3) the statistical approaches. The studies which have been conducted in each of these categories are reviewed in some detail in order to establish an understanding of the underlying principles involved in each method and to develop an appreciation for the limitations which are inherent in each of these approaches.

This review is followed by a discussion of the recent studies concerning the distribution of pore sizes in porous media and the complicated manner in which the flow channels through a porous medium are branched and interconnected. Finally, the limitation of these approaches are considered in light of the probable structure of a sheet of paper. It is concluded that the hydraulic radius theories represent the only approach which has been developed to the point of practical usefulness in the present investigation. The major limitation in applying the hydraulic radius theories to a normal sheet of paper is that such a structure has a broad distribution of pore sizes which has heretofore not been accounted for in these theories. A "modified hydraulic radius theory" is developed in which variations in pore size are taken into account and by which the permeability of a porous medium is expressed in terms of the pore size distribution and certain empirical parameters.

The experimental techniques and equipment used in this study are described next. This is followed by the presentation of the data obtained on thick mats

of wood pulp fibers, on beds of certain synthetic fibers, and on thin handsheets of wood pulp fibers. The specific experimental objectives of this thesis were: (1) to measure the permeability and pore size distribution properties of carefully prepared handsheets of wood pulp fibers, (2) to relate the permeability of these sheets to the surface area exposed to flow and the fractional void volume in the sheet, and (3) to determine the effect of pore size distribution on the permeability properties of paper. It was hoped that these objectives would also lead to an elucidation of the basic factors which are important in determining the permeability properties of a sheet of paper.

It is well known that a large number of variables have an effect on the porous structure of a sheet of paper. For example, the permeability of paper can be changed by the degree of refining of the fibers, by the presence or absence of fillers, by the type of coating applied to the sheet, by the amount of wet pressure applied to the sheet, and by a myriad of other variables. It was not the purpose of this study to investigate all of the possible variables which might influence the porous structure of paper. Rather, this thesis was limited to the above objectives while utilizing whatever variables seemed appropriate to alter the properties under consideration. Therefore, in a sense, this study must be considered to be preliminary in nature.

Because of the extreme complexity of fibrous structures, this study has necessarily been quite empirical in nature. However, a number of interesting and informative observations have been brought to light which should be of significant value in future studies on the structure of fibrous sheets.

HISTORICAL REVIEW

FUNDAMENTAL CONSIDERATIONS

A sheet of paper may be visualized as an assemblage of elongated fibers which are bonded together at many points along their length, and among which passages exist allowing the flow of fluids through the sheet. These passages are of indefinite size and shape and are branched or interconnected in such a manner that it is not possible to discern a definite dimension which is characteristic of a particular pore space. As a result of this structure, liquids and gases are able to penetrate into and through the sheet.

A porous medium, such as a fibrous sheet, may be defined as a material in which the solid substance is distributed over a space larger than the volume of the solid substance itself. As such, a porous material has a number of properties that are related closely to the manner in which the solid matter is distributed over the space and by which the porous structure of the material can be characterized. A porous medium may be further classified as compressible or incompressible, consolidated or unconsolidated, and isotropic or anisotropic.

A sheet of paper is compressible in that its bulk dimensions can be changed by the application of an external load. It is also anisotropic since the fibers generally lie with their axes preferentially in the plane of the sheet (the x-y plane) thereby resulting in different permeabilities in the lateral and transverse directions. Since the fibers in a sheet of paper are bonded together to form a more or less continuous solid phase, paper is classified as a consolidated porous medium. A sheet of paper may therefore be described as a compressible, anisotropic, consolidated porous medium.

It is virtually impossible to achieve an exact geometrical description of the porous structure of a sheet of paper. This is readily apparent from examination of the simulated cross section of a sheet of paper shown in Fig. 1.

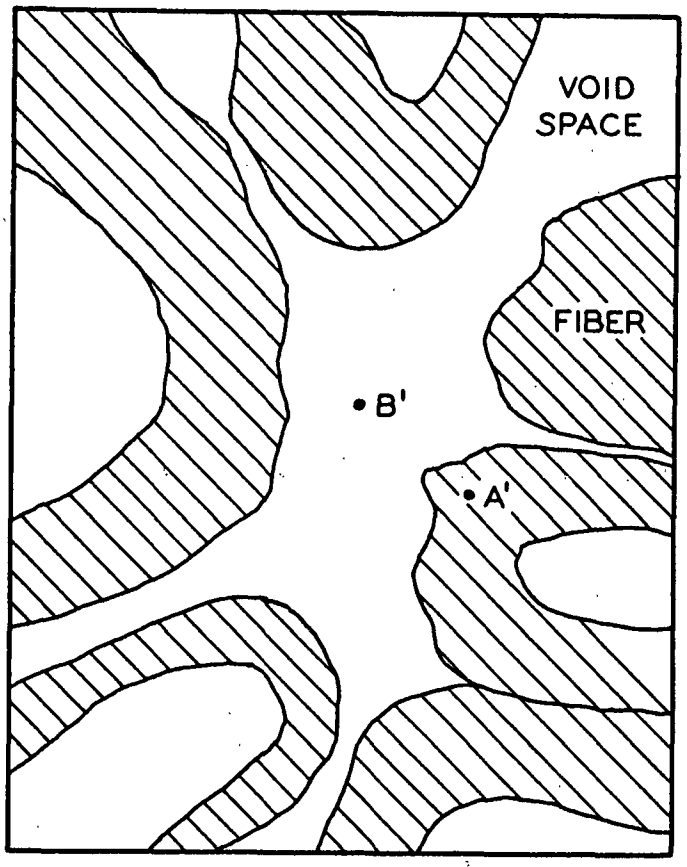

Figure 1. Simulated Random Section Through a Sheet of Paper

In the above figure, A' and B' are randomly located points in a random plane through the sheet. To achieve an exact geometrical description of the sheet, it is necessary to construct a model in which there is a point-to-point identity between an infinite number of these points in an infinite number of plane sections through both the model and the sheet of paper. Then, and only then, can it be said that exact geometrical similitude has been achieved. This is obviously not possible. Furthermore, the geometrical description of a

sheet of paper is only the first step. A complete description of the porous structure of the sheet would require a knowledge of the distance from each randomly located point to a solid surface, the orientation of the surface, and textural properties of the surface. In view of these considerations, it is not surprising that it has been necessary to describe the structure of porous media by other, less rigorous, means.

An alternative approach to describing the structure of porous media which has been studied intensively is the mathematical description of the flow of fluids through the porous medium. The description of fluid motion in any geometrical system is found in the differential equations based on the three conservation principles. These are: (1) the conservation of matter, or equation of continuity; (2) the conservation of momentum, or equations of motion, and (3) the conservation of energy, or equation of state. These general equations are discussed in detail in the literature (1, 2).

In theory, the differential equations describing the three conservation principles are sufficient to predict all of the details of the motion of a fluid flowing through any confined space, regardless of its shape or complexity. However, even a cursory inspection of the classical texts on hydrodynamics (2) discloses that, except for the case of relatively simple geometries, the mathematical solution of these differential equations is quite impossible. In order to obtain a rigorous solution of these general equations, it is necessary, among other things, to completely specify the boundary conditions of the flow. This would amount to a complete geometrical description of the porous medium, which is not feasible. In view of these considerations, it has been necessary to adopt a more empirical approach to the description of the flow of fluids through porous media.

A tenable, quantitative description of flow through porous media begins with the Darcy equation. This equation describes the steady-state, isothermal flow of a nonreacting, incompressible fluid through a homogeneous porous medium and may be written as

$$u = Q/A = K_o \, \Delta P/L \qquad (1)$$

where:

u = superficial linear velocity

Q = volumetric rate of flow

A = cross-sectional area of the test specimen

ΔP = frictional pressure drop across the test specimen

L = thickness of the test specimen, and

K_o = a proportionality factor which is dependent on the properties of the porous medium and the permeating fluid

The region of flow in which Equation (1) is experimentally valid is designated as laminar, streamline, or viscous flow. This does not infer that inertial effects are entirely absent. On the contrary, local velocity fluctuations must exist in the fluid as it passes through the complex pore space of a porous medium. However, in the flow region where Darcy's equation applies, the inertial effects are negligibly small and the frictional pressure drop may be considered to be due entirely to the viscous drag of the fluid.

As mentioned above, the proportionality factor, K_o, includes the properties of the permeating fluid. Since it has been demonstrated both experimentally and theoretically that the fluid density is not a factor in the region where Equation (1) applies (1), the effects of the fluid on K_o may be separated in a simple manner:

$$K_o = K/\eta \qquad (2)$$

where K is a new proportionality factor known as the permeability coefficient or simply the permeability of the porous medium. The permeability coefficient is determined only by the structure of the porous medium and is independent of the nature of the permeating fluid.

A combination of Equations (1) and (2) results in the generalized form of Darcy's equation, more often referred to as Darcy's law:

$$u = Q/A = K \Delta P/(\eta L) \qquad (3)$$

The formal definition of permeability may therefore be stated as the volume of fluid of unit viscosity passing through a unit cross section of the medium in unit time under the influence of a unit pressure gradient.

While Darcy's equation was formulated from experimental data over a century ago, it was only recently proved theoretically. By means of the reasoning of irreversible thermodynamics, Mokadam (3) was able to derive a general equation for flow through porous media. He further demonstrated that Darcy's equation was a special case of this general relationship. It may therefore be stated that Darcy's equation is a theoretically and experimentally valid law in the flow regime known as viscous or laminar flow. It has been amply demonstrated experimentally that Darcy's law is applicable to paper and fibrous beds (4-6).

STUDIES ON THE STRUCTURE OF POROUS MEDIA

The separation of the permeability coefficient into the geometrical properties of the porous medium has been much more difficult than separating the fluid properties from those of the solid phase. There have been three different

approaches to this problem: (1) the phenomenological approach, which includes the hydraulic radius theories, (2) the analytical approach as represented by the drag theories of permeability, and (3) the statistical approach.

PHENOMENOLOGICAL APPROACHES

In the phenomenological approaches, the flow of fluids through porous media is considered to be analogous to flow through a system of capillaries. These approaches may be further divided into studies on cylindrical capillary models and studies on noncylindrical capillary models. Studies of the latter models are also referred to as hydraulic radius theories.

In order to relate the flow of fluids through porous materials to more fundamental quantities, Kozeny (7) developed a widely used theory based on the hydraulic radius concept. The Kozeny equation was later modified by Carman (8), who applied the equation to the determination of the surface area of porous materials. Because of the importance attached to this relationship and the necessity for realizing the assumptions made in evolving the Kozeny-Carman equation, a brief outline of the derivation is given below.

The Poiseuille equation for viscous flow through a long, straight capillary tube of radius, R, cross-sectional area, A, and length, ℓ, is

$$u = Q/A = R^2 \Delta P/(8 \eta \ell) \qquad (4).$$

This relationship can be extended to channels of noncircular cross section by introducing the concept of the hydraulic radius, m. For a cylindrical channel,

$$m = \frac{\text{volume of channel}}{\text{wetted area of channel}} = \frac{\pi R^2 \ell}{2 \pi R \ell} = \frac{R}{2} \qquad (5).$$

Substituting this value of $\underline{m}$ for $\underline{R}$ in Equation (4) and replacing the resulting factor of 2 by the shape factor, $\underline{k_o}$, results in the generalized form of Poiseuille's equation:

$$u = \frac{Q}{A} = \frac{m^2 \Delta P}{k_o \eta \ell} \tag{6}$$

Kozeny (7) noted the similarity between Darcy's law and the generalized form of Poiseuille's equation and proceeded to relate the permeability coefficient to the size, shape, and mode of packing of the solid material making up the porous medium. The total cross-sectional area of the pore space was shown to equal $\epsilon \underline{A}$, where ϵ is the porosity or fractional volume of voids and $\underline{A}$ is the cross-sectional area of the medium. Kozeny considered the porous material to be equivalent to groups of parallel, similar channels of complex cross-sectional shape and oriented in the direction of macroscopic flow. The total volume and internal area of these channels were considered to be equal, respectively, to the total void volume and the total surface area of the medium. The mean hydraulic radius is then given by

$$\overline{m} = \frac{\epsilon}{S_o} \tag{7}$$

where $\underline{S_o}$ is the surface area per unit volume of the medium.

Carman (8) reasoned, first, because cross-sectional area available to fluid flow within the porous medium is restricted and, second, because it is qualitatively apparent that the fluid is constrained from flowing in a straight line through the medium, that the actual average velocity of the fluid, $\underline{u_e}$, is given by

$$u_e = (u/\epsilon)(L_e/L) \tag{8}.$$

In Equation (8), $\underline{u}$ is the superficial approach velocity of the fluid, $\underline{L}$ is the actual thickness of the porous medium, and $\underline{L_e}$ is the apparent length of the equivalent channels in the direction of macroscopic flow.

Combining Equations (6), (7), and (8), one obtains

$$u = Q/A = \epsilon^3 \Delta P/[k_o(L_e/L)^2 S_o^2 \eta L] \qquad (9)$$

The product of the pore shape factor, $\underline{k_o}$, and the tortuosity factor, $(\underline{L_e}/\underline{L})^2$, is referred to as the Kozeny factor* and is designated by $\underline{k}$. The surface area of the particles per unit volume of the medium, $\underline{S_o}$, may be written in terms of the surface area per unit volume of the particles, $\underline{S_v}$, by assuming that the area of contact between the particles in the medium is negligible. Thus,

$$S_o = S_v(1 - \epsilon) \qquad (10)$$

Substituting for $\underline{k_o}(\underline{L_e}/\underline{L})^2$ and $\underline{S_o}$ in Equation (9) gives the usual form of the Kozeny-Carman equation.

$$u = Q/A = \epsilon^3 \Delta P/[kS_v^2(1 - \epsilon)^2 \eta L] \qquad (11).$$

Comparing Equation (11) with Darcy's law, it is seen that the permeability coefficient is represented by

$$K = \epsilon^3/[kS_v^2 (1 - \epsilon)^2] \qquad (12).$$

The specific surface area may also be written on a mass basis since

$$S_w = vS_v \qquad (13)$$

*The factor $\underline{k}$ is referred to by some authors as the "Kozeny constant." However, since it is now recognized that $\underline{k}$ is not a constant but can vary with porosity and other properties of the porous medium, the term Kozeny factor is preferred.

where S_w is the hydrodynamic surface area[1] per unit mass of solid material and v is the hydrodynamic specific volume[2] of the particles which compose the porous medium. The combination of Equations (12) and (13) yields

$$K = \epsilon^3 v^2 / [k S_w^2 (1 - \epsilon)^2] \qquad (14).$$

Recent monographs by Scheidegger (9) and Carman (10) discuss in detail much of the large volume of literature which has grown out of the Kozeny-Carman theory, and a review of this type will not be given here. Instead, the general conclusions of significance to the present study will be discussed, particularly those relating to fibrous beds and to consolidated porous media.

A considerable amount of effort on the application of the Kozeny-Carman equation has centered about selecting a proper value of the Kozeny factor, k. In the terminology used in deriving Equation (11), the factor k is considered to be the product of a shape factor, k_o, and a tortuosity term, $(L_e/L)^2$. The theoretical values of k_o for flow channels of various cross-sectional shapes have been presented by Carman (8). These are listed in Table I and were derived from solutions of the general equations of fluid flow.

In a simple experiment in which a dye was injected into water flowing through a bed of large glass spheres, Carman (10) observed that the instantaneous velocity was generally at an angle of 45° with the direction of macroscopic flow. From this he concluded that the average length of the path for

---

[1] For microporous materials such as wood pulp fibers, the term "hydrodynamic specific surface area," in which the intrafiber surfaces are excluded and slight surface roughnesses are considered unimportant, is preferred.

[2] For wood pulp fibers, the "hydrodynamic specific volume" includes the volume of solid material plus the volume of nonflowing fluid. As a result, v is always larger than the reciprocal of the pycnometric density of the solid material.

fluid flow was $\sqrt{2}$ times the bed thickness. Since the data obtained on beds of glass spheres and packed sand indicated a value of about 5 for the Kozeny factor, Carman concluded that the shape factor must have an average value of 2.5. These conclusions are not unreasonable in view of the theoretical values of k_o listed in Table I.

TABLE I

THEORETICAL VALUES OF k_o FOR VARIOUS CROSS-SECTIONAL SHAPES

[After Carman (8)]

Shape	k_o
1. Circle	2.00
2. Ellipses	
a. Major axis = 2 x minor axis	2.13
b. Major axis = 10 x minor axis	2.45
3. Rectangles	
a. Length = breadth (square)	1.78
b. Length = 2 x breadth	1.94
c. Length = 10 x breadth	2.65
d. Length is infinite	3.00
4. Equilateral triangle	1.67

* A rather complete study of the effect of porosity and particle shape on the value of the Kozeny factor has recently been published by Wyllie and Gregory (11). These authors determined the surface area of a number of different particle shapes as a function of porosity using a statistical "pin-drop" method. These particles were then formed into beds and subjected to permeability tests. From the known surface areas and porosities, Wyllie and Gregory were able to calculate values of the Kozeny factor. A portion of the results presented by these authors is recorded in Table II. The column labeled k_c represents the

corrected values of Kozeny factor in which the area of contact between particles was taken into account. The column labeled $\underline{k}$ represents the values of Kozeny factor assuming point contact between particles.

TABLE II

EFFECT OF PARTICLE SHAPE ON THE KOZENY FACTOR

[After Wyllie and Gregory (11)]

Particles	Corrected Area, sq. cm./cc.	Porosity, ϵ	Kozeny Factors, $\underline{k}$	$\underline{k_c}$
Cubes				
$\underline{S_v}$ = 18.6 sq. cm./cc. (uncorrected)	10.40	0.190	5.40	17.17
	10.75	0.205	5.32	15.84
	11.95	0.274	4.88	11.76
	12.70	0.317	4.74	10.11
	13.25	0.345	4.58	8.98
	13.60	0.358	4.59	8.54
	15.05	0.425	4.37	8.64
Disks				
$\underline{S_v}$ = 25.2 sq. cm./cc. (uncorrected)	21.35	0.343	4.09	5.69
	21.85	0.351	4.10	5.44
	22.25	0.369	4.11	5.26
	23.40	0.398	4.28	4.96
	24.75	0.429	4.70	4.87
Prisms				
$\underline{S_v}$ = 24.1 sq. cm./cc. (uncorrected)	15.15	0.361	3.21	8.15
	15.65	0.378	3.31	7.87
	16.00	0.408	3.41	7.76
	16.54	0.434	3.83	8.25
	17.05	0.466	4.29	8.60
	18.00	0.518	4.86	8.74

It is readily seen from the data of Table II that the Kozeny factor is greatly affected by particle shape, particularly for the more angular-shaped particles. While the uncorrected values of $\underline{k}$ are near the value of 5 suggested by Carman, when account is taken of the area in contact, the Kozeny factors are significantly higher.

Wyllie and Gregory (11) also studied the effect of particle size on the Kozeny factor by determining the permeability of mixtures of spherical particles of

different sizes. The surface areas were calculated from the particle diameters and, since the requirement of point contact between particles is probably justified with these beds, no corrections were applied to the Kozeny factors. A summary of the results of these studies, together with the particle dimensions, are presented in Table III. It can be seen from these data that, as the distribution of particle sizes (and presumably the pore size distribution) becomes broader, the calculated Kozeny factors increase. From the studies of Wyllie and Gregory (11), it may be concluded that porosity, particle shape, and pore size distribution all affect the value of the Kozeny factor, k.

TABLE III

EFFECT OF PARTICLE SIZE ON THE KOZENY FACTOR

[After Wyllie and Gregory (11)]

Particle sizes:

Particle	Diameter, mm.
Glass spheres	3.0
3M Superbrite beads:	
Grade 5	0.711
Grade 9	0.279
Grade 16	0.057
Grade 19	0.028

Calculated Kozeny Factors:

Bed Composition	S_v, sq. cm./cc.	Porosity, ϵ	Kozeny Factor, k
100% 3-mm. Spheres	19.8	0.368	4.81
61% 3 mm.; 41.7% Grade 5	44.64	0.294	5.53
58.3% 3 mm.; 41.7% Grade 5	46.39	0.283	6.40
51.3% 3 mm.; 48.7% Grade 9	111.7	0.254	6.94
61.1% 3 mm.; 38.9% Grade 9	96.18	0.235	7.00
70% 3 mm.; 30% Grade 16	347.2	0.187	7.14
60.5% 3 mm.; 22% Grade 5; 12.5% Grade 19	569.2	0.139	7.36

Fowler and Hertel (12) and Sullivan and Hertel (13) have tested the validity of the Kozeny-Carman equation when applied to the air permeability of fibrous materials such as glass wool, cotton, and other textile fibers whose external surface area and density could be determined with fair accuracy by other means. Using an air permeability apparatus in which the bed could be compacted to varying degrees by means of a movable piston, Fowler and Hertel determined the permeability properties of these fibrous beds over a wide range of porosity. These data were analyzed using a form of the Kozeny-Carman equation which allowed the hydrodynamic specific surface area and the hydrodynamic specific volume of the fibers to be evaluated simultaneously. The equation used by Fowler and Hertel may be developed in the following way.

One can consider a fibrous bed so highly compressed that the effective porosity is zero and all flowing fluid is excluded from the bed. Then, the fiber density must be equal to the bed density, and

$$\rho_s = \rho_b = W/AL_o \qquad (15)$$

where ρ_s and ρ_b are the effective densities of the fibers and the bed, respectively, W is the mass of fibers in the bed whose cross-sectional area is A, and L_o is the bed thickness at zero porosity. At any thickness of the bed, L, greater than L_o, the solid fraction of the bed must be equal to the ratio of the bed density to the effective density of the fibers, and the porosity or void fraction is given by

$$\epsilon = 1 - \rho_b/\rho_s = 1 - L_o/L \qquad (16)$$

Substituting this expression for ϵ into the Kozeny-Carman relationship [Equation (12)] and rearranging terms gives

$$(KL)^{1/3} = (1/kS_v^2 L_o^2)^{1/3} (L - L_o) \qquad (17)$$

where K is the permeability coefficient from Darcy's law, S_v is the hydrodynamic specific surface area per unit volume of the fibers, and the remaining quantities were defined above.

According to Equation (17), a plot of the quantity $(K/L)^{1/3}$ against L should be linear if the Kozeny-Carman equation is applicable. Furthermore, the value of S_v may be calculated from the slope of this plot, and the hydrodynamic specific volume may be calculated from the intercept, L_o, since

$$v = AL_o/W \qquad (18)$$

Equation (17) may also be written on a mass basis by introducing the value of v from Equation (18). Such a substitution results in

$$(KL)^{1/3} = [A^2/(kS_w^2 W^2)]^{1/3} (L - L_o) \qquad (19)$$

Fowler and Hertel (12) applied Equation (23) to beds of fibers in which the fibers were oriented perpendicular to the direction of macroscopic flow. For this orientation, the Kozeny factor was found to have an average value of 5.55 (over a range from 5.0 to 6.0) and was relatively independent of porosity. The range of porosity studied was restricted to 0.55 to 0.86 (14). These authors also investigated the case of flow through beds of fibers whose axes were oriented parallel to the direction of macroscopic flow. For this case, the Kozeny factor was found to have a value of 3.0 at a porosity of 0.86. Since the tortuosity must equal 1.0 for fibers oriented parallel to the direction of flow, the shape factor, k_o, was assigned a value of 3.0 for this case.

Sullivan (14, 15) applied the Kozeny-Carman equation to the air permeability of textile fibers in the higher porosity range from 0.82 to 0.995. He found that the Kozeny factor increased sharply with porosity in these highly porous beds.

Brown (16) has applied a modified form of the Kozeny-Carman equation to the determination of the surface area exposed to flow in thin handsheets of paper and beds of dry, "unbonded" pulp fibers. He concluded that the pore shape factor, k_o, "...appears to be a constant, independent of porosity for moderately compacted beds of fibers and handsheets." He also noted that, for the fiber beds, the Kozeny factor apparently increased with decreasing porosity. This variation was attributed to an increase in the tortuosity term, $(L_e/L)^2$, and the fact that the area of contact between the fibers became appreciable at lower porosities. Brown also conducted air permeability tests on glass fiber beds and utilized the slip phenomenon* at low pressures in an effort to separate the effects of pore shape and tortuosity. The results of these tests are presented in Table IV.

The results recorded in Table IV indicate a relatively constant tortuosity which is near the value of $\sqrt{2}$ suggested by Carman (8), whereas the pore shape factor, k_o, increases regularly with porosity. In view of the theoretical values of pore shape factor recorded in Table I, the physical significance of the higher values of k_o (those above about 3.0) would seem questionable. It should also be pointed out that the results recorded above for glass fibers are in opposition to the conclusions of Brown regarding his beds of pulp fibers. In the latter case, the increase in the Kozeny factor was attributed to an increase in tortuosity with the shape factor remaining essentially constant.

*Slip flow is the condition which exists when the velocity of the fluid at the solid boundary is not zero. This phenomenon becomes important when the dimensions of the flow channel approach the mean free path of the gas (17).

TABLE IV

VARIATION OF PORE SHAPE FACTOR AND TORTUOSITY WITH POROSITY

[After Brown (16)]

Porosity	Kozeny Factor	Pore Shape Factor	Tortuosity
0.953	12.0	5.35	1.50
0.944	10.9	5.30	1.44
0.929	9.65	4.25	1.51
0.911	8.60	3.50	1.57
0.869	7.04	3.29	1.47
0.828	6.40	2.91	1.48
0.782	6.17	2.98	1.43
0.738	5.90	2.78	1.46

Ingmanson, et al. (18) have recently applied the Kozeny-Carman equation to beds of cylindrical glass and synthetic fibers using water as the permeating fluid. They concluded that the Kozeny factor had an average value of about 5.5 over the porosity range from 0.7 to 0.8 in agreement with the results of Fowler and Hertel (12). These authors also found an increase in the Kozeny factor at higher porosities and suggested the following empirical equation to describe this variation:

$$k = \frac{3.5\,\epsilon^3}{\sqrt{(1-\epsilon)}}\left[1 + 57(1-\epsilon)^3\right] \qquad (20)$$

Macklem (19) has applied the Kozeny-Carman equation to the flow of liquids through woven wool felts. Several different types of felts were investigated in both lateral and transverse permeability tests. For the case of transverse flow (i.e., perpendicular to the specimen), the Kozeny factor was found to decrease

from about 8.0 at a porosity of 0.68 to approximately 1.0 at porosities of 0.1 to 0.2. The unreasonably small values of $\underline{k}$ at the lower porosities were attributed to a decrease in the swollen specific volume at higher levels of compaction.

For the case of lateral flow (i.e., along the felt), Macklem corrected the data for the deswelling of the fibers at larger compressive loads. While a large variation in the calculated values of $\underline{k}$ was found, it appeared that the Kozeny factor increased with decreasing porosity. Calculated values of $\underline{k}$ as large as 26 were observed.

From the studies reviewed above, it appears that the validity of the Kozeny-Carman equation has been fairly well established for flow through unconsolidated fibrous beds, provided that a proper value is selected for the Kozeny factor, $\underline{k}$. However, in view of the variations in the Kozeny factor, the accuracy of the equation is probably no better than $\pm$ 10% in many cases. Nonetheless, the Kozeny-Carman equation does yield concordant values for specific surface area, and it appears to be adequate for many engineering applications.

Relatively little work has been done on the application of the Kozeny-Carman equation to the viscous flow of fluids through consolidated porous media. For the purposes of this discussion, a consolidated porous medium may be defined as one in which the particles making up the structure are bonded or fused together to produce a continuous solid medium which is more or less rigid. Such porous media as natural rocks, sintered glass, and a sheet of paper would fall under this definition.

Many of the investigations on consolidated porous media have been made on porous rocks (20, 21) which are of particular interest in the oil industry. In these studies, the "tortuosity" was evaluated using a method originally

proposed by Archie (22). Archie defined a "formation resistivity factor," F, as the ratio of the electrical resistance offered by a porous medium saturated with electrolyte, R_o, to that of the free electrolyte solution, R_w,

$$F = R_o/R_w \tag{21}$$

It has been demonstrated by Wyllie and Spangler (21) that the "tortuosity" is related to F by

$$(L_e/L)^2 = F^2 \epsilon^2 \tag{22}$$

where ϵ is the porosity of the porous medium.

The basic assumption made in arriving at Equation (22) is the identification of the ratio (L_e/L) of the electrical system with the corresponding ratio of the fluid flow system which is involved in the derivation of the Kozeny-Carman equation. As pointed out by Bikerman (23), in the case of swollen gels and some membranes, ionic migration along the surfaces and through the gel structure is possible. For such systems, then, the paths for ionic transfer and for fluid flow are clearly not the same. Since cellulose is a polyelectrolyte, Equation (22) would not be expected to apply to beds of pulp fibers. This conclusion has been supported by the experimental work of Goring and Mason (24).

In the case of consolidated porous rocks such as sandstone, Equation (22) has been found to yield concordant values of "tortuosity." While the equivalence of the ratio (L_e/L) in the electrical and fluid flow systems is certainly debatable, Wyllie and Spangler (21) have applied this equation to a number of samples of sandstone with reasonably good results. These authors determined the surface area and porosity of several samples of sandstone from fluid flow measurements and from statistical tests. A summary of their results is presented in Table V.

TABLE V

PERMEABILITY DATA OF WYLLIE AND SPANGLER (21)

Sample	Permeability Coefficient, 10^{-13} sq. cm.	Porosity, ϵ	$(L_e/L)^2$, electrical	Apparent k_o	S_v (flow), sq. cm./cc. [a]	S_v (stat.), sq. cm./cc.
Oligocene S.S.	3.76	0.218	8.66	2.40	497	507
Penn. S.S. F151	1.21	0.163	10.70	3.20	437	386
Penn. S.S. F154	2.66	0.181	6.42	2.72	457	438
Penn. S.S. F228	2.75	0.201	12.35	2.36	387	398
Penn. S.S. F250	5.10	0.205	7.11	2.13	388	421
Penn. S.S. F252	2.91	0.185	9.78	2.54	365	362
Penn. S.S. F220	3.32	0.195	7.74	3.32	433	376

[a] S_v values from fluid flow measurements were calculated assuming a value of 2.5 for k_o as suggested by Carman (8).

The values listed under the heading "apparent k_o" are the values of the pore shape factor in the Kozeny-Carman equation required to produce agreement between the surface areas calculated from fluid flow measurements and those predicted statistically.

The data of Table V indicate an arithmetic average shape factor of 2.69, which is reasonably close to the value of 2.5 suggested by Carman (8). It is also apparent that these consolidated rocks had a much higher "tortuosity" than the unconsolidated sand beds investigated by Carman and other workers. Thus, it might also be expected that other consolidated porous media such as an ordinary sheet of bonded pulp fiber would exhibit an abnormally high Kozeny factor.

However, it should be pointed out that extreme caution must be exercised in any attempt to translate the results obtained on porous rocks to fibrous systems. One need only consider the following basic differences between the two systems:

1. Porous rocks have a low porosity (below 0.5) compared to fibrous structures (above 0.5).

2. Porous rocks are more or less isotropic while fibrous structures are quite anisotropic with respect to permeability properties.

3. Porous rocks are incompressible media while fibrous mats are compressible.

4. While porous rocks are made up of more or less spherical particles, fibrous structures are formed from elongated, ribbonlike fibers.

A few studies have been reported in which the Kozeny-Carman equation was applied to thin handsheets of bonded pulp fibers. Brown (16) reported a hydrodynamic specific surface area of about 12,000 sq. cm. per g. for an unrefined pulp wet pressed at 50 p.s.i. The corresponding value for dry, "unbonded" fibers

was approximately 8600 sq. cm./g. In both cases, the value of the Kozeny factor was assumed to be 6.0. Brown attributed these differences to a larger tortuosity in the case of the handsheets.

Sanborn (25) was unable to apply the Kozeny-Carman approach to evaluate the stress-induced changes in the interfiber exposed surface area of paper. For a specimen formed from a lightly refined, classified pulp and wet pressed at 50 p.s.i., he found that the hydrodynamic specific surface area (calculated using $k = 5.55$) was reduced from 11,000 sq. cm. per g. for the unstressed sample to 8750 sq. cm./g. for the same specimen after repeated stress-recovery cycles. These anomalies were attributed to large changes in the pore size distribution, which had a considerable effect on the permeability characteristics of the sheet. Sanborn concluded, "This means that the Kozeny-Carman method of data reduction should not be used to analyze air-permeability data gathered on relatively thin sheets of paper. If the method is used to rectify such data....the calculated values of interfiber exposed surface area are too high by a factor of about two..."

Recently, McDonald (26) has shown that the Kozeny-Carman equation can be applied to thick mats prepared from an unbeaten, classified pulp. Using an apparatus which employs a movable piston to compact the mat and the method of data reduction suggested by Fowler and Hertel (12) [see Equation (19)], McDonald found that the Kozeny-Carman equation described his data very well for the porosity range from 0.4 to 0.75.

Thus, it appears that the Kozeny-Carman approach does apply to thick mats of bonded pulp fibers. However, in the case of thin sheets of paper, the value of the Kozeny factor is apparently greater than the value of 5.55 suggested by Fowler and Hertel (12). Whether this difference is due to a higher tortuosity

as suggested by Brown (16) or to effects of the pore size distribution as proposed by Sanborn (25) is a moot question.

Another approach which has been applied to the description of porous media and which may also be classified as phenomenological in nature is the various cylindrical capillary models. If a bundle of cylindrical capillary tubes is taken as the model of a porous medium, equations describing nearly all of the flow properties can be derived by comparatively simple mathematical operations. The equations which relate the properties of porous media to the capillary radius distribution of the equivalent bundle of capillaries have been given by Childs and Collis-George (27), Fatt and Dykstra (28), Tollenaar and Blokhuis (29), and Burdine, et al. (30).

The advantages which are gained by being able to make rigorous calculations from these models are more than offset by the failure of the models to represent accurately the porous medium. Several obvious characteristics of real porous media are not accounted for by a bundle of parallel cylindrical capillaries. For example, most real porous media exhibit a different permeability in different directions and are therefore somewhat anisotropic. In contrast, a bundle of capillaries is perfectly anisotropic. Many other differences between the bundle of cylindrical capillaries model and real porous media are revealed when the flow properties of the model are compared with those of the real porous media.

ANALYTICAL APPROACHES

As mentioned earlier, the analytical approaches are represented by the various drag theories of permeability. The basic premise of these theories is that the pressure drop across a porous medium through which uniform flow is occurring is equal to the total drag force experienced by the particles which

compose the medium. Theoretically, the drag force on each individual particle may be evaluated by solving the basic hydrodynamic equations under the appropriate boundary conditions. In the idealized case where the particles are assumed to be independent of each other, the drag force on an individual particle has been derived for such simple geometries as spheres and cylinders (2). In actual porous media, flow interferences due to neighboring particles are always present even at very high void fractions.

An example of the application of the drag theory to fibrous porous media is found in the recent work of Iberall (31). He considered a unit volume of a bed composed of N randomly oriented cylinders in which N/3 cylinders were oriented in each of the three perpendicular directions. It was estimated by Emersleben (32) that the drag force per unit length of a single cylinder oriented along the direction of flow is approximately

$$F_d = 4\pi\eta V' \qquad (23)$$

where F_d is the drag force per unit length, V' is the approach velocity or the stream velocity approaching the cylinder, and η is the viscosity of the permeating fluid.

The drag force per unit length over a cylinder of infinite length oriented perpendicular to the direction of flow is given by [see Lamb (2)]

$$F_d = 4\pi\eta V'/(2 - \ln Re) \qquad (24)$$

in which:

ln Re = natural logarithm of the local Reynolds number

Re = du ρ/η

d = cylinder diameter

$\underline{u}$ = local velocity, and

ρ = fluid density.

Iberall proceeded to combine the drag forces for the $\underline{N}/3$ cylinders in each of the three perpendicular directions and he then equated this result with the over-all pressure gradient. The work of Iberall has been severely criticized by Han (32a). The major limitation of Iberall's work lies in the faulty assumption of noninterference between neighboring cylinders. Such an interference must exist even at porosities approaching 1.0. In addition, Lamb's solution predicts that the product of the Reynolds number and the drag coefficient (for a single fiber) should increase with Reynolds number when, in fact, it has been demonstrated experimentally on highly porous beds that this product is a constant (32a).

As mentioned earlier, the basic idea of the drag theories is that the pressure drop required to maintain uniform flow through a porous medium is equal to the total drag force experienced by the particles in the medium. For $\underline{N}$ particles, this may be stated mathematically as

$$\Delta P = NF_t/A \tag{25}$$

where $\underline{F_t}$ is the <u>total</u> drag force on $\underline{N}$ particles.

For cylindrical particles of diameter $\underline{d}$ and length $\underline{L_c}$

$$N = 4(1 - \epsilon)AL/(\pi d^2 L_c) \tag{26}$$

and therefore,

$$\Delta P = 4L(1 - \epsilon)F_t/(\pi d^2 L_c) \tag{27}$$

In the absence of interference by neighboring cylinders, $\underline{F}_t$ may be evaluated for the drag over a single, infinite cylinder (2). If this result is then compared with Darcy's law, it can be shown (32a) that

$$K = (d^2/16)(2 - \ln Re)[\epsilon/(1 - \epsilon)] \qquad (28)$$

But, for cylinders

$$S_v^2 = 16/d^2 \qquad (29)$$

and therefore

$$K = [(2 - \ln Re)/S_v^2][\epsilon/(1 - \epsilon)] \qquad (30)$$

Comparing this result with the Kozeny-Carman equation, it can be shown that the Kozeny factor must vary with porosity. This variation is even more graphically shown by the recent work of Happel (33) in which the interference between neighboring cylinders is also considered.

Happel was able to solve the Navier-Stokes equations for flow parallel to and perpendicular to an array of cylinders using a "free surface model," With this model, each cylinder is considered to be surrounded by an envelope of fluid with a free surface. (Fig. 2).

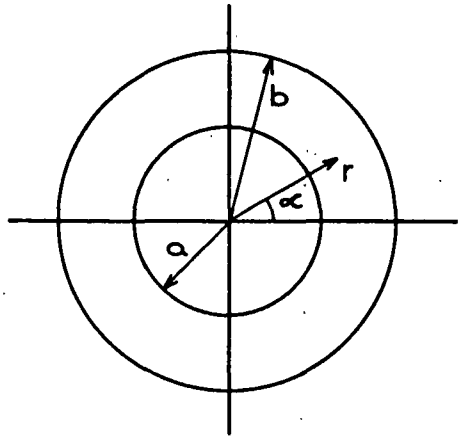

Figure 2. Free Surface Model

The case of fluid flow perpendicular to an array of cylinders is of particular interest to this study and will be considered in some detail. For this orientation, it is assumed that the cylinder is moving with a uniform velocity $\underline{V}'$ in a stationary fluid. This is equivalent to the case of the cylinder being stationary with fluid flow past it at a uniform velocity $\underline{V}'$. The boundary conditions for the free surface model are: (1) no slippage of the fluid at the surface of the cylinder and (2) no shearing stress at the free surface. These conditions are expressed mathematically as (see Fig. 2):

$$u = V'$$

$$v_r = V' \cos\alpha \qquad \text{at } \underline{r} = \underline{a}, \text{ and}$$

$$v_\alpha = -V' \sin\alpha$$

$$v_r = 0$$

$$\frac{\partial v_\alpha}{\partial r} + \frac{1}{r}\frac{\partial v_r}{\partial \alpha} - \frac{v_\alpha}{r} = 0 \qquad \text{at } \underline{r} = \underline{b}$$

where $\underline{v}_{\underline{r}}$ and $\underline{v}_{\underline{\alpha}}$ are the local velocity components in the directions of $\underline{r}$ and α, respectively.

For an incompressible fluid, the equation of continuity in two-dimensional cylindrical co-ordinates is

$$\frac{\partial v_r}{\partial r} + \frac{v_r}{r} + \frac{1}{r}\frac{\partial v_\alpha}{\partial \alpha} = 0 \tag{31}$$

The Navier-Stokes equations for steady-state, viscous flow (neglecting inertial effects) are:

$$\frac{\partial p}{\partial r} = \eta\left[\nabla^2 v_r - \frac{v_r}{r^2} - \frac{2}{r^2}\frac{\partial v_\alpha}{\partial \alpha}\right] \tag{32}$$

and

$$\frac{1}{r}\frac{\partial p}{\partial \alpha} = \left[\nabla^2 v_\alpha - \frac{v_\alpha}{r^2} + \frac{2}{r^2}\frac{\partial v_r}{\partial \alpha}\right] \tag{33}$$

where p is the local fluid pressure and ∇^2 is the Laplacian operator.

Applying the above boundary conditions to the Navier-Stokes equations and the equation of continuity, Happel (33) was able to show that the drag force per unit length of the cylinder is given by

$$F_d = 4\pi\eta V'/\left[\ln(b/a) - 1/2\left(\frac{b^4 - a^4}{b^4 + a^4}\right)\right] \tag{34}$$

From Fig. 2 it can be seen that the porosity of a unit cell in the free surface model is given by

$$\epsilon = 1 - (a/b)^2 \tag{35}$$

Thus, the drag force per unit length of the cylinder may be expressed in terms of porosity as

$$F_d = \frac{8\pi\eta V'}{\left[\ln\left(\frac{1}{1-\epsilon}\right) - \left(\frac{1 - (1-\epsilon)^2}{1 + (1-\epsilon)^2}\right)\right]} \tag{36}$$

From a simple force balance, the pressure drop across an assemblage of cylinders of diameter d required to maintain a uniform velocity V' is related to F_d by

$$\Delta P = 4L(1 - \epsilon)F_d/(\pi d^2) \tag{37}$$

where L is the thickness of the assembly. The permeability coefficient is

therefore given by

$$K = \eta LV'/\Delta P = \left\{d^2/[32(1-\epsilon)]\right\}\left\{\ln[1/(1-\epsilon)] - \frac{1-(1-\epsilon)^2}{1+(1-\epsilon)^2}\right\} \qquad (38).$$

Since the specific surface area, S_v, for cylinders is equal to $4/d$, the Kozeny factor is represented by

$$k = \frac{\epsilon^3}{KS_v^2(1-\epsilon)} = \frac{2\epsilon^2}{(1-\epsilon)\left\{\ln[1/(1-\epsilon)] - \frac{1-(1-\epsilon)^2}{1+(1-\epsilon)^2}\right\}} \qquad (39)$$

Equation (39) contains no empirical factors and is rigorously correct for flow perpendicular to an array of cylinders. Happel's contribution seems to be in the elimination of the ill-defined and misunderstood factors of pore shape and tortuosity in the Kozeny-Carman equation. A comparison of Happel's equations with experimental results on beds of cylindrical fibers may be achieved by comparing the Kozeny factor predicted by means of Equation (45) with the empirical correlation of Ingmanson, et al. (18) Equation (20). Such a comparison is presented in Fig. 3. Happel's equation for flow parallel to an array of cylinders is also plotted in Fig. 3.

It can be seen that the agreement is excellent at a porosity of 0.6. At higher porosities, Happel's equation for flow perpendicular to cylinders predicts a higher Kozeny factor than is found experimentally. This may be due to a combination of two factors. First, since the free surface model is based on a uniform arrangement of cylinders, there is no provision for a variation in pore size. Physically, if the fiber mats investigated by Ingmanson, et al. (18) had an appreciably large pore size distribution, the fluid would tend to flow preferentially through the large pores, thereby resulting in a higher permeability and a

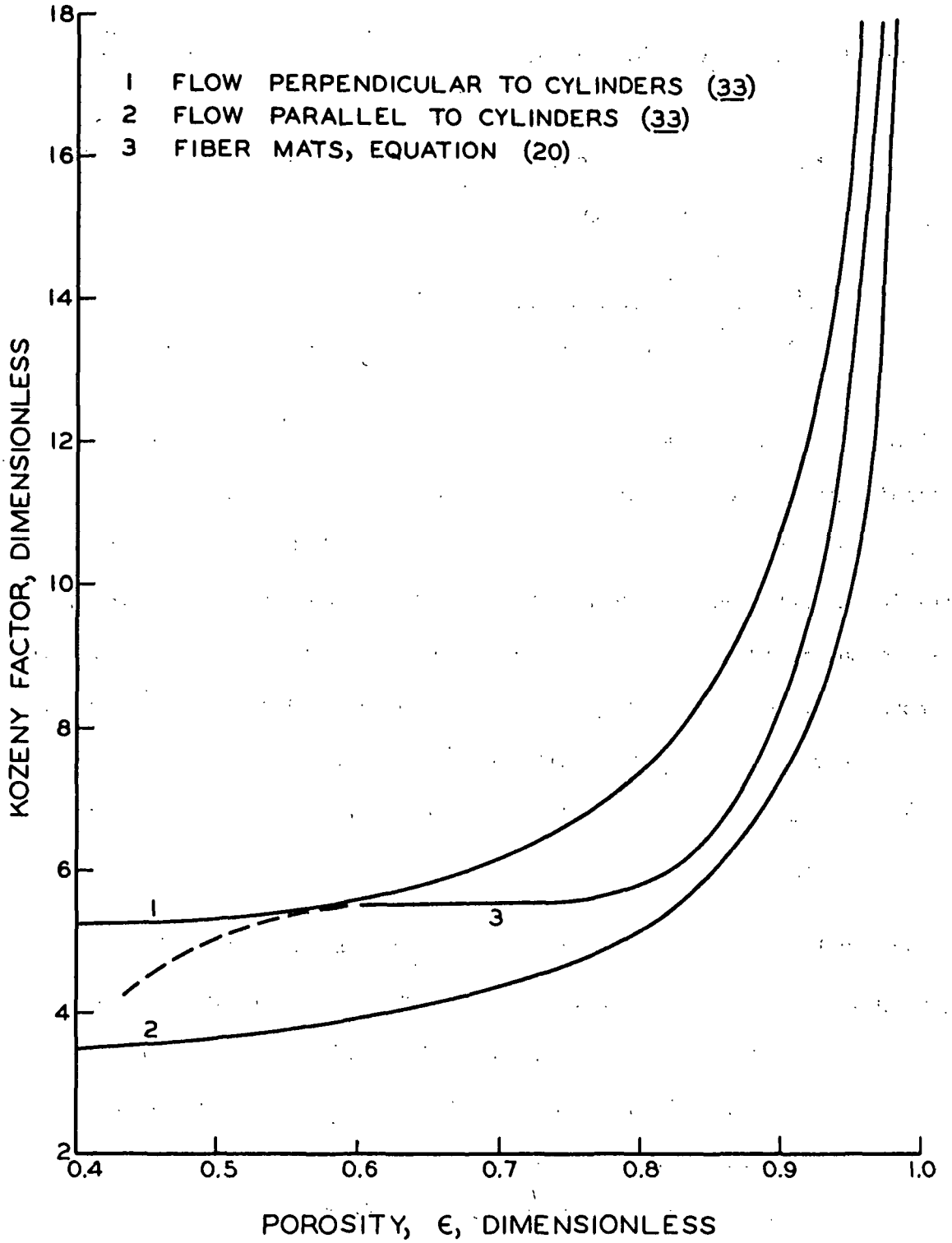

Figure 3. Variation of Kozeny Factor with Porosity

lower Kozeny factor, at a given porosity, than the prediction based on uniform pore size. Secondly, the Happel equation is based on flow perpendicular to an array of cylinders which are aligned parallel to one another. The cylinders thus lie in only one direction, whereas the fiber mats of Ingmanson, et al. were formed in such a manner that the fibers were more or less randomly oriented in a plane perpendicular to flow. It is possible that the flow interference between neighboring fibers might be different for a random orientation in the plane perpendicular to the direction of macroscopic flow than for a parallel array of cylinders in the same plane.

Nonetheless, the theoretical derivations of Happel (33) have placed the hydraulic radius theories on a much sounder basis for the special case of beds of cylindrical fibers. In addition, since the free surface model takes account of flow interference between adjacent particles in the bed, the Happel equations represent a significant advance in the drag theories of permeability.

STATISTICAL APPROACHES

Both the phenomenological approach and the analytical approach are based on an orderly model for the description of flow through porous media. The opposite approach is represented by the various statistical theories in which a completely disordered model is assumed. The statistical theories assume that the randomness or disorder of the porous medium may be predicted on the basis of ordinary probability considerations. The randomness may be attributed to the fluid as suggested by Scheidegger (9) or to the porous medium as suggested by other authors. Scheidegger's approach leads to a modification of Darcy's law in which a new macroscopic quantity termed "dispersivity" is introduced. This quantity is taken to be indicative of the sideways dispersion which the stream of fluid undergoes in passing

through the porous medium. His approach has not yet led to a useful permeability expression and will not be discussed further.

The first problem in the statistical approach is to describe the pore geometry, and since a point-by-point specification is not possible, the description must be a statistical one. Debye and co-workers (34) define a function, $\underline{g}(\vec{r})$, of a position vector $\vec{r}$ within the porous medium such that $\underline{g}(\vec{r}) = 1$ if $\vec{r}$ is in a void region and $\underline{g}(\vec{r}) = 0$ if $\vec{r}$ is in a solid region. A complete knowledge of the correlation function $\underline{g}(\vec{r})$ would amount to a detailed description of the porous medium. Since this is not possible, a partial description of the medium may be obtained by considering various average values of $\underline{g}(\vec{r})$. Thus, the volume average of $\underline{g}(\vec{r})$ itself is the porosity or void fraction of the medium:

$$\epsilon = \langle\langle g(\vec{r}) \rangle\rangle = \frac{1}{V} \int_V g(\vec{r}) d\vec{r} \qquad (40)$$

where $\langle\langle g(\vec{r}) \rangle\rangle$ is referred to as the one-point average. The one-point average represents the probability that a point selected at random in a section of the porous medium will lie within a void region. Or,

$$\langle\langle g(\vec{r}) \rangle\rangle = \lim_{N \to \infty} N_o/N \qquad (41)$$

where $\underline{N}_o$ denotes the number of times the point lies in a void region, and $\underline{N}$ is the total number of points selected.

Information about the shape of the void region may be obtained by adding a length vector, $\vec{\delta}$, to the position vector, $\vec{r}$, and averaging the product $\underline{g}(\vec{r}) \cdot \underline{g}(\vec{r} + \vec{\delta})$ with respect to $\vec{r}$ while keeping $\vec{\delta}$ fixed (35). The resulting two-point average,

$$S(\vec{\delta}) = g(\vec{r}) \cdot g(\vec{r} + \vec{\delta}) \tag{42}$$

represents the probability that a line segment having the direction and length of the vector $\vec{\delta}$ will, when thrown randomly on a cross section of the porous medium, land with both of its ends in a void region. For an isotropic porous medium, $\underline{S}(\vec{\delta})$ will depend only on the magnitude of $\vec{\delta}$. When $\delta = 0$, the product of $\underline{g}(\vec{\underline{r}})$ by itself is simply unity and its volume average is the porosity, ϵ. When $\delta = \infty$, the probabilities of two events in voids a large distance apart are independent of each other; the volume average of each event is ϵ, and the product of the two probabilities is therefore ϵ^2. Thus, the correlation function $\underline{S}(\vec{\delta})$ decays continuously from ϵ to ϵ^2 as δ is changed from zero to infinity.

Debye, et al. (34) proceeded to establish the mathematical form of the correlation function $\underline{S}(\vec{\delta})$ for a completely random, isotropic porous medium. If $\vec{\underline{r}}$ is considered to be a pin of fixed length which is thrown randomly into a porous medium, one may define $\underline{P}_{\underline{ab}}$ as the probability that the ends land in an environment $\underline{ab}$. There are four such probabilities*: $\underline{P}_{01}$, $\underline{P}_{10}$, $\underline{P}_{00}$, and $\underline{P}_{11}$, where the subscript 0 stands for a void and 1 for a solid environment. These four probabilities are related as follows:

$$P_{00} + P_{01} = 1 \tag{43}$$

$$P_{10} + P_{11} = 1 \tag{44}$$

and

$$\epsilon P_{01} = (1 - \epsilon)P_{10} \tag{45}$$

where the last equation represents the two equally probable ways in which the ends of the pin may land in different environments.

*These are conditional probabilities in that $\underline{P}_{00}$ represents the probability that, if one end of the vector lies in a void space, the other end also lies in a void region, and so forth.

Since $\underline{S}(\vec{\delta})$ decays from ϵ to ϵ^2 when δ changes from 0 to ∞, it may be reasoned that if one end of the pin is fixed in a void, the probability that the other end also lies in a void is

$$P_{00} = S(\vec{\delta})/\epsilon \tag{46}$$

Therefore, the probability that the free end lies in a solid environment is given by

$$P_{01} = 1 - P_{00} = 1 - S(\vec{\delta})/\epsilon \tag{47}$$

Since $\epsilon P_{01} = (1 - \epsilon)P_{10}$, if the pin is thrown randomly there is an equal probability that the ends will fall into different environments; hence,

$$P_{10} = (\epsilon/1 - \epsilon)P_{01} = \frac{\epsilon - S(\vec{\delta})}{1 - \epsilon} \tag{48}$$

Thus, the probability of "dissimilar ends," $\underline{P_D}$, can be written as

$$P_D = \epsilon P_{01} + (1 - \epsilon)P_{10} = 2[\epsilon - S(\vec{\delta})] \tag{49}$$

From Equation (49), one may proceed directly to a calculation of the specific surface area. If $\vec{\delta}$ is allowed to become very small and to take on all possible spatial orientations, while imposing the restriction that the two ends must always remain in different environments, the pin must cut and follow the surface between the void and solid spaces. From geometric considerations, the probability of "dissimilar ends," $\underline{P_D}$, may be calculated as follows* (Fig. 4):

*In order to calculate the "probability of dissimilar ends" from these geometric considerations, it is also necessary that the length, δ, be small compared to the radius of curvature of the surface, $\underline{S}$.

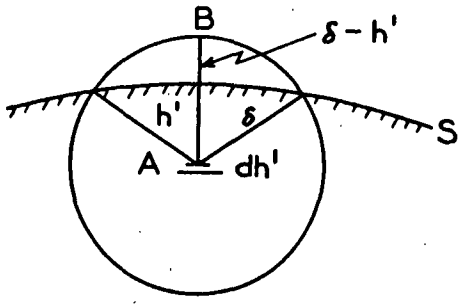

Figure 4. Calculation of the Probability of "Dissimilar Ends," P_D

For the case where one end of the pin, A, is fixed in the solid while the other end, B, is in a void space, it is apparent that point A must lie within a distance $h' < \delta$ from the surface S (see Fig. 4). If the distance h' is increased by an amount dh', the volume which can be covered by the pin per unit volume of porous medium is $S_o\, dh'$. Furthermore, only certain orientations of the pin will allow the free end of the pin, point B, to penetrate the surface. From the geometry of Fig. 4, the probability of penetration, P_p, is given by

$$P_p = \frac{2\pi\delta(\delta - h')}{4\pi\delta^2} \tag{50}$$

Since one end of the pin, point A, may also be fixed in a void space, a similar argument may be applied to this case, and the probability of "dissimilar ends" is twice the integrated probability of penetration,

$$P_D = 2S_o \int_{h'=0}^{h'=\delta} \frac{\delta - h'}{2\delta}\, dh' = S_o\, \delta/2 \tag{51}$$

Comparing Equation (51) with Equation (49), it is seen that the specific surface area is given by

$$S_o = -4\left[\frac{S(\vec{\delta}) - \epsilon}{\delta}\right] \tag{52}$$

But, as mentioned previously, as δ approaches zero, $\underline{S}(\vec{\delta})$ approaches ϵ, so that the value in the bracket approaches the derivative of $\underline{S}(\vec{\delta})$ with respect to δ at $\delta=0$. Therefore, the specific surface area, $\underline{S}_o$, is simply minus four times the initial slope of the plot of $\underline{S}(\vec{\delta})$ versus δ.

It is now possible to proceed with the development of the mathematical form of the correlation function, $\underline{S}(\vec{\delta})$. For a pin of length δ which has one end fixed in a solid environment, $\underline{P}_{11}$ can be affected by a change, $\Delta\delta$, in the length of the pin. The probability $\underline{P}_{11}$ will change only if the addition of $\Delta\delta$ to the length of the pin will allow the pin to cross the surface of the solid environment into a void space or vice versa. If ϕ is the angle between $\vec{\delta}$ and the normal to the surface, the free end of the pin must lie within $\Delta\delta \cos\phi$ to allow a pin of length $\delta + \Delta\delta$ to cross into a void space. The average value of $\Delta\delta \cos\phi$ over all possible orientations is given by

$$\frac{\Delta\delta}{2} \int_0^{\pi/2} \cos\phi \sin\phi d\phi \tag{53}$$

the integral of which is $\Delta\delta/4$.

As a result, the change, $\Delta\underline{P}_{11}$, in $\underline{P}_{11}$ when δ is changed by $\Delta\delta$ is given by

$$\Delta P_{11} = -\left(\frac{S_o}{1 - \epsilon}\right)\left(\frac{\Delta\delta}{4}\right)P_{11} \tag{54}$$

However, since it is possible for the free end of $\vec{\delta}$ to be already in a void, an extra term must be added to the expression for $\Delta\underline{P}_{11}$ to account for the positive contribution which would be made to $\underline{P}_{11}$ by the growth of $\vec{\delta}$ into another solid region. The final expression of $\Delta\underline{P}_{11}$ is

$$\Delta P_{11} = -\left(\frac{S_o}{1-\epsilon}\right)\left(\frac{\Delta\delta}{4}\right)P_{11} + \left(\frac{S_o}{\epsilon}\right)\left(\frac{\Delta\delta}{4}\right)P_{10} \tag{55}$$

In the limit, as $\Delta\delta$ approaches zero, Equation (55) becomes

$$\frac{dP_{11}}{d\delta} = -\frac{S_o}{4}\left[\frac{P_{11}}{1-\epsilon} - \frac{P_{10}}{\epsilon}\right] \tag{56}$$

But,

$$P_{11} = 1 - P_{10} = 1 - \left[\frac{\epsilon - S(\vec{\delta})}{1-\epsilon}\right] \tag{57}$$

and

$$P_{10} = \frac{\epsilon - S(\vec{\delta})}{1-\epsilon} \tag{48}$$

Substituting Equations (57) and (48) for $\underline{P}_{11}$ and $\underline{P}_{10}$, respectively, into Equation (56), one obtains

$$\frac{dS(\vec{\delta})}{d\delta} = -\frac{S_o}{4}\left[\frac{S(\vec{\delta}) - \epsilon^2}{\epsilon\,(1-\epsilon)}\right] \tag{58}$$

the solution for which is

$$S(\vec{\delta}) = [\epsilon\,(1-\epsilon)]\,\exp^*\left[-\frac{S_o\,\delta}{4\,(1-\epsilon)}\right] + \epsilon^2 \tag{59}$$

Thus, it may be concluded that the correlation function $\underline{S}(\vec{\delta})$, is exponential for an isotropic medium with a random distribution of voids and solids. It should also be noted that Equation (59) predicts that $\underline{S}(\vec{\delta})$ approaches ϵ when δ approaches zero and $\underline{S}(\vec{\delta})$ approaches ϵ^2 as δ approaches infinity. These results are in agreement with arguments presented earlier.

Using the two-point average, $\underline{S}(\vec{\delta})$, and applying the Helmholtz principle of least action, Prager (35) was able to show that

*exp is used in this thesis to denote the power of e, the base of Naperian logarithms, i.e., $\exp(\underline{x}) = e^{\underline{x}}$.

$$K < \frac{9}{10} \frac{\int_0^\infty [S(\vec{\delta}) - \epsilon^2] \, \delta d\delta}{(1 - \epsilon)^2} \tag{60}$$

The Helmholtz principle of least action, as applied by Prager, was described as requiring that "...the stress distribution within the sample of porous material be such as to minimize the rate of energy dissipation, subject to the condition that the stresses on the exterior faces of the sample take on specified values."

The inequality of Equation (60) is of little practical value, but it does indicate the potentiality of the statistical method. For instance, if Equation (59) is combined with Equation (60) and the resulting expression is integrated, one obtains

$$K < \frac{9}{10} \frac{16 \epsilon^3 (1 - \epsilon)}{S_o^2} \tag{61}$$

Comparing this equation with the Kozeny-Carman equation ($\underline{K} = \epsilon^3 / \underline{k} S_o^2$), it is seen that

$$\frac{1}{k} < 14.4(1 - \epsilon) \tag{62}$$

which is true, but of little practical value. However, Prager (35) claimed that by using a more elaborate function such as a three-point average, the structure of the porous medium could be determined more closely. Unfortunately, there is no known function for the three-point average, and the theory of the three-, four-, and five-point averages, and so on, have not yet been formulated or tested.

The two-point average has also been derived by Cornfield and Chalkeley (36), and the method has been applied to porous materials by Chalkeley, et al. (37) and by Wyllie and Gregory (11).

Chalkeley and co-workers (37) demonstrated that if a pin is thrown randomly onto a porous medium, the specific surface area is represented by

$$S_o = 4 \epsilon C/H \tag{63}$$

where C is the number of "cuts" (number of times the pin crosses the surface between the voids and the solid) and H is the number of "hits" (number of times the ends of the pin fall within void spaces). These authors found that after 2000 throws, Equation (63) predicted the value of S_o within $\pm$ 8% of the true value.

While the statistical theories have been applied successfully to a number of consolidated and unconsolidated porous media, it appears that nowhere in the literature have attempts been made to apply these theories to fibrous structures.

DISTRIBUTION OF PORE SIZES IN POROUS MEDIA

In both the hydraulic radius and drag theories of permeability, the pore size of the porous medium is assumed to be uniform or very nearly uniform. Many real porous media have a rather broad distribution of pore sizes, and it seems advisable to review the recent studies on the determination of the pore size distribution of porous media with special reference to thin sheets of paper.

As pointed out by Scheidegger (9), many problems arise when the deceptively simple term "pore size" is used. He suggested that the pore diameter may best be defined as the diameter of the largest sphere which will fit within the pore space at the point in question. While this definition might be acceptable for some instances, it has the disadvantage that a method of making the appropriate measurements is unknown. In addition, one need only consider a pore having a long, slitlike cross section to see that the "pore size" defined by Scheidegger

is not the correct value to be used in fluid flow calculations. For example, a rectangular pore cross section of unit width and of length, say, four units would certainly offer less resistance to flow than would a circular pore cross section of unit diameter.

The pore space of a porous medium is an extremely complex maze of branched and interconnected flow channels. A given flow passage may exist at one position in the structure as a small slitlike opening and, at a neighboring point, it may open into a large cavernous space. As a result of this complex structure, it must be emphasized that the pore size or pore size distribution of a porous medium is defined only by the experimental techniques used to measure these properties. In addition, the manner in which the experimental data is analyzed will also influence the computed pore size distribution. For example, the pore size distribution calculated on a cylindrical capillary model will differ from the pore size distribution calculated from the same experimental data using a hydraulic radius model.

Very recently, Banacki and Bowers (38) have described an experimental technique for measuring the pore size distribution of filter papers which is closely analogous to the pore diameter definition of Scheidegger (9). Briefly, the method involves passing a liquid, in which a large number of small, spherical beads of different diameters are suspended, through the test specimen. The beads which are passed by the test specimen are retained on an absolute filter and are analyzed microscopically for size and number. A pore size distribution is then constructed on the count and size of the beads passed by the test specimen.

This method measures the distribution of some equivalent pore diameter and is therefore closely related to the pore size definition of Scheidegger.

However, Banacki and Bowers (38) found that the order in which the different sized beads were presented to the test specimen did not affect the results obtained. Since one would expect that the larger beads might become lodged in pores which would otherwise pass beads of a smaller size, this observation would raise serious doubts as to the validity of the test.

It appears that the only acceptable techniques which give data reflecting on the size of pores in a porous medium—or at least the sizes which control the entry of fluids—are injection of a nonwetting fluid into an evacuated porous medium or the injection of a nonwetting phase into a porous medium which is saturated with a wetting fluid. Basic capillary theory shows that the pressure difference across a curved interface between two fluid phases is given by the relationship:

$$\Delta P = \gamma(1/R_1 + 1/R_2) \tag{64}$$

where R_1 and R_2 are the principal radii of curvature of the interfacial meniscus, and γ is the interfacial surface tension. When the meniscus is confined in a circular capillary, Equation (64) takes the form (for imperfect wetting):

$$\Delta P = 2\,\gamma\cos\theta/R \tag{65}$$

where R is the capillary radius and θ is the angle of contact between the fluid and the solid material. If a porous medium is considered to be a system of interconnected cylindrical capillaries of varying sizes, a quantity of wetting liquid will distribute itself in the pores in accordance with Equation (65), and all of the liquid interfaces will have the same radius of curvature. [This condition is termed capillary equilibrium.] Conversely, if a pressure difference, ΔP, is imposed on a porous medium completely saturated with a wetting liquid, the

liquid will be displaced from all pores having radii larger than that given by Equation (65). Therefore, by varying the applied pressure difference over a sufficiently wide range, an estimate of the pore size distribution of the porous medium may be obtained. However, the cylindrical capillary models do not adequately describe most porous media, and the pore radius defined by Equation (65) is correct only for the special case of cylindrical pores.

Schultze (38a) has investigated the capillary rise in a variety of non-circular capillaries, and the data which he obtained may be correlated with reasonable accuracy using the concept of a hydraulic radius. Thus,

$$m = \gamma/\rho gh \tag{66}$$

where m is the hydraulic radius, ρ is the liquid density, g is the acceleration due to gravity, and h is the height of capillary rise.

Carman (10) has shown that for unconsolidated porous media, such as beds of sand, the hydraulic radius is closely related to the capillary pressure by

$$m = \gamma/\Delta P = \epsilon/S_o \tag{67}$$

Equations (66) and (67) are, of course, equivalent, and the latter equation has recently been applied to consolidated porous media (20). Strictly speaking, the above equation applies only to porous media of uniform pore size. Wyllie and Rose (20) have tested Equation (67) for several synthetic samples which were specially prepared by fusing together uniformly sized particles of alundum and pyrex glass, thereby producing samples of relatively uniform pore size. The permeability and "tortuosity" (by electrical means) were then measured on these samples. The surface areas were calculated from Equation (67) and from the Kozeny-Carman equation, assuming a shape factor, k_o, of 2.5. These results, together

with the results obtained on two natural sandstone samples, are presented in Table VI. It can be seen that the agreement between Equation (67) and the Kozeny-Carman equation is reasonably good in most cases.

TABLE VI

PERMEABILITY DATA OF WYLLIE AND ROSE (20)

Sample	K, 10^{-11} sq. cm.	Porosity, ϵ	$(L_e/L)^2$, electrical	S_v [Eq. (67)], sq. cm./cc.	S_v (flow), sq. cm./cc.
Alundum	680	0.258	12.52	418	384
Alundum	660	0.254	8.25	572	466
Alundum	63	0.236	7.35	1670	1390
Pyrex	8.1	0.374	2.72	13,700	15,600
Pyrex	3900	0.286	3.15	413	349
Nichols Bluff S.S.	230	0.200	6.25	690	590
Berea S.S.	890	0.224	6.94	406	348

Only a few methods for determining pore size distribution have been applied to fibrous structures. Ritter and Drake (39) have described a method which involves the stepwise penetration of mercury into the voids of a porous medium. These workers demonstrated the applicability of this "mercury intrusion" method to a number of incompressible porous materials. The mercury intrusion method has been applied to woven felts by Grace (40) and to wood pulp fibers by McKnight and co-workers (41).

The following objections to the mercury intrusion method seem to reject its application to a study of the flow of fluids into and through a sheet of paper:

1. Because of the high surface tension of mercury, very high pressures are necessary to obtain a closed distribution curve. McKnight and co-workers found

it necessary to reach pressures of over 1000 p.s.i. in order to obtain a complete distribution of pore sizes. At such pressures, one is probably destroying the very property which is to be measured.

2. At high pressures, the mercury penetrates into the fibers and it is not possible to distinguish between intrafiber pores and interfiber pores. McKnight, et al. (41) found that after removing the mercury from the samples as completely as possible, examination of the fibers under a microscope clearly revealed droplets of mercury in the fiber lumen.

McKnight and co-workers (41) also calculated the pore size distribution of one sample of wood pulp fibers using the benzene desorption isotherm method described by Pierce (42). This method involves the assumptions that (1) the sorbed vapor is held as a liquid in the pores, (2) the pores can be treated as cylinders, and (3) the Kelvin equation for the depression of the vapor pressure of a capillary-held liquid is applicable for computing the pore radii from the vapor pressure at which desorption occurs. The results obtained by McKnight and co-workers using the benzene desorption method did not agree well with that obtained by mercury intrusion techniques, and the former method does not appear to be applicable to paper.

Another method of estimating pore size distribution which has been widely used (27, 43-45) is the measurement of capillary pressure as a function of the saturation of a porous medium. The saturation is defined as the volume of liquid retained in the porous medium per unit volume of void space and therefore this method also measures the volume distribution of pore sizes. The capillary suction method, as this technique is called, has been applied to thick beds of glass fibers by Parker (44) with good results. Recently, White and Marceau (45) have used the capillary suction methods in studying the porous structure of wetted

sheets of blotter stock. The method might also be applied to dry sheets of paper if a nonswelling liquid were used as a saturant. However, experimental difficulties would render such determinations relatively inaccurate. With this method, the saturation of the sample is determined by measuring the volume of saturant removed at each increment of capillary suction. Since the total volume of liquid held by a normal sheet of paper is quite small, the accurate measurement of these incremental volumes would be extremely difficult.

Corte (46) has described a "dioxane method" which appears to be better adapted to pore size distribution studies in thin sheets of paper. A more general term for this method, which is also based on a capillary concept, is the gas-drive method. The gas-drive technique involves the stepwise penetration of a gas through a sample of porous medium above which is a column of liquid. Any number of liquids may be used with this method, the only requirements being that the liquid does not interact with the porous medium and that it has a relatively lower surface tension.

The determination of pore size distribution using the gas-drive method is basically quite simple. The pressure beneath the sample is increased slowly until bubbles appear in the liquid. The size of the pores which correspond to this pressure may be estimated from the basic equation of capillarity [Equation (64)] or some modification of this equation. The pressure beneath the sample is then increased slightly. According to Darcy's law, the gas flow rate should be proportional to the pressure drop if no new flow channels are opened to flow. However, new flow channels of smaller size are opened to flow as predicted by Equation (64), and the additional increase in flow rate is proportional to the number of new flow channels opened to flow. Thus, by measuring the pressure drops

and flow rates over a sufficiently wide range of pressures, the number distribution of pore sizes can be calculated.

That the gas-drive method does, in fact, give the number distribution of pore sizes can best be seen by considering a parallel arrangement of cylindrical capillaries of varying radii. Assume that there are n_i capillaries of radius R_i in this bundle. The total volume of capillaries of radius R_i is then proportional to $n_i R_i^2$. However, from Poiseuille's equation, the flow rate through this group of capillaries is proportional to $n_i R_i^4$. Since, in the gas-drive method, the frequency of occurrence of each pore size is computed from the contribution of pores of that size to the over-all flow, the resulting frequency distribution must be proportional to $n_i R_i^4$. On the other hand, in the capillary suction methods, the frequency of occurrence of each pore size is computed from the volume of pores of that size. Hence, in such a distribution, the frequency is proportional to $n_i R_i^2$, and the pore size distribution function determined by these two methods is distinctly different. In order to distinguish between the pore size distribution determined by capillary suction and that measured in the gas-drive test, the former distribution is referred to as a volume distribution and the latter as a number distribution (46). In the simple case of a model of parallel cylindrical capillaries, it is easily seen that these two distributions differ and presumably they would also differ in real porous media.

The gas-drive method was applied to paper formed from lightly refined, classified pulp by Sanborn (25) and to glassine and greaseproof papers by Corte (46). Hence, it appears that the method can be applied to paper over a wide range of pore sizes.

It has been shown experimentally by Corte (46) that the distribution of pore sizes in a sheet of paper can be described by a logarithmic Gaussian

distribution, that is, a normal distribution for the logarithm of the pore size. He also offered several arguments to support this distribution function for describing the pore size distribution of paper. The advantages of fitting the pore size distribution data to a known statistical distribution function are many. In addition to smoothing the experimental data, this allows one to specify the distribution by means of the usual statistical parameters.

Such methods as low-temperature gas adsorption, optical examination, and calculation of the pore size distribution from particle sizes have been applied to a number of porous media. However, these methods either cannot be applied to paper or do not yield information which can be interpreted in terms of the penetration of fluids into and through a sheet of paper.

PORE INTERCONNECTION IN POROUS MEDIA

In order to describe the structure of a porous medium adequately, not only the pore size but also the manner in which the pore spaces are interconnected must be considered. An interesting and unique approach to this problem has been presented recently by Fatt (47). He considered a network model composed of cylindrical tubes of various sizes which were interconnected according to some regular geometric pattern. In order to eliminate a large amount of labor, Fatt found it necessary to reduce the three-dimensional network models to two dimensions. He stated:

> "This is equivalent to assuming that the change produced by making the porous medium thin, and thereby eliminating a number of cross-connections in the third dimension, may be compensated by introducing additional channels within the two-dimensional network."

While the assumptions made by Fatt are certainly open to question, the results which he obtained have provided some extremely useful insights into the nature of flow through porous media.

The first step in applying the network model to a porous medium is to select a regular geometric network with which the porous medium is to be represented. The four networks studied by Fatt are shown in Fig. 5. The only parameter used to describe the network is the number of tubes connected to each tube in the network. This parameter is referred to as the β-factor, and the values for the four networks shown in Fig. 5 along with the values of the β-factor for a parallel and series capillary model are given in Table VII.

TABLE VII

VALUES OF β-FACTOR FOR VARIOUS NETWORKS

[After Fatt (47)]

Network	β-Factor
Series capillary model	2
Single hexagonal network	4
Square network	6
Double hexagonal network	7
Triple hexagonal network	10
Parallel capillary model	∞

Fatt (47) investigated several arbitrary tube size distributions and studied the effect of network type and tube size distribution on the capillary suction curve of the model. He found that all of the networks studied gave capillary suction curves similar to those found experimentally on sandstone and other porous media. In addition, he noted that as the β-factor increased (i.e., more tubes connected to a given tube), the capillary suction curve approached that of the parallel capillary model which has an infinite β-factor. Fatt also found that the shape of the capillary suction curve was not particularly sensitive to the network model selected but was determined almost entirely by the assumed tube

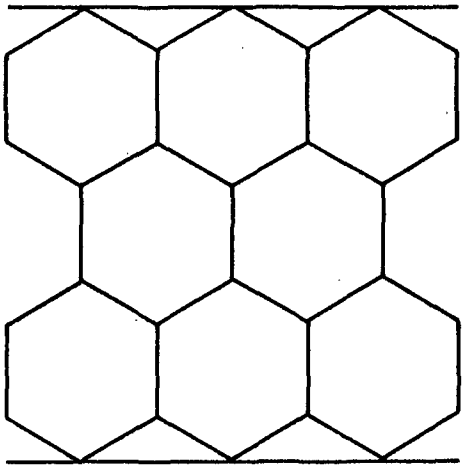

SINGLE HEXAGONAL NETWORK

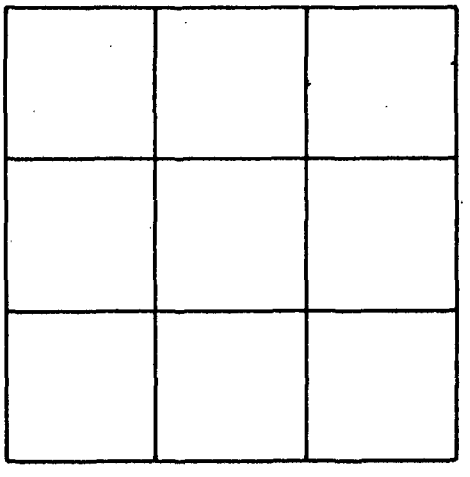

SQUARE NETWORK

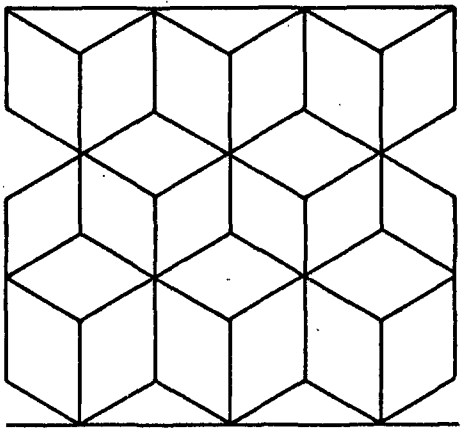

DOUBLE HEXAGONAL NETWORK

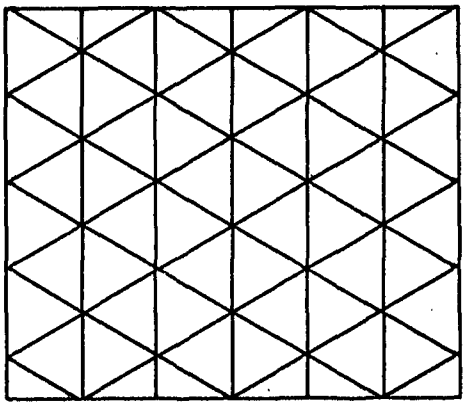

TRIPLE HEXAGONAL NETWORK

Figure 5. Network Models Studied by Fatt (47)

radius distribution. From this he concluded that the capillary suction curve of a porous medium can be used to estimate the pore size distribution of the medium.

Fatt also studied the dynamic (flow) properties of the network models and compared the results predicted from the models with the available permeability data on porous materials. With regard to calculating the resistance to flow of a network model, Fatt pointed out:

> "In practice, the calculation of the total network resistance of a network of several hundred tubes is impossibly laborious. Network theory leads to a determinant as the solution of the total network resistance. The network models used in this study lead to determinants of several hundred rows and columns; that is, determinants of order 100 or more. Such determinants cannot be evaluated by any reasonable amount of labor. Even modern, high-speed computers cannot evaluate determinants of greater than 30th order unless the determinant has some symmetry which permits reduction to a lower order. The determinants derived from network models have no symmetry and, therefore, cannot be reduced."

These conclusions led Fatt to the use of analog techniques to determine the dynamic properties of his network models.

From these studies, Fatt (47) concluded that the dynamic properties of porous media, such as permeability, are strongly influenced by the network form assumed while the pore size distribution has relatively little effect. In other words, the branching and interconnecting of the tubes in the network models determined, to a large extent, the permeability characteristics of the model.

Rose (48) has recently extended the pioneering work of Fatt to network models in three dimensions. In doing so, he introduced several new concepts. Rose suggested that the best three-dimensional model available was the tetrahedron model shown in Fig. 6. This model has a β-factor [as defined by Fatt (47)] of 22. With the three-dimensional tetrahedron model, then, it is possible

to consider as many as 22 tubes connected to a given tube and, as Rose pointed out, "...in all probability, no porous media will ever be found in nature where such a high degree of pore branching will be required in the corresponding network model."

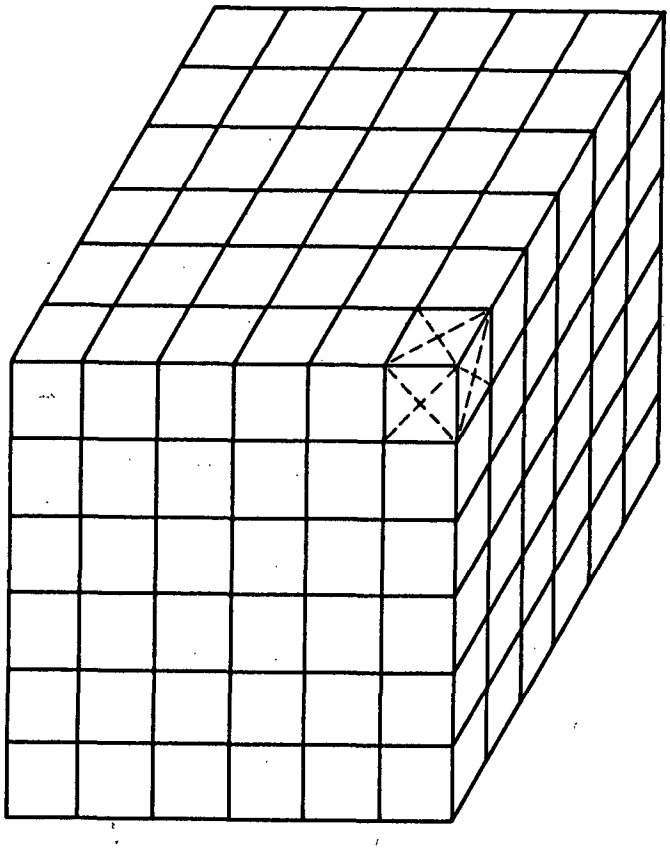

Figure 6. Three-dimensional Tetrahedron Model of Rose (48)

Rose also introduced the concept of a "path characterizing number" which defines the possible number of single, double, triple, and quadruple pore path interconnections between adjacent mesh points in the network. For the three-dimensional tetrahedron model, the path characterizing numbers are: 1:4:8. That is, there is one direct path, four double-length paths, etc., between adjacent mesh points in the tetrahedron model.

Rose further pointed out the possibility of assigning zero pore sizes to some of the tubes in the tetrahedron model. This, in effect, reduced the β-factor (and path characterizing number) and results in a different network model. In this way it was shown that one could reduce the three-dimensional tetrahedron model to any of Fatt's two-dimensional models.

The general procedures outlined by Rose (48) would serve as a useful guide for applying these three-dimensional models to the analysis of flow through porous media. However, as he pointed out, the problem of calculating the results of such an application is quite staggering. For example, for a three-dimensional model of 1728 tubes (12^3), a solution of a 1729-order determinant is required. This is obviously not possible. The large computer which Rose had available for his work (the ILLIAC) is capable of solving up to 143 simultaneous equations, whereas most present-day computers are limited to about 40 simultaneous equations. While Rose was able to obtain some preliminary information through the use of special programming techniques, the general application of such models is not yet possible. In spite of this, the work of Rose (48) and Fatt (47) certainly represents one of the more promising approaches yet considered in the field of flow through porous media.

Even though the network models described above achieve a degree of point-to-point identity with real porous media which has heretofore not been attained, they omit consideration of such properties as pore shape. Thus, even with such elaborate models, some empirical factors may still have to be introduced to produce complete agreement between the predictions of the models and the experimental data.

DEVELOPMENT OF A MODIFIED HYDRAULIC RADIUS THEORY FOR SINGLE-PHASE FLOW THROUGH POROUS MEDIA

The several approaches to the description of flow through porous media which have been described in the literature have been used with varying degrees of success. It is necessary at this point to examine each of these approaches in light of the probable structure of a sheet of paper.

The statistical theories described earlier are applicable only to completely random, isotropic porous media. Since the fibers in a sheet of paper are preferentially oriented in the plane of the sheet (the x-y plane), a normal sheet of paper is quite anisotropic with respect to flow. Furthermore, the porosity and specific surface areas determined from these statistical theories include sealed-off pores which could conceivably occur in a sheet of paper. Such pores, if they occur, would not be active in the transportation of fluids through the sheet. Therefore, the extension of the statistical theories of permeability to fibrous structures may involve some rather important modifications.

While the drag theories of permeability have been applied successfully to fibrous systems, the work in this area has so far been limited to flow past regular arrays of cylinders. In a sheet of dry, bonded fibers, the individual fibers are more in the form of flat ribbons than cylinders. It is possible that the drag force on such a fiber would be quite different from that of a cylinder. In addition, the drag theories are based on a uniform pore size whereas a normal sheet of paper undoubtedly has a broad distribution of pore sizes.

The network models of Fatt (47) and Rose (48) present some interesting possibilities, but, as pointed out earlier, the calculations involved in the application of these models are quite insurmountable.

It appears that the only practical methods of describing the flow through porous media presently available are the hydraulic radius theories. However, the Kozeny-Carman approach, which is the most widely used hydraulic radius theory, does not apply to a thin sheet of paper, as shown by Brown (16) and Sanborn (25). The Kozeny-Carman model is essentially an analog model and can only have a pretense of rigor when applied to a porous medium which possesses a uniform pore size. From a practical standpoint, because of the adjustable parameter k, some variation in pore sizes can be tolerated without introduction of appreciable errors provided it is possible to assign a meaningful value to the mean hydraulic radius and to the Kozeny factor. If the pores are not reasonably uniform in size, the Kozeny-Carman model must break down seriously. According to Poiseuille's equation, the quantity of fluid flowing through a cylindrical capillary is proportional to the fourth power of the capillary radius. As a result, the quantity of fluid flowing through a porous medium of nonuniform pore size must be dominated by the larger pores. On the other hand, the exposed surface area is greatly affected by the large surface-to-volume ratio of the smaller pores. The Kozeny-Carman model disregards the presence of individual pores by lumping all pores together into a single hydraulic radius term, ϵ/S_o. This can be done with any degree of accuracy only if the range of pore sizes is small.

The major contribution of the hydraulic radius theories, including the Kozeny-Carman approach, seems to be in recognizing the factors of first-order importance which influence the permeability of porous media. It has been quite adequately established that porosity and surface area are the primary factors which influence the permeability coefficient. There are, of course, a myriad of other factors which influence the flow of fluids through porous media. Among these factors are: pore branching and interconnection, pore shape, particle shape,

pore size distribution, tortuosity, etc. In the Kozeny-Carman equation, all of these factors are lumped together in the parameter referred to as the Kozeny factor. In many cases, these factors are relatively unimportant as shown by the fact that the experimental values of the Kozeny factor do not vary widely for many different porous media.

Much of the confusion found in the literature on the application of the Kozeny-Carman equation is due to attempts to attach a physical significance to the parameter k. The contention of some authors that the Kozeny factor involves only the product of a pore shape factor and a tortuosity term is an obvious over-simplification of the problem.

In consolidated porous media where the pore sizes vary widely, the original Kozeny-Carman equation is no longer valid. It was for this reason that Wyllie and co-workers (21, 43) introduced a "generalized Kozeny-Carman equation" in which the variations in pore size were taken into account. The choice of nomenclature of these authors is unfortunate since the concept of pore size distribution is basically incompatible with the Kozeny-Carman theory. While the model upon which Wyllie and co-workers based their "generalized" equation is somewhat similar to that used in the original Kozeny-Carman equation, the two models are nonetheless distinct and the parameters calculated from one model are not necessarily applicable to the other.

In developing a model for flow through porous media in which pore size distribution is taken into account, it is necessary to use an experimental technique and method of data reduction which are consistent with the selected model. Although there are several methods for measuring the pore size distribution of a porous medium, the gas-drive method was selected for use in this study. The

basic principle involved in the gas-drive technique is that an increase in the pressure drop across a porous medium which is partially saturated with liquid causes more pores to be drained of liquid. By measuring the flow rates and pressure drops, the pore size distribution may be estimated in the following manner.

Consider a porous medium initially in equilibrium with a wetting liquid which does not interact with the medium. The pressure in the gas below the specimen is then increased slowly until flow occurs. From Darcy's law, it is possible to define an apparent permeability coefficient, $\underline{K}_a$, from

$$K_a = Q\eta L/(A\Delta P) \tag{68}$$

where $\underline{A}$ is the area and $\underline{L}$ is the thickness of the test specimen, η is the viscosity of the permeating gas, and $\underline{Q}$ and $\underline{\Delta P}$ are, respectively, the observed flow rate and pressure drop.

If the pressure drop across the specimen is increased slightly, the flow rate will increase because of two effects. First, a portion of the increase in flow rate will be due to the increased pressure drop across flow channels already participating in flow and, secondly, new and smaller channels are opened to flow and this also contributes to the over-all increase in flow rate. The additional increase in flow rate due to the opening of new flow channels will produce a corresponding increase in $\underline{K}_a$ as defined by Equation (68). If the pressure drop is increased incrementally to sufficiently high values, the apparent permeability coefficient calculated from Equation (68) will become constant, indicating that no additional (detectable) channels are being opened to flow. When this point is reached, it is possible to calculate a relative permeability for each pressure drop from

$$K_r = K_a/(K_a)_{max.} \tag{69}$$

where $(\underline{K_a})_{max.}$ is the limiting value of $\underline{K_a}$ from Equation (68). The conversion of the values of $\underline{K_a}$ to a relative basis in Equation (69) is analogous to the conversion of the incremental volumes of pore saturant to relative saturation values in the capillary suction method and the values of $\underline{K_r}$ from Equation (69) represent the cumulative distribution of pore sizes. The frequency of occurrence of each pore size, $\Delta\underline{K_r}$, may be calculated by subtracting the preceding value of $\underline{K_r}$ from the value at the data point under consideration [see Appendix I].

The problem of defining the illusive term "pore size" has been discussed earlier. From a review of the literature, it was concluded that an acceptable measure of the pore size may be obtained from

$$m = \gamma/\Delta P \tag{67}$$

where $\underline{m}$ is the hydraulic radius of the pores, γ is the surface tension of the wetting liquid, and $\Delta\underline{P}$ is the pressure drop required to drain the liquid from pores of the given hydraulic radius. Equation (67) is not rigorous but has been shown by Carman (10) to be a good approximation for several regular cross-sectional shapes. Comparing Equation (67) with the basic equation of capillarity, Equation (64), it is seen that for the case of perfect wetting (i.e., $\cos\theta = 1.0$).

$$m = \gamma/\Delta P = \frac{1}{(1/R_1 + 1/R_2)} \tag{70}$$

Thus, the value of $\underline{m}$ in Equation (67) is simply one half of the harmonic mean radius of curvature of the liquid-gas interface in the pore space and Equation (67) is therefore rigorously correct only for the case of a cylindrical pore and perfect wetting.

In spite of these limitations, it was felt that Equations (67) and (69) would produce an acceptable measure of the pore size distribution of a porous medium. It must again be emphasized, however, that the pore size distribution is defined only by the experimental technique used to measure the property and by the model used to analyze the experimental data.

It is now possible to proceed with the development of a model to be used to describe the flow of fluids through a porous medium. The following development is similar to that of Wyllie and Gardner (43) except that the gas-drive method is incorporated for measuring the pore size distribution whereas Wyllie and Gardner used the capillary suction technique. For lack of a better term, this development will be referred to as a "modified hydraulic radius theory" in order to distinguish this theory from that of Kozeny and Carman.

Instead of assuming that the porous medium has a uniform pore size and a uniform hydraulic radius, ϵ/S_o, it is viewed as being composed of a number of smaller, idealized media in a parallel arrangement. Each ideal medium is considered to have a porosity, ϵ, equal to the porosity of the original medium and a hydraulic radius given by

$$m_i = \epsilon/S_{oi} = \gamma/\Delta P_i \qquad (67)$$

Thus, the model used in the modified hydraulic radius theory may be visualized as a "mosaic" arrangement of small, idealized media each of which is composed of a number of noncylindrical capillaries embedded in a solid matrix. The effective area of each idealized medium is represented by $A\Delta K_r$ where A is the total area of the test specimen and ΔK_r is the contribution of the flow channels of size m_i to the relative permeability of the porous medium.

The basic hydraulic radius theory assumes that the permeability coefficient of the porous medium is proportional to the porosity of the medium and to the square of a characteristic length. The characteristic length is taken as the ratio of the cross-sectional area of the flow channels to their wetted perimeter; that is, the hydraulic radius. The basic hydraulic radius theory may be stated mathematically as

$$K = \epsilon m^2/\psi \tag{70}$$

where K is the permeability coefficient, ϵ is the porosity of the medium, and ψ is a proportionality factor which may be termed a "flow parameter." The flow parameter incorporates the effects of pore shape, tortuosity, pore branching, etc., and may be expected to vary from one porous medium to another. Combining Equations (67) and (70), the permeability of each idealized medium in the model is represented by

$$K_i = \epsilon \gamma^2/[\psi(\Delta P)^2] \tag{71}$$

The incremental rate of flow through each idealized medium is given by

$$\Delta Q/A\Delta K_r) = K_i \Delta P/(\eta L) \tag{72}$$

and the total rate of flow through the entire model is

$$u = Q/A = \frac{\Sigma \Delta Q}{A} = [\Delta P/(\eta L)] \cdot \Sigma K_i \Delta K_r \tag{73}$$

Substituting Equation (71) for K_i into Equation (73), it is seen that the permeability coefficient of the real porous medium is represented by

$$K = [\epsilon \gamma^2/\psi] \cdot \Sigma \Delta K_r/(\Delta P_i)^2 = [\epsilon \gamma^2/\psi] \int_0^1 dK_r/(\Delta P)^2 \tag{74}$$

where the integral corresponds to a continuous variation of pore size. By a simple rearrangement of Equation (74), it is apparent that the flow parameter, ψ, may be calculated from

$$\psi = [\epsilon\ \gamma^2/K] \int_0^1 dK_r/(\Delta P)^2 \qquad (74)$$

since all of the quantities on the right side of this equation are easily determined experimentally from the gas-drive and permeability tests.

The model used in developing the modified hydraulic radius theory differs physically from real porous media in several important respects.

1. In real porous media the flow channels of various sizes are distributed more or less randomly throughout the medium. In contrast, in the model described above, the flow channels of a given size are considered to be gathered together in a single idealized medium which occupies a fraction ΔK_r of the total area perpendicular to the direction of macroscopic flow.

2. In the real porous medium, the pore space is made up of branched and interconnected flow channels of various sizes whereas in the above model, it is tacitly assumed that flow through the uniform flow channels of each idealized medium is possible without any contribution being made by flow channels which are either larger or smaller than those being considered. Therefore, the components of flow from each idealized medium are presumed to be independent of, and suffer no interference from, all other components.

3. It is also implicit in Equation (74) that the flow parameter is identical for each hypothetical ideal medium of uniform pore size; that is, ψ was not included in the summation of Equation (74).

These physical requirements are clearly not realized in real porous media. The assumption that each pore size contributes to the flow independently of all

other pore sizes is obviously untrue in real porous media which have interconnecting and branching pores of various sizes. A similar assumption was made by Wyllie and Spangler (21) in their development of equations relating permeability to measured capillary and electrical parameters. These authors suggested that this assumption may be rationalized by considering that the flow through pores of a given size occurs by way of interconnecting pores of different sizes. The flow resistance of the connecting pores may be ignored since this resistance is incorporated in an appropriate, experimentally determined hydraulic radius. In spite of these arguments, the assumption of noninterference between flow components remains one of the more obvious defects of this theory.

As mentioned earlier, it is also assumed in this development that the flow parameter is not dependent on pore size. Since all of the idealized media are considered to have the same porosity, this is equivalent to assuming that ψ is a function of porosity only for a given porous medium. While this assumption is not easily justified, a similar argument was followed by Wyllie and Gardner (43) and by Burdine, Gournay, and Reichertz (30).

At this point it may be helpful to analyze the essential differences between the modified hydraulic radius theory described above and the "generalized Kozeny-Carman equation" of Wyllie and Gardner (43). The permeability equation given by these authors is

$$K = \epsilon \gamma^2/k \cdot \Sigma \Delta s/(\Delta P)^2 \qquad (75)$$

where k is the Kozeny factor and Δs is an incremental change in saturation. In arriving at Equation (75) Wyllie and Gardner considered the porosity of each idealized medium to be less than the over-all porosity of the real medium by a fraction Δs; that is, the contribution of each ideal medium to the over-all

porosity was considered to be $\Delta\epsilon = \epsilon\Delta\underline{s}$ where $\Delta\underline{s}$ is the incremental change in saturation which occurs when pores of size $\underline{m}_i$ are drained of liquid. Wyllie and Gardner then summed the contributions of each ideal medium to the porosity of the original medium. Thus, these authors carried out the summation over the volume-dependent property of porosity (or saturation) and the capillary suction method was used to determine the values of $\underline{m}_i$ and $\Delta\underline{s}$.

In contrast, in the model used in the development of the modified hydraulic radius theory, the idealized media are all assumed to have the same porosity as the original medium. However, in this model, the effective area of each hypothetical medium is considered to be restricted to a fraction $\Delta\underline{K}_r$ of the bulk area of the real porous medium (taken in a direction perpendicular to the direction of macroscopic flow). The summation is then carried out over the area-dependent property of relative permeability. Thus, the essential difference between the model used by Wyllie and Gardner and that employed in the modified hydraulic radius theory lies in the method used to determine the pore size distribution of the porous medium. The physical models upon which each of these theories is constructed differ only in relatively minor detail. It is felt that the major advantage of the modified hydraulic radius theory lies in the fact that a dynamic (flow) technique is used to determine the pore size distribution. Since the gas-drive method is basically a permeability technique, the pore size distribution determined by this test should be closely related to the hydraulic radii which are effective in offering resistance to fluid flow.

Comparing Equation (70) with Equation (74), it is seen that in the modified hydraulic radius theory, the value of $\underline{m}$ is replaced by

$$m = \sqrt{\gamma^2 \int_0^1 dK_r/(\Delta P)^2} \tag{76}$$

But $\underline{m}$ may also be expressed as the ratio $\epsilon/\underline{S}_o$ so that

$$\epsilon/S_o = \sqrt{\gamma^2 \int_0^1 dK_r/(\Delta P)^2} \tag{77}$$

Expressing the specific surface area on a mass basis and solving for $\underline{S}_w$,

$$S_w = \left\{v\,\epsilon/[\gamma(1 - \epsilon)]\right\} \sqrt{\frac{1}{\int_0^1 dK_r/(\Delta P)^2}} \tag{78}$$

Since Equation (78) involves only experimentally determined quantities, $\underline{S}_w$ may be calculated directly from this relationship.

It should be pointed out that Equation (78) involves the implicit assumption that the hydraulic radii determined in the gas-drive test are identical with those which are effective in offering resistance to the flow of fluids through the porous medium.

PRESENTATION OF THE PROBLEM

A common method of studying the structure of porous media is to describe the flow of fluids through such materials. A review of the literature reveals that studies on the flow of fluids through porous media have been limited to three approaches. These are: (1) the phenomenological approach, such as the hydraulic radius theories; (2) the analytical approach, represented by the drag theories; and (3) the statistical approach. The last two approaches have not yet been developed to the point of practical usefulness in the present study. On the other hand, the hydraulic radius theories, such as that of Kozeny and Carman, have been applied to flow through fibrous porous media with moderate degrees of success. However, the Kozeny-Carman theory is not applicable to porous media which have a broad distribution of pore sizes.

It is expected that a thin sheet of paper has a relatively broad pore size distribution. Consequently, the Kozeny-Carman equation would not be expected to apply to such a structure. A modified hydraulic radius theory has been developed in an effort to extend the applicability of this approach. In this theory, the permeability coefficient is expressed in terms of the pore size distribution and certain empirical parameters which are presumed to be characteristic of the porous medium. Since this approach is somewhat similar to that of Kozeny and Carman, it is subject to some of the same limitations which apply to the Kozeny-Carman theory. Some of these limitations are (10): No pores are sealed off; the void spaces are distributed at random in the structure; viscous flow is maintained; and molecular effects such as interactions between the permeating fluid and the medium and "slip flow" are either absent or insignificant. All of these conditions were observed, insofar as possible, in the experimental program.

Specifically, the experimental objectives of this study are: (1) to measure the permeability and pore size distribution properties of carefully prepared handsheets of paper, (2) to relate the permeability of these sheets to the surface area exposed to flow and the porosity of the sheet, and (3) to determine what relationship, if any, exists between the pore size distribution and permeability properties of paper. From the pore size distribution and permeability data the empirical factors in the modified hydraulic radius theory can be evaluated. The differences in the porous structure of the various test specimens should be manifested in different values of this parameter. In this way, it is hoped that some of the basic factors which influence the permeability characteristics of thin sheets of paper can be elucidated.

EXPERIMENTAL EQUIPMENT AND TECHNIQUES

Before describing the details of the experimental techniques used in this investigation, a general outline of the experimental program will be presented. It is convenient, for the purposes of this discussion, to divide the experimental program into three areas of study. These are: (1) the air permeability tests on thick mats of wood pulp fibers, (2) the air permeability tests on thin handsheets of these fibers, and (3) the pore size distribution tests on these thin handsheets.

As was mentioned earlier, in the case of wood pulp, the specific volume of the fibers is not simply the reciprocal of the pycnometric density. For such fibers, the hydrodynamic specific volume, in which the volume of stagnant fluid within the fiber structure is taken into account, must be used. The experimental techniques and method of data reduction described by Fowler and Hertel (12) provide a convenient method of determining the hydrodynamic specific volume of pulp fibers. At the same time, by noting the range of porosity over which the rectified plot of the data is linear, an idea of the applicability of the hydraulic radius theories, such as the Kozeny-Carman equation, can be obtained.

The specific objectives of the air permeability studies on thick mats of pulp fibers were therefore twofold: (1) to determine the hydrodynamic specific volume of the fibers used in this study as a function of the mat apparent density, and (2) to establish the range of porosity over which the hydraulic radius theories might be expected to apply to such structures.

Air permeability tests were conducted on thin handsheets prepared from the same pulp used in the mat permeability studies. The results of these tests were used to estimate the hydrodynamic specific surface area and porosity of the sheets. The basis weight of the sheets and the wet pressure applied to the sheets were

varied in these studies. The data from these tests were analyzed using the usual form of the Kozeny-Carman equation and the modified hydraulic radius theory developed earlier in this thesis.

In order to apply the latter method of data reduction, the pore size distribution of these test specimens was also determined using the gas-drive technique. Since both the pore size distribution and the permeability were measured on each of the thin handsheets, it was possible to assess the effect of pore size distribution on the permeability characteristics of paper.

PREPARATION OF TEST SPECIMENS

In order to avoid the problems related to fines distribution in the sheet, it was decided that sheets with a relatively simple porous structure should be used. Therefore, a long-fibered, bleached sulfite pulp was obtained in dry lap form for use in this study. This pulp was subjected to the following treatment before it was used to prepare the test specimens:

1. Eighty 30-gram batches of the unrefined pulp were classified using a modification of Institute method 415 (49) in which the slurry was classified for 30 minutes on a Bauer-McNett classifier and only the portion held on a 20-mesh screen was retained. Ordinary tap water was used for this classification except for the last five minutes when deionized water was used.

2. Each of the 80 batches of fines-free pulp was dewatered on a large Buchner funnel, and then all 80 batches were blended at a consistency of about 3% using a Williams pulp breaker.

3. The resulting pulp was dewatered with a laboratory washbox and stored at a consistency of about 20% in polyethylene bags in a cold room at 40°F. Approximately 2% formaldehyde (ovendry basis) was added to each bag as a preservative.

It was considered essential to this study that the formation of the test specimens, both the thick mats and the handsheets, be uniform and reproducible. In order to achieve these ends, the constant-rate filtration apparatus shown in Fig. 7 was used. This equipment is a modification of that used by Jones (50) and proved to be very satisfactory.

The slurry was contained in a 50-gallon stainless steel tank from which it passed through a 1-inch diameter Tygon tube into the forming tube. The forming tube was made up of two sections of Lucite tubing. The upper portion was 4 inches in diameter and 36 inches long. A flow stabilizer positioned near the top of this tube served to break up the excessive turbulence from the inlet. The upper section was fastened to the 5-inch diameter lower section by four brass bolts and was sealed with a rubber O-ring. The lower section of the forming tube is positioned on the septum and was held in place by four threaded brass rods. An O-ring seal was also provided between the lower section of the forming tube and the septum assembly.

The septum was made from a drilled brass plate over which a 150-mesh brass screen was securely clamped. The septum was held to the base cylinder by four brass screws and was sealed by a rubber O-ring.

The outlet pipe from the base of the apparatus served as a filling line for introducing water into the storage tank and as an outlet during the formation of a specimen. In filling the storage tank, deionized, deaerated water* was fed to the inlet side of a rubber-impeller, "positive-displacement" pump. A recycle

*During the summer months, the deionized water supply was found to be contaminated with algae and other particulate matter. Since this material could not be removed with the usual filtering techniques, distilled, deaerated water was used in some cases.

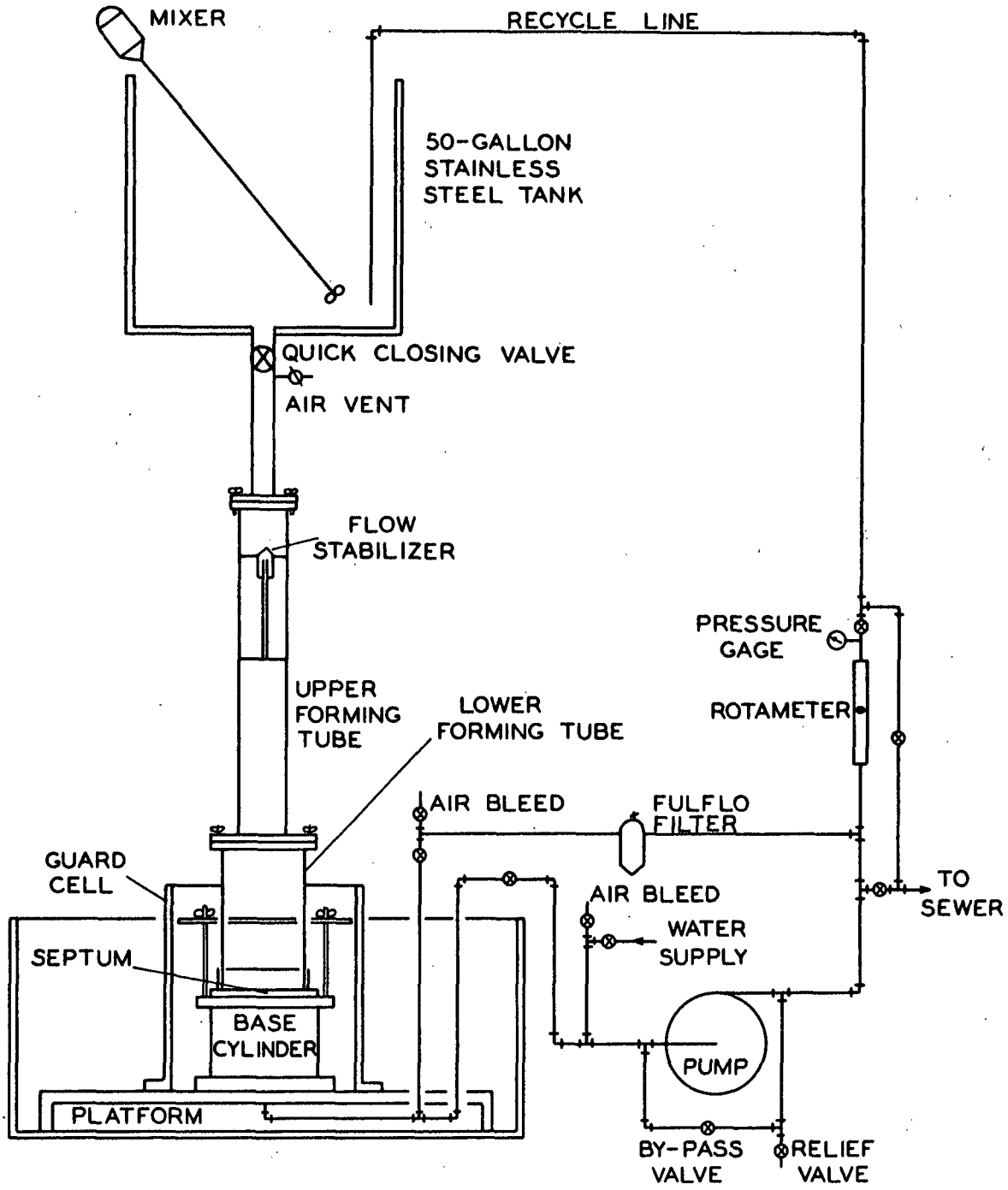

Figure 7. Constant-Rate Filtration Apparatus

line containing a by-pass valve and a relief valve was placed around the pump to prevent excessively high pressures in the system. The outlet of the pump was connected through a Fulflo filter to the base of the apparatus. The filter element was wrapped with Whatman no. 1 filter paper in order to improve the filtering efficiency.

By filling the forming tube and storage tank from below the septum, trapped air in the system was effectively eliminated. Several air-bleed valves on the apparatus served to eliminate trapped air from the flow lines.

In forming a specimen, the water was recycled back to the storage tank or was pumped to the sewer through a rotameter. The flow rate was controlled by a globe valve on the downstream side of the rotameter. A second globe valve on the upstream side of the rotameter was adjusted to provide a constant back pressure of 7 p.s.i. on the rotameter.

A small mixer in the storage tank was used to keep the slurry in suspension. All pipe and fittings on the apparatus were either brass or stainless steel.

In forming the thick mats, the required amount of pulp was weighed out on a triple-beam balance in 2.5-gram (ovendry) portions. This pulp was then added to 2 liters of deionized water and was disintegrated for 150 counts in a British disintegrator. The resulting slurry was deaerated under vacuum in 4-liter suction flasks.

The constant-rate filtration apparatus was filled with deionized, deaerated water, and 5 grams of pulp were added to the storage tank to provide an initial consistency of approximately 0.0025%. The pump was then started with the water recycled back to the storage tank, and the flow rate was adjusted to 4 gallons

per minute. The superficial linear velocity approaching the septum was approximately 2 cm./sec. at this flow rate. An additional 2.5 grams of pulp were added to the storage tank every ten minutes until the desired total mass of fiber had been added. From preliminary experiments, it was determined that 2.75 grams of fiber were deposited in ten minutes from a slurry with an initial consistency of 0.0025%. Thus, while the consistency varied during a run, it was easily controlled and never exceeded the initial consistency of 0.0025%.

Ten minutes after adding the last portion of pulp, the by-pass valve was opened allowing the water to be pumped through the rotameter to the sewer. In this way, the flow rate was maintained constant throughout the entire formation. When the water level had passed below the septum, the pump was shut off. The mat was then covered with a sheet of Whatman no. 1 filter paper and the septum was removed from the forming apparatus.

The thin handsheets were also formed with the constant-rate filtration apparatus, but a somewhat different procedure was used. After the storage tank had been filled to the proper level, the quick-closing valve beneath the storage tank was closed, the air vent was opened, and the water was drained from the forming tube. Approximately 5 grams of an unrefined, unclassified pulp were added to the lower section of the forming tube. The forming tube was then refilled, and the water in the storage tank was recycled through this pulp pad for two hours at a flow rate of four gallons per minute to further clarify the water. The forming tube was then drained, and the pulp pad was removed and discarded.

The unrefined, classified pulp from which the handsheets were to be formed was weighed out on a triple-beam balance. This pulp (6.25 grams, ovendry) was added to 2 liters of deionized water and was disintegrated for 150 counts in a

British disintegrator. The resulting slurry was deaerated under vacuum, then added to the storage tank. The dilute slurry (approximately 0.0025% consistency) was kept in suspension by means of the small mixer.

The handsheets were formed by pumping the water through the rotameter to the sewer at a constant rate of 4 gallons per minute. When the desired basis weight was attained (as calculated from the consistency and the flow rate), the quick-closing valve was closed, and the air vent was opened simultaneously. In this way, the flow rate was maintained constant until the water level had passed below the septum. The pump was then shut off, and the forming tube was disassembled. The wet handsheet was covered with a single layer of filter paper, and the septum was removed from the forming apparatus.

The handsheet was couched from the septum (using a technique which will be described later), the forming tube was reassembled, and the above procedure was repeated. Three handsheets with a basis weight of 100 g./sq.m. could be formed in this manner from each tank of slurry.

Early in the experimental program, it was found that special procedures were necessary for couching the thick mats. When pressure was applied to the thick mats (which were essentially saturated with water), a lateral expansion of the mat occurred. This resulted in a significant and uncontrollable change in the porous structure of the mat. As a result, it was necessary to couch the mat in such a way that the water was forced from the structure while the mat was restrained from expanding laterally. The apparatus shown in Fig. 8 was designed and built to satisfy these requirements.

A 2-inch section was cut off the lower (5-inch diameter) forming tube of the constant-rate filtration apparatus. This section was placed on the septum

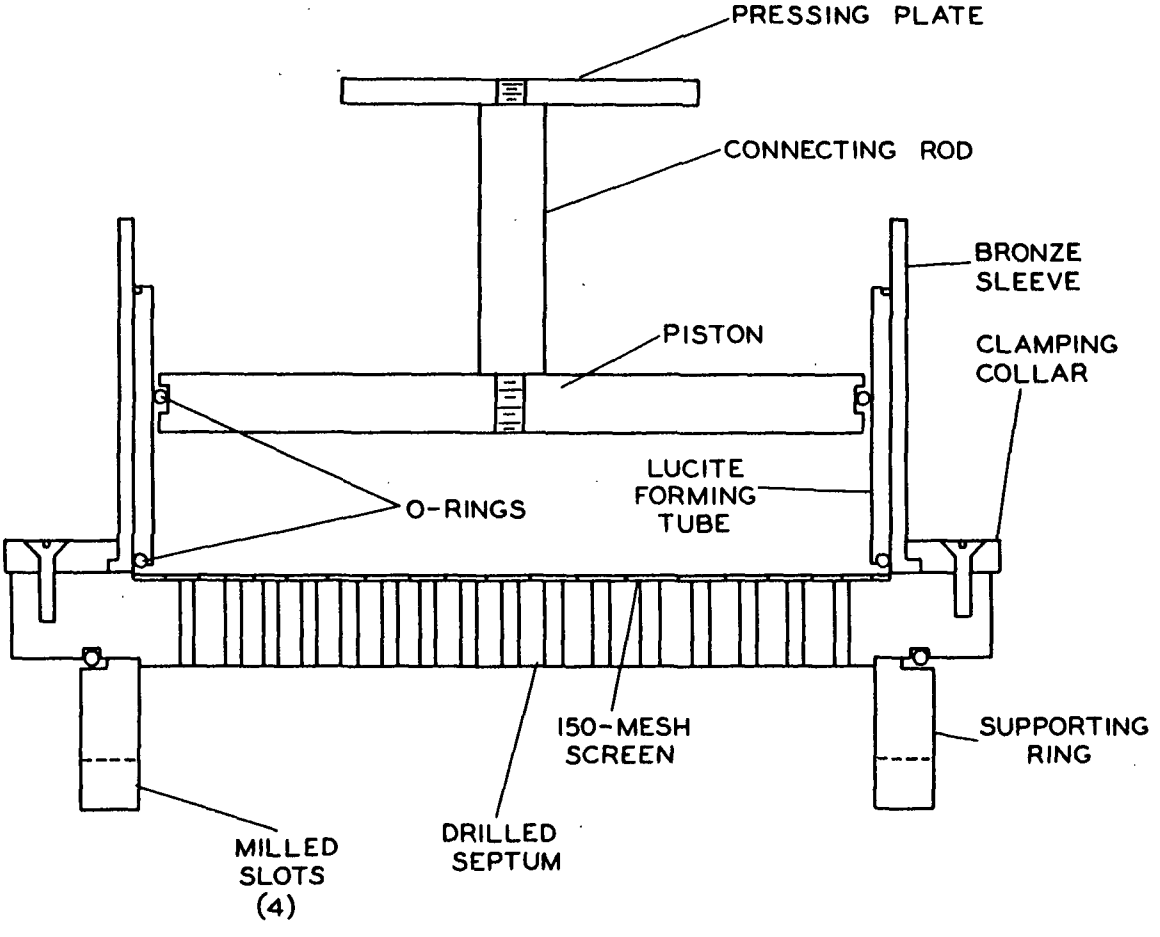

Figure 8. Couching Apparatus

and was surrounded by a bronze supporting sleeve, 1/8-inch thick. The Lucite tube and bronze sleeve were held to the septum by four machine screws through a clamping collar.

A brass piston with a dynamic O-ring seal was fitted inside the Lucite sleeve. The piston was connected to a flat pressing plate by a short brass rod. A supporting ring was placed beneath the septum. Four 1/4-inch slots were machined into the supporting ring to allow the water to escape from beneath the septum.

After forming a thick mat, the septum and bronze sleeve were removed from the constant-rate filtration apparatus and placed over the supporting ring. Three layers of standard blotter stock (cut to a 5-inch diameter) were placed over the thick mat and the filter paper. The piston assembly was then inserted inside the Lucite sleeve, and the entire couching apparatus was placed in a Williams press. The pressure was raised slowly to 10 p.s.i.* and allowed to remain there for one minute. The couching apparatus was then removed from the press, and the thick mat was removed for wet pressing.

A sheet of Whatman no. 1 filter paper and eight blotters were placed on either side of the mat, which was then centered, "wire side" down, on a British sheet press. The pressure applied to the mat was raised to the desired level in 60 seconds. After five minutes, the mat was removed from the press. A second press of 15 minutes, with five dry blotters on either side of the mat, concluded the pressing cycle. The mat was turned "felt side" down for the final press.

*This pressure was corrected for the pressure required to overcome the friction between the piston assembly and the Lucite sleeve.

When the wet-pressing cycle was completed, the mat was transferred to a humidity room maintained at 50% relative humidity and 73°F. where it was allowed to equilibrate with the atmosphere.

The handsheets prepared in this study were couched in the same manner as the thick mats except that the O-ring seal between the piston assembly and the Lucite tube was not used. The couched handsheets were removed from the couching apparatus and placed on a filter paper. The handsheets were then labeled and placed "wire side" down on three standard blotters. Thus, a stack was formed consisting of three blotters, a filter paper, a handsheet, a filter paper, three blotters, etc.

The handsheets were wet pressed at the desired level in a British sheet press for five minutes. The wet blotters were then replaced with dry blotters, and the handsheets were subjected to a second press for 15 minutes. Again, the handsheets were turned "felt side" down for the second press. The handsheets were then transferred to the humidity room and were allowed to equilibrate with the atmosphere.

In order to insure the reproducibility of the drying conditions and prevent "curling" of the samples, the apparatus shown in Fig. 9 was designed and constructed. With this apparatus, which was constructed entirely of brass, it was possible to condition the samples under a constant load corresponding to 0.1 p.s.i. (based on a 5-inch diameter sample).

The baseplate (A) of the apparatus contained three leveling screws (B) and a spirit level (C). The lower septum (D) was a brass plate, 6-3/4 inches in diameter and 1/4-inch thick. The plate was drilled with 1/4-inch holes on 5/16-inch

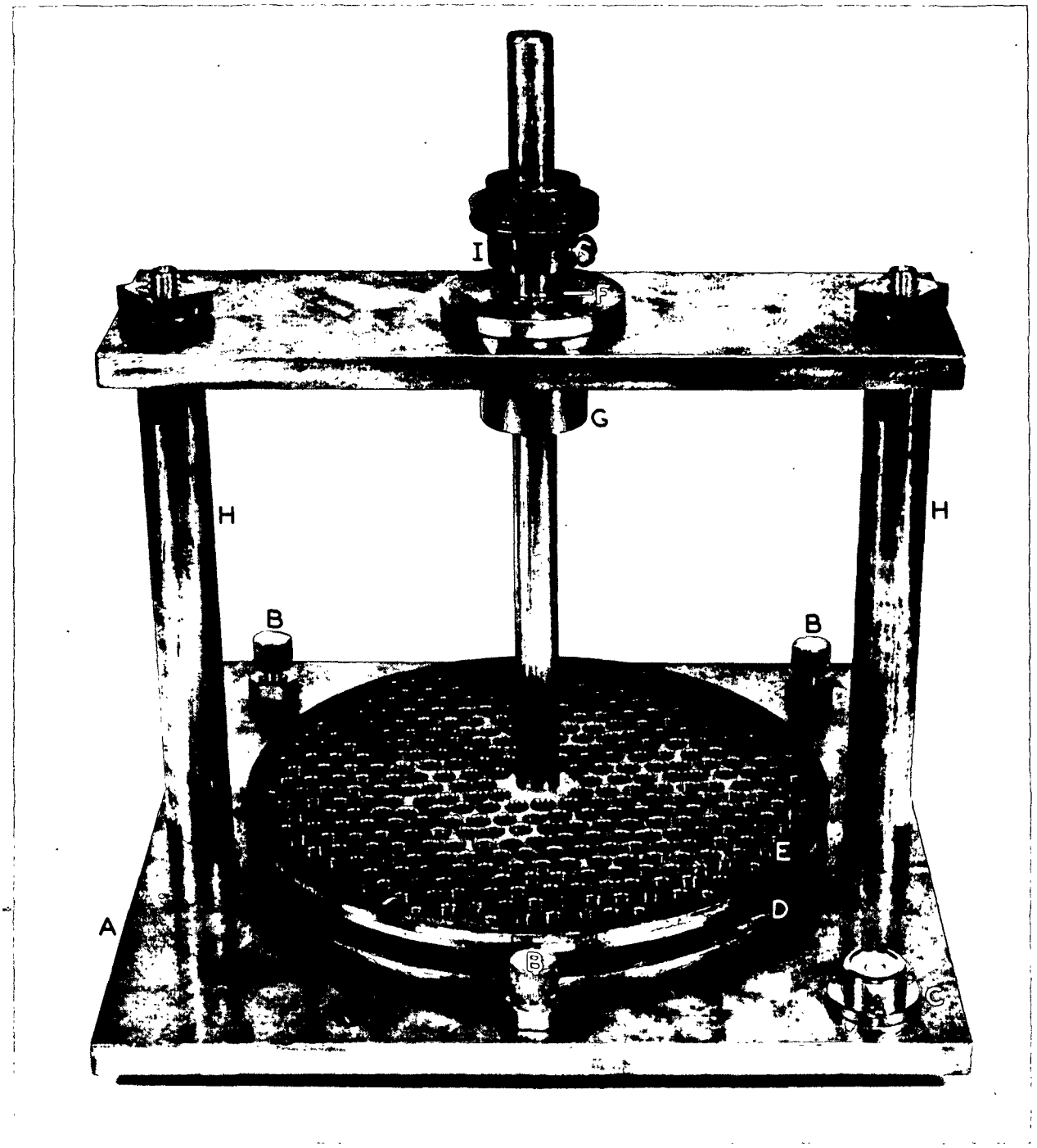

Figure 9. Drying Apparatus

centers to provide 58.3% open area. A 28-mesh screen was soldered on the top of the lower septum, and the septum was machined to fit into the baseplate (A).

The upper septum (E) had the same dimensions as the lower septum and was tapped in the center to receive a 1/2-inch diameter brass rod. The upper septum was also drilled with 1/4-inch holes on 5/16-inch centers to provide 57.3% open area. A 28-mesh brass screen was soldered to the underside of the upper septum.

The upper septum was free to travel in the vertical direction and was held in position by a ball bushing (F). The ball bushing was mounted in a housing (G) which was, in turn, press fitted into the cross member. The entire top assembly was held in position by two 3/4-inch diameter brass rods (H). The ball bushing (F) was designed to provide an antifriction bearing for linear motion in much the same manner as a ball bearing does for rotary motion. In addition, the ball bushing provided a rigid support for the upper septum to insure that the upper and lower septa were parallel.

The load applied to the samples could be varied by placing weights on the collar (I) as shown in Fig. 9. A load which corresponded to a compacting pressure of 0.1 p.s.i. was used throughout this study. In conditioning a sample, air was gently circulated around the drying apparatus by a small electric fan in a humidity room maintained at 50% relative humidity and 73°F. Preliminary tests indicated that 48 hours were required for the thick mats to reach constant weight while the handsheets reached equilibrium with the humidity room within 24 hours.

After the mats had equilibrated with the air in the humidity room, they were nailed to a block of wood and further dried for 24 hours in a vacuum desiccator over calcium chloride. Three test specimens, 2.01 inches in diameter, were then

cut from each mat using a special cutter on a drill press. The specimens were positioned so that at no time did the edges of the test specimens come closer than within 1/4 inch of the edges of the mats. In this way, any edge effects in forming the mats were avoided by drilling the specimens from the center portion of the mats. The individual test specimens were returned to the desiccator where they were stored to await future testing.

AIR PERMEABILITY STUDIES ON THICK MATS

As mentioned earlier, one of the objectives of the mat permeability studies was to determine the hydrodynamic specific volume of the fibers as a function of the apparent density of the mats. In order to calculate the apparent density of the mats, it was necessary to know the initial thickness of the specimens. In this study, "initial conditions" were arbitrarily selected as the "dry" state (moisture content of less than 2% above oven dry) and under a load of 0.1 p.s.i.— the load under which the samples were conditioned.

The mat specimens were removed from the desiccator and were transferred to the mat permeability cell (to be described later) where they were conditioned, uncompressed, with dry nitrogen for several hours. The specimen was then quickly removed from the permeability cell and transferred to a polyethylene bag.

In order to determine the initial specimen thickness, a compressibility test was run on each specimen using an Instron tester. A 5-pound weight, 4 inches in diameter, was suspended from the strain cell and a second 4-inch diameter platen was secured to the crosshead of the Instron tester. The initial separation of the two surfaces was set with an accurately machined steel gage block. Because a slight curling at the edges of the test specimen was produced by drilling the specimens from the mat, gage blocks of 1.615-inch diameter (the

diameter of the permeability test area) were placed above and below the test specimens.

The assembly, consisting of the bottom gage block, the test specimen in a polyethylene bag, and the top gage block, was then carefully centered on the bottom platen. The crosshead of the Instron tester was then slowly moved up until contact was made between the top gage block and the weight. A crosshead speed of 0.02 inch per minute and a chart speed of 20 inches per minute were used so that 1 inch on the chart trace corresponded to 0.001 inch on the specimen.

The specimen was compressed to a total load of four to five pounds, and several points of load-thickness data were selected from the resulting chart trace. The loads were corrected for the mass of the top gage block, and thickness data were corrected for the thickness of the polyethylene bag and the strain error in the Instron tester. The corrected data were converted to compacting pressures in p.s.i. and thickness in centimeters. These data were then fitted to the empirical equation, $\underline{L} = \underline{A}\underline{P}^{\underline{B}}$, where $\underline{L}$ is the specimen thickness, $\underline{P}$ is the compacting pressure, and $\underline{A}$ and $\underline{B}$ are constants. An IBM 1620 computer was used for these computations, and the best fit to the above equation was determined by least squares analysis of the data. This equation was then used to calculate the thickness of the specimen at a load of 0.1 p.s.i. The correlation was quite good in most cases with a correlation coefficient of over 99%, and it was estimated that the calculated initial thicknesses were accurate to within $\pm$ 0.001 inch. After completing the compressibility test, the specimen was returned to the mat permeability cell, where it was further conditioned with dry nitrogen before being subjected to permeability tests.

Several considerations were thought to be important in the design of the air permeability apparatus used in this study. These included:

1. The apparatus should be designed to allow the experimental determination of the permeability of thick mats as a function of compacting load, the permeability of thin handsheets, and the pore size distribution of thin handsheets using the gas-drive method.

2. The permeability tests should be conducted at high pressures to avoid the complications of slip and diffusional flow (5, 17).

3. In order to maintain laminar flow in the permeability tests, it was anticipated that relatively low flow rates should be employed. Consequently, the permeability apparatus should be designed to measure relatively small pressure drops.

4. Provisions should be made to insure that the same area of the test specimens was measured in both the permeability and gas-drive tests on thin handsheets.

The apparatus shown schematically in Fig. 10 was designed and built to satisfy the above requirements. This equipment is a modification of that used by Sanborn (25) and McDonald (26). Water-pumped nitrogen was bled through a two-stage pressure regulator (PR1) and a shutoff valve (V1) into two drying columns connected in series. The drying columns were constructed from 3-inch diameter steel pipes and were filled with refrigeration-grade silica gel. After flowing through the drying columns, the nitrogen passed through a Norgren 30-AE filter trap (F) where any fine particles, which might affect the operation of the needle valves, were removed. A Hoke model 4RB281 micrometer needle valve (MV1) was used to regulate the flow rate to the gas-drive cell and was left open during the permeability tests. A second pressure regulator (PR2) was used to adjust the pressure in the permeability cells and was left in an open position for the gas-drive tests. The nitrogen then passed through a temperature-sensing

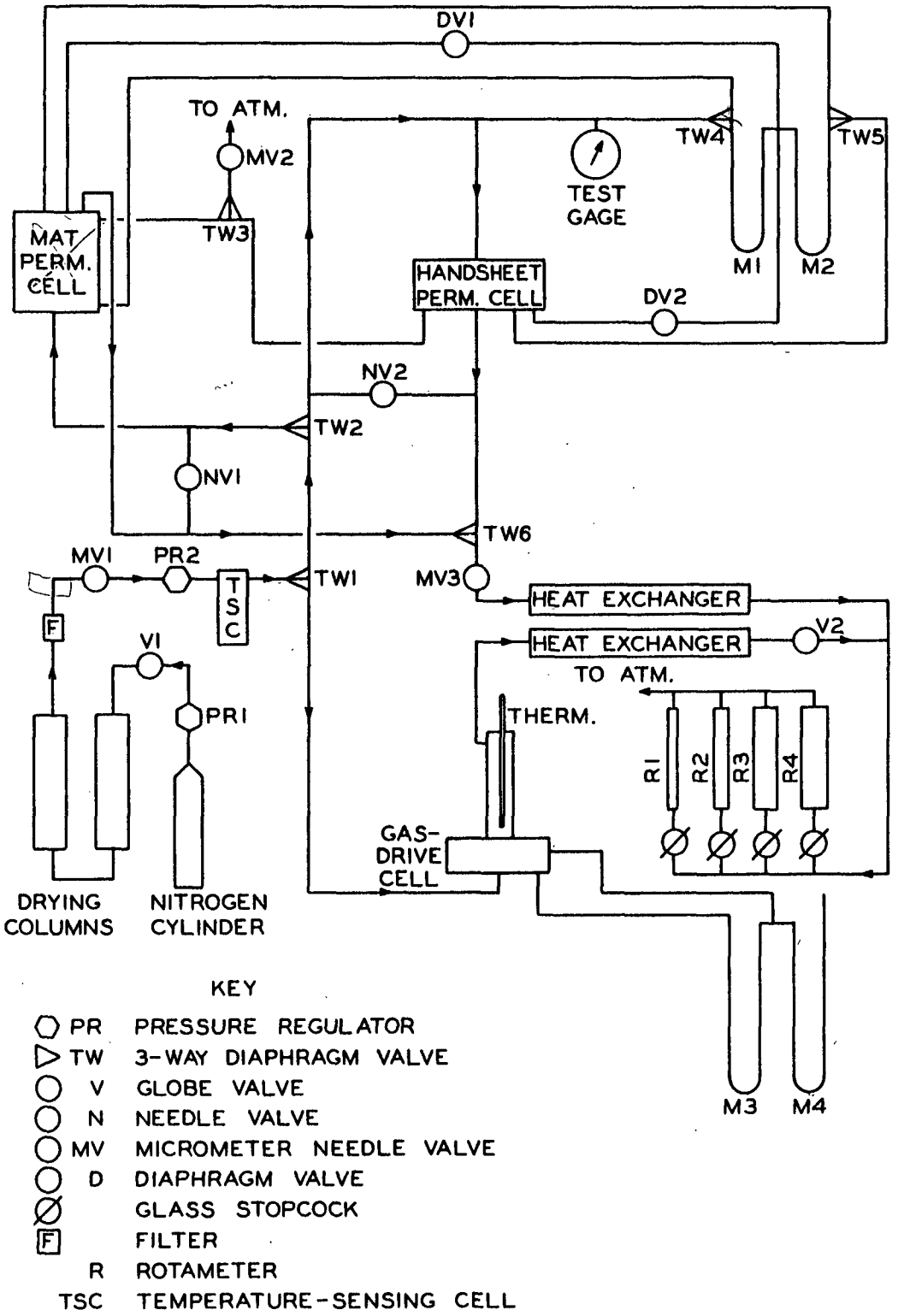

Figure 10. Flow Diagram of Permeability Apparatus

cell (TSC) which contained a system of hygrometers (not used in this study) and a thermister for measuring the gas temperature. The thermister was connected to the terminals of an Aminco no. 15-3000 electric hygrometer unit.*

From the temperature-sensing cell, the gas flowed into a three-way diaphragm valve (TW1) where it was directed either to the gas-drive cell or to the permeability cells. A second three-way diaphragm valve (TW2) was used to direct the flow of nitrogen into either the handsheet permeability cell or the mat permeability cell.

The permeability cells and the gas-drive cell will be described later in detail. Manometer M1 was filled with octoil-s containing a small amount of brown dye and was used to measure the pressure drop across either the mat or handsheet permeability cell. For the latter case, this manometer was mounted in a slanted position. A large test gage was attached to one side of manometer M1 and was used to measure the pressure in the permeability cells. Both the mat and handsheet permeability cells used in this study employed the guard ring principle described by Carson (51). Manometer M2, which was also filled with octoil-s, was used to balance the pressure between the test area and the guard-ring area in either the mat or handsheet permeability cell. Two three-way valves (TW4 and TW5) were used to connect manometers M1 and M2 to either the mat or handsheet permeability cell. Two Hoke needle valves (NV1 and NV2) were provided as bypasses around the mat and handsheet permeability cells, respectively. These valves were opened when raising or lowering the pressure in the permeability cells to prevent blowing the fluid from the manometers.

*Manufactured by American Instrument Co., Silver Springs, Md.

A Hoke model 4RB281 micrometer needle valve (MV2) was connected through a three-way valve (TW3) to the guard-ring area of either the mat or handsheet permeability cell. This valve was used to bleed gas from the guard ring in order to balance the pressure between the guard-ring area and the test area.

Two diaphragm valves (DV1 and DV2) were inserted in the downstream pressure tap lines from the mat and handsheet permeability cells. When a mat permeability test was being conducted, DV1 was opened and DV2 was shut off. The opposite was true for the handsheet permeability tests.

The gas outlet lines from the permeability cells were connected through a three-way valve (TW6) to a Hoke model 4RB281 micrometer needle valve (MV3) which was used to control the flow rate from these cells. The gas was then passed through a series of finned-tube heat exchangers to insure that the gas was in thermal equilibrium with the surroundings. The gas flow rate was measured on one of four Fisher-Porter triflat rotameters mounted in parallel. These rotameters were calibrated against a wet-test meter and were found to have the following approximate ranges at 760 mm. Hg and 73°F.:

Rotameter	Range, cc./sec.
R1	0.2 to 3.2
R2	2.5 to 26.4
R3	5.3 to 120
R4	100 to 535

The entire permeability apparatus was located in a humidity room in which the temperature and relative humidity were controlled at 73°F. and 50%, respectively. The flow lines leading from the heat exchangers to the rotameter complex were black rubber tubing. All other connections on the permeability apparatus

were made with 1/4-inch copper tubing, and the entire apparatus (excepting the gas-drive cell) was designed to withstand pressures up to 200 p.s.i.

A diagram of the mat permeability cell used in this study is shown in Fig. 11. This cell is a modification of that used by McDonald (26) and employs the guard ring principle described by Carson (51) to minimize the complications due to edge effects. The mat permeability cell was constructed primarily of brass and consisted of three main parts: the upper assembly, the lower assembly, and the piston assembly.

The upper assembly was composed of the top cell plate (A), the septum (B), and the upper guard ring (C). The top cell plate (A) was fastened to the drilled septum (B) by six 1/4-inch brass bolts and was sealed by a rubber O-ring (OR-1). Also attached to the top cell plate was the upper guard ring (C), which was likewise sealed by rubber O-rings (OR-2) to the top cell plate (A) and to the septum (B). The upper guard ring divided the space above the septum into an inner space (the test area) and an outer annulus (the guard ring).

A piece of porous sintered metal* approximately 1/4 inch thick by 1.600 inches in diameter was recessed into the bottom face of the septum (B) to cover the test area. A ring of the same material, 1.630 in. by 2.160 in. by approximately 1/4 in. thick, was recessed into the bottom of the septum (B) to cover the guard-ring area of the cell. A thin brass ring, which was 1.600 inches inside diameter by 1.630 inches outside diameter, was allowed to protrude about 0.015 in. below the bottom surface of the sintered metal. This lower guard ring (D) served to define the area of the test specimen.

*Type 304 porous stainless steel, grade "C", manufactured by Micrometalics Division of The Pall Corporation, Glen Cove, N. Y.

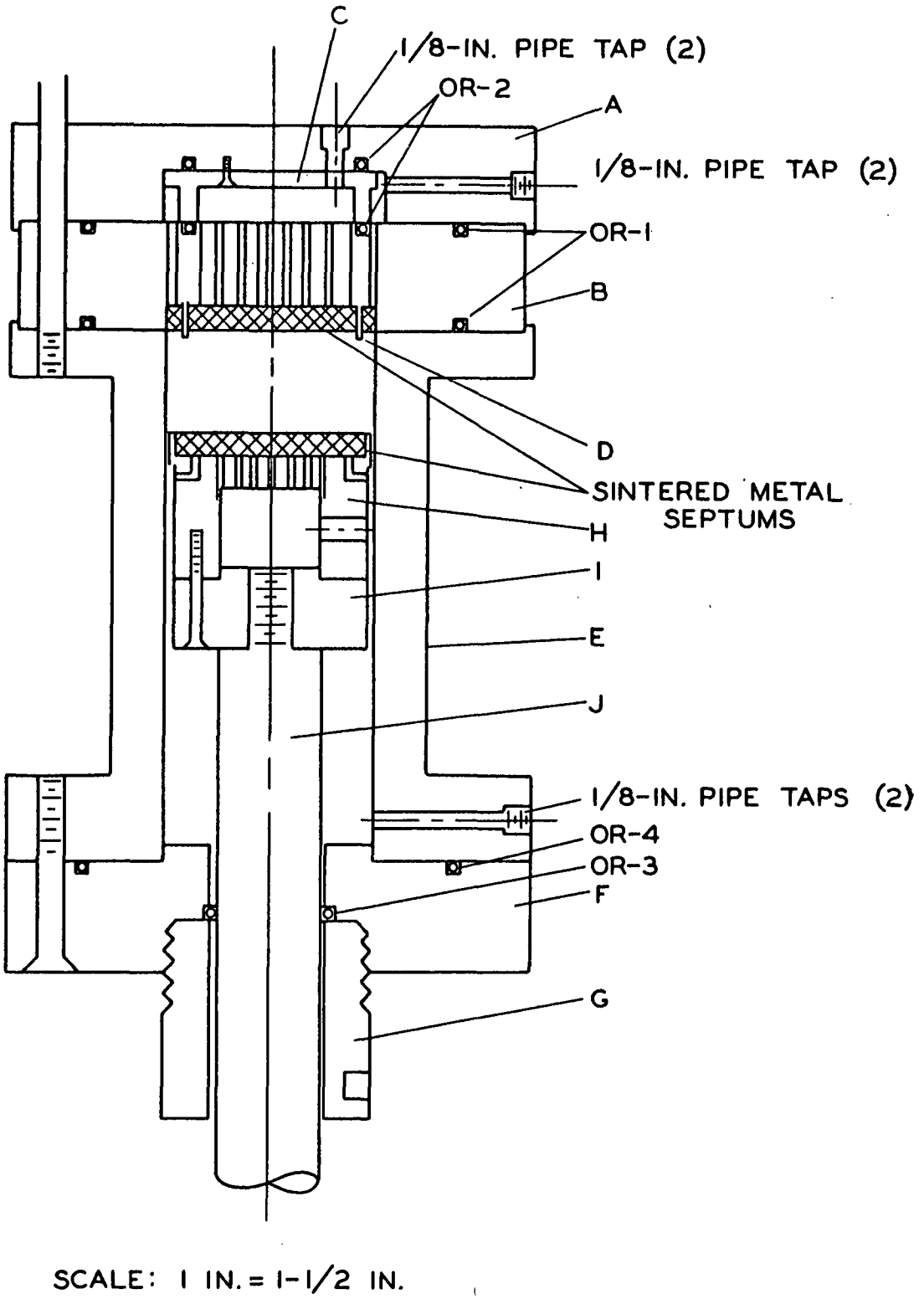

Figure 11. Cross Section of Mat Permeability Cell

Four 1/8-in. pipe taps were located in the top cell plate (A). Two of these taps were positioned in the test area and served as a gas outlet and a downstream pressure tap. The remaining two pipe taps were located in the guard-ring area and served as a guard-ring bleed and a guard-ring pressure tap.

The upper assembly was machined to fit into the top of the lower assembly to insure a close alignment of the septum and the permeable piston. The two assemblies were held together by six 1/4-in. steel bolts and were sealed by a rubber O-ring (OR-1). The upper and lower assemblies could be separated by removing these bolts to insert or remove a test specimen.

The lower assembly consisted of the cell chamber (E), the bottom cell plate (F), and the sealing gland (G). The cell chamber (E) was held to the bottom cell plate (F) by six machine screws and was sealed by a rubber O-ring (OR-3). The sealing gland (G) was screwed into the base of the bottom cell plate and compressed a rubber O-ring (OR-4) to provide a dynamic seal between the bottom cell plate and the piston rod. Two 1/8-in. pipe taps were located in the bottom flange of the cell chamber (E) to provide an inlet to the cell and an upstream pressure tap.

The piston assembly consisted of the permeable piston (H), the piston connector (I), and the piston rod (J). The permeable piston was a drilled septum with a piece of porous sintered metal approximately 1/4 in. thick by 2.010 in. in diameter set into its top surface. The permeable piston was machined to an outside diameter of 2.010 in. and fitted closely inside the cell chamber, which was 2.015 in. inside diameter. The piston connector (I) was tapped to receive the stainless steel piston rod (J) and was held to the permeable piston by four machine screws.

The mat permeability cell was mounted on a supporting frame, as shown in Fig. 12. The stand (A) was constructed of 2-in. angle iron and was bolted to the bottom support plate (B). The top support plate (C) and the bottom support plate (B) were connected by two 1-1/2-in. diameter steel rods (D) which were threaded on both ends. The tops of the supporting rods (D) shouldered on the top support plate, which was held in place by two large nuts. A support spacer plate (E) was clamped to the supporting rods between the top and bottom support plates and acted as a support for the lower assembly of the mat permeability cell when the upper assembly was removed to insert a test specimen.

A hydraulic cylinder holder (F) was fastened beneath the lower support plate to hold and position a 4-ton hydraulic jack (G). The hydraulic jack was used to compress the test specimen. A supporting nut (H) was screwed onto the lower end of the piston rod. After the specimen was compressed, this nut was tightened against the hydraulic cylinder holder (F) to provide a positive stop of any downward motion of the piston rod.

The thickness of the test specimen was measured by means of a dial caliper attached to the bottom of the mat permeability cell. The foot of this caliper rested on an arm which was clamped to the piston rod as shown in Fig. 12. It was estimated that the mat thicknesses determined with this arrangement were accurate to within a few thousandths of an inch.

The entire permeability cell was designed to withstand an internal pressure of 250 p.s.i. The cell and the supporting stand would withstand mechanical loads in excess of 3 tons—about 2000 p.s.i. mechanical compacting pressure on the permeable piston.

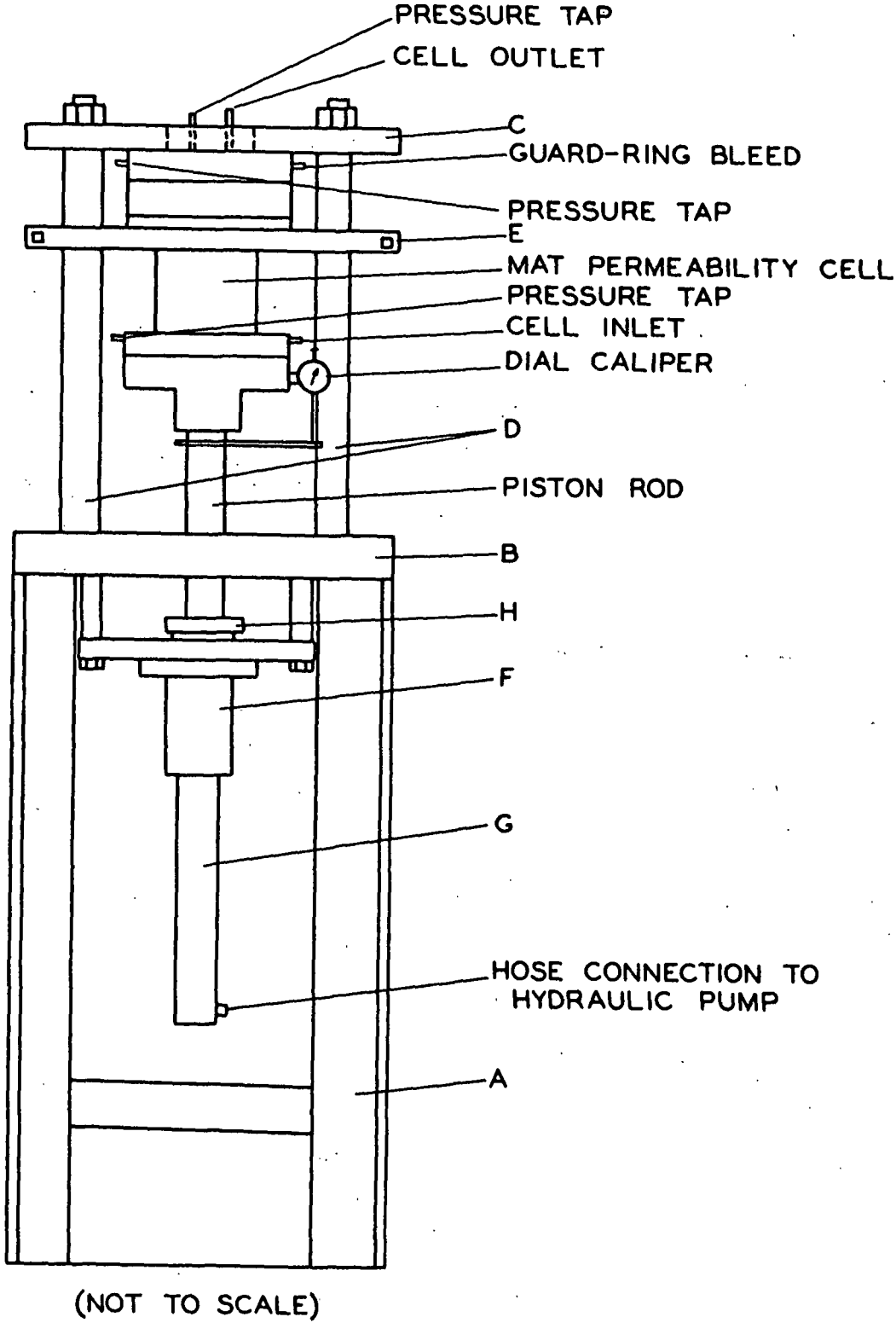

Figure 12. Supporting Stand for Mat Permeability Cell

After completing the compressibility test for initial mat thickness, the specimens were returned to the permeability cell where they were further conditioned with dry nitrogen. The following experimental technique was then used to characterize the permeability properties of the specimens.

1. The pressure in the permeability cell was adjusted to 100 p.s.i. and the specimen was compressed to the initial compacting pressure by means of the hydraulic jack. Six levels of compacting pressure from approximately 200 to 1500 p.s.i. (based on piston area) were used on each specimen.

2. Four flow rate-pressure drop readings were taken at each level of compaction. At each reading, the pressure between the test area and the guard ring was balanced by means of the guard-ring bleed valve to within $\pm$ 0.5 mm. of octoil-s (density 0.911 g./cc.). The pressure drop across the specimen was measured within $\pm$ 0.5 mm. of octoil-s on a U-tube manometer, and the flow rate was measured on one of four calibrated rotameters.

3. The dial caliper reading, the gage reading on the hydraulic jack, and the thermister reading (a measure of the temperature of the gas entering the permeability cell) were also measured at each level of compaction. The specimen thickness was determined as the difference between the dial caliper reading and the zero caliper at that compacting pressure. The zero caliper readings were obtained from a curve of zero caliper versus compacting pressure. This calibration curve was established by inserting a carefully machined gage block in the permeability cell and noting the dial caliper readings for several compacting loads.

4. When sufficient flow rate-pressure drop data had been obtained, the specimen was quickly transferred to a weighing bottle where the conditioned weight was determined. The specimen was then oven dried overnight at 105°C.,

and the moisture content was calculated. In general, the moisture content of the specimens varied between 0.5 and 1.25% above oven dry.

5. Finally, the thickness and flow rate-pressure drop data were used to calculate the specimen permeability coefficients as a function of compacting pressure. These data were then plotted according to Equation (19) in order to obtain an estimate of the hydrodynamic specific surface area and the fiber hydrodynamic specific volume of each specimen. These calculations were all carried out on an IBM 1620 computer, and the best fit of the data to straight lines was obtained by the method of least squares.

AIR PERMEABILITY STUDIES ON HANDSHEETS

One of the objectives of this thesis was to measure the permeability properties of carefully prepared handsheets. The air permeability data were used in two ways. First, they were used to determine the effect of basis weight and wet pressure on the permeability characteristics of paper; second, they were used together with pore size distribution data to estimate the hydrodynamic specific surface area from the modified hydraulic radius theory developed earlier.

In order to calculate the permeability coefficients, the porosities, and the apparent densities of the thin handsheets tested in this study, it was necessary to have a reliable measure of the average sheet thickness. As pointed out by Brown (16), this average thickness is not an easily defined property. In the case of permeability calculations, the proper average thickness is the harmonic mean rather than the arithmetic average—disregarding any point-to-point variations in the permeability coefficients. If the thickness varies widely from point to point on the specimen, the harmonic mean can be considerably smaller than the arithmetic mean thickness. However, for fairly uniform specimens, the two averages should not differ greatly.

Brown (16) has investigated several methods for determining the thickness of thin sheets of paper. Among the methods investigated were: a TAPPI standard method employing a small micrometer, the Federal compressibility gage, a mercury displacement method, and a mercury capacitance method. For the first two methods, it was found that it was necessary to extrapolate the data for various compacting pressures to zero load to determine the "free" thickness of the test specimen. These extrapolations proved to be open to question in most cases. Brown concluded that the mercury capacitance method was the most satisfactory, and this method was selected for use in this study. As Brown (16) pointed out, "The method is theoretically sound and quite reproducible, particularly for the thinner samples."

The mercury condenser constructed for use in this study is shown in the photographs of Fig. 13 and 14. Figure 13 shows only the lower portion of the cell, while Fig. 14 shows the assembled cell with a specimen in place.

A 500-ml. cork-type bottle was sawed in half 1-1/4 inches above the base, taking care that the cut was made parallel to the base. The two surfaces were then ground smooth with a fine carborundum powder in light mineral oil. A 1/2-inch hole was drilled into the bottom section of the bottle to accept the lower electrode (A) and a 1/4-inch hole (B) was drilled in the upper section of the bottle to allow mercury to be admitted to the cell. The bottom section of the bottle was fitted between positioning pins (C) in a brass base plate (D). The base plate was leveled with three screws (E), and a small spirit level (F) was used to indicate when the base plate had been properly leveled.

Two 3/16-in. rods (G) were also mounted in the base plate to position the test specimen. These rods were placed so as to correspond to those on the gas-drive and handsheet permeability cells in order to insure that the same area of

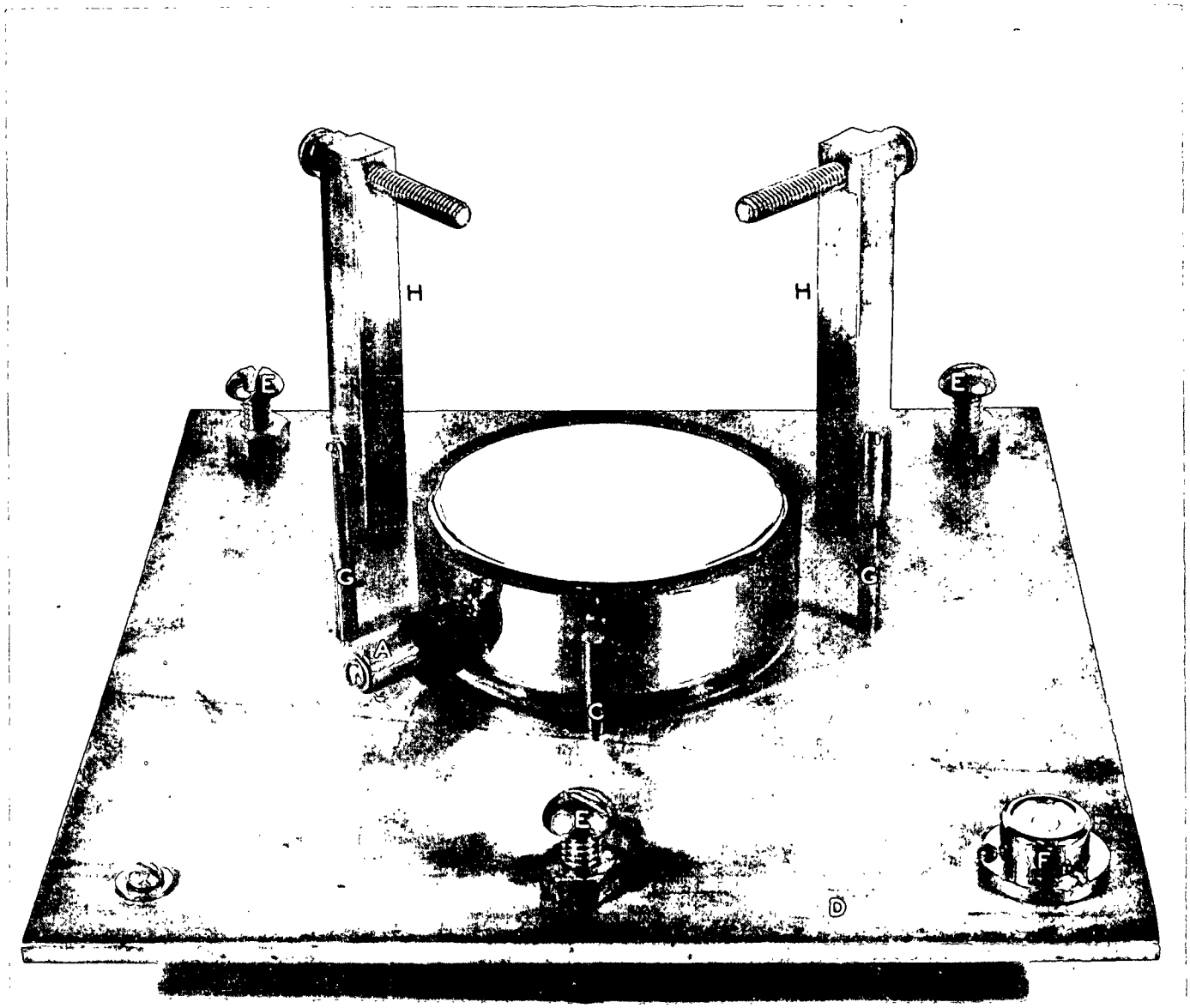

Figure 13. Mercury Condenser Cell (Open)

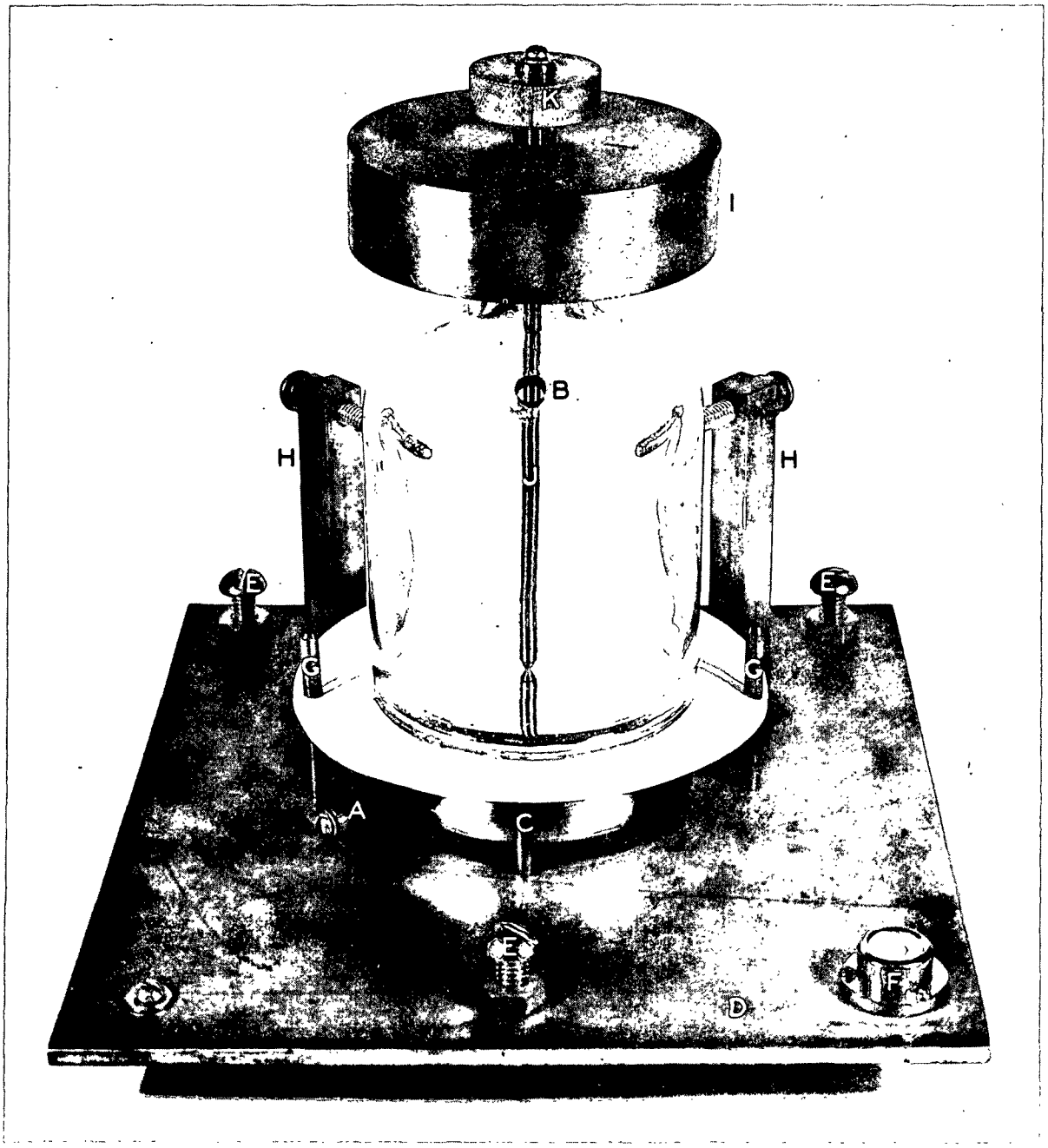

Figure 14. Mercury Condenser Cell (with Specimen in Place)

the specimen was tested in all three tests. The effective area of the mercury condenser was calibrated using a piece of Mylar film and was found to be 46.5 sq. cm.

The lower electrode (A) was machined from magnetic iron and was fitted through a rubber stopper into a pool of mercury in the bottom of the cell. A small screw was tapped into the end of this electrode to provide an electrical connection.

The two centering posts (H) were provided with adjusting screws which served to position the top of the cell over the bottom section once the test specimen was in place. By adjusting these two screws and aligning the mold lines on the bottle, the position of the two halves of the cell could be accurately aligned.

The upper section of the cell was held in place by a large bronze weight (I). A recess was machined into the bottom of this weight to fit over the top of the bottle. The upper electrode (J) was also machined from magnetic iron and was threaded through the bronze weight with a 1/4-inch-40 tap. Thus, one full turn of the knurled knob (K) corresponded to a linear movement of 0.025 inch on the upper electrode. This arrangement allowed the level of mercury above the test specimen to be carefully controlled. A small screw was tapped into the top of the upper electrode to provide an electrical connection.

The mercury condenser cell was connected to a General Radio Type 650A impedance bridge by means of shielded conductors. The shielding of all leads and the lower electrode (A) were grounded. A frequency of 1 kilocycle was used for all capacitance tests, and a Heathkit oscilloscope was used to indicate the balance of the impedance bridge.

The lead capacitance and the internal capacitance of the bridge were measured and found to be 8 micromicrofarads and 7 micromicrofarads, respectively. Corrections were applied for these capacitances in all tests.

After the handsheets had been conditioned in the humidity room, they were separated from the filter papers, and two 3/16-in. holes were punched in each sheet. These holes were placed so as to fit over the specimen-positioning pins on the mercury condenser, the gas-drive cell, and the handsheet permeability cell. The handsheets were then transferred to a dry box in which the air was circulated externally over calcium chloride. In preliminary tests, it was found that a relative humidity of about 7-9% could be maintained in the dry box.

After drying for 24 hours, the handsheets were weighed individually on an analytical balance. Each specimen was then subjected to a mercury capacitance test using a mercury head above the specimen which corresponded to a compacting pressure of 0.1 p.s.i. As mentioned earlier, this pressure was selected arbitrarily as initial conditions and was used in all tests.

When the necessary measurements had been completed, the mercury was drawn off the specimen by vacuum into a filter flask and the test specimen was transferred to a desiccator to await further testing. After a few tests, the mercury became contaminated and it was necessary to clean the mercury periodically by passing it through a pinhole in a sheet of filter paper.

The method of calculating the sheet thickness from the mercury capacitance data is described in detail by Brown (16) and need not be repeated here. The final working equation from which the sheet thickness may be calculated is

$$L = \frac{(1.11A^2 + 4\pi C'\emptyset'W) + \sqrt{(1.11A^2 + 4\pi C'\emptyset'W^2) + 4[8.88\pi C'A^2W]}}{8\pi C'A} \qquad (79)$$

where L is the sheet thickness in cm., A is the area of the mercury condenser in sq. cm., C' is the measure capacitance in micromicrofarads, ø' is a constant, and W is the mass of the specimen under the mercury electrodes. Since Equation (79) involves only measurable quantities, the harmonic mean thickness of the test specimens were calculated directly from this relationship.

The apparatus used to gather the flow rate-pressure drop data on thin handsheets was the same as that shown diagrammatically in Fig. 10. The different test cell was used, and manometer M1 was mounted in a slanted position, but the method of operation was exactly the same as that used on thick mats.

A diagram of the permeability cell used in this study is shown in Fig. 15. This cell is similar to that used by Bublitz (5) and employs the guard-ring principle described by Carson (51) to accurately define the test area. The main body of the cell was constructed of brass and was divided into an upper and lower section. The upper section (A) was 6 inches in diameter and 2 inches thick. The test area (B) was 3.000 inches inside diameter and was surrounded by a guard ring (C). A steel bearing plate (D) 2 inches in diameter by 3/8 inch thick was recessed into the top of the upper section. This plate was used to distribute the clamping load and prevent damage to the soft brass. Two 1/8-inch pipe taps in the test area served as a gas inlet and an upstream pressure tap. The gas inlet was baffled to prevent direct impingement of the gas on the test specimen. Several small holes were drilled between the test area and the guard-ring area to insure that the pressure was properly balanced on the upstream side of the specimen.

The lower section of the cell (E) was 6 inches in diameter and 2-1/2 inches thick. The test area and guard-ring area had identical dimensions with the

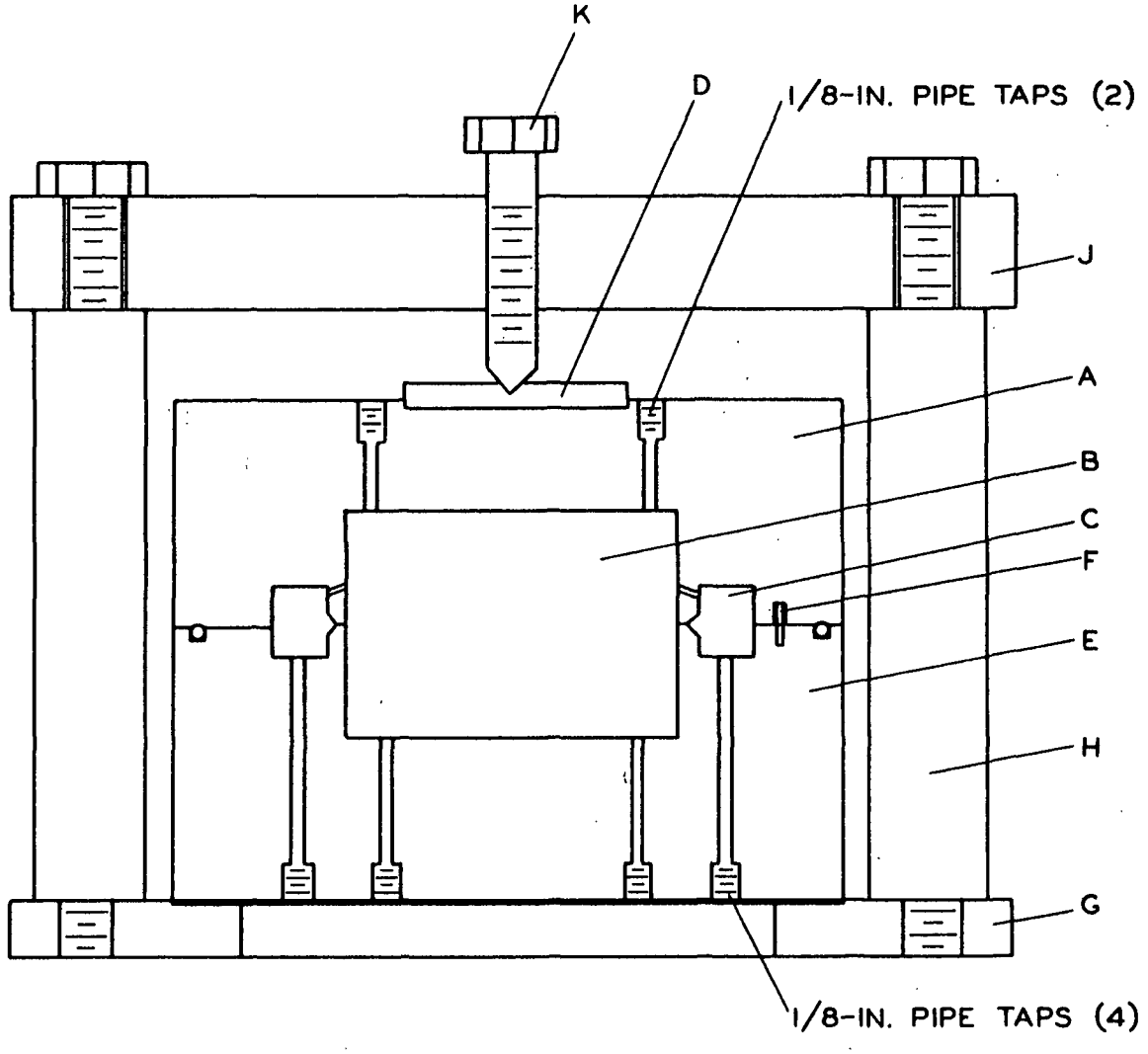

Figure 15. Cross Section of Handsheet Permeability Cell

upper section of the cell. Two 1/8-inch pipe taps in the guard-ring area acted as a guard-ring pressure tap and a guard-ring bleed outlet. The two 1/8-inch pipe taps in the test area served as a gas outlet and a downstream pressure tap.

The two sections of the handsheet permeability cell were aligned by two 3/16-in. taper pins (F). These pins were placed so as to correspond to those on the mercury capacitor cell and the gas-drive cell, and therefore they also served to position the test specimen. A rubber O-ring provided a seal between the guard ring and the atmosphere. The cell was designed to withstand pressures of about 250 p.s.i.

The lower section of the cell was recessed into a 9-inch square by 1/2-inch thick steel base plate (G). Two 1-inch diameter steel upright rods (H) were threaded into the base plate, and a 1-in. square clamping bar (J) was bolted onto the tops of these uprights. A 1/2-in. tempered steel bolt (K) was tapped into the center of the clamping bar.

To clamp a test specimen in the cell, the two sections were separated, and the specimen was placed over the taper pins. The upper section was positioned over the taper pins, and the clamping bar was then securely tightened against the steel bearing plate to apply pressure to the rubber O-ring and seal the cell.

The following procedure was used to gather the necessary flow rate-pressure drop data on the thin handsheets:

1. A specimen of known thickness was carefully clamped in the handsheet permeability cell, and the cell pressure was adjusted to 100 p.s.i.

2. After the specimen had been conditioned with dry nitrogen, several—usually ten—flow rate-pressure drop readings were taken. The pressure drop

across the cell was measured to within ± 0.5 mm. of octoil-s (density 0.911 g./cc.) on a slant-mounted manometer (magnification = 12.7). The flow rate was measured on one of four calibrated rotameters. The thermister reading (a measure of the gas temperature) was also recorded for each flow rate.

3. When sufficient data had been collected, the specimen was removed from the cell and transferred to a desiccator to await further testing.

4. Finally, the flow rate-pressure drop data and the data from the mercury capacitance tests were used to calculate the permeability of the sheet. These calculations were carried out on an IBM 1620 computer, and the flow rate-pressure drop data were fitted to a straight line by the method of least squares.

PORE SIZE DISTRIBUTION STUDIES ON HANDSHEETS

An important objective of this thesis was to evaluate the pore size distribution properties of carefully prepared handsheets. The data from these tests were used in two ways. First, they were used to evaluate the effect of pore size distribution on the permeability properties of paper. Secondly, these data were used together with the air permeability data to estimate the hydrodynamic specific surface area using the modified hydraulic radius theory developed earlier.

Although there are several methods for measuring the pore size distribution of a porous medium, the gas-drive technique was selected for use in this study. This technique, or a modification of this technique, has been used for a number of years by soil scientists (9), but it has only recently been applied to paper (25, 46, 52). The basic principle involved in the gas-drive technique is that an increase in the pressure drop across a porous medium partially saturated with a liquid causes more pores to be drained of liquid. By measuring the flow rates and pressure drops over a sufficiently wide range of pressures, the pore size distribution may be calculated using the method of analysis described earlier.

The gas-drive method was selected for use in this study for several reasons:

1. Even the smallest pores can be detected at reasonably low pressures, and therefore anomalies due to compression of the test specimen are minimized.

2. Since the gas-drive method is a dynamic (energy dissipative) method, the pore size distribution determined by this test is probably closely related to the pore sizes which are effective in offering resistance to fluid flow.

3. It is relatively easy to obtain a closed distribution curve using the gas-drive technique.

As pointed out earlier, any number of liquids may be used in the gas-drive test. It has recently been demonstrated experimentally by Pouradier and Chateau (52) that the pore size measured by the gas-drive technique is independent of the liquid used provided that the liquid does not swell cellulose. Following Sanborn (25), normal hexyl alcohol was used in this study for the following reasons:

1. Hexyl alcohol has a relatively low surface tension so that the smaller pores may be penetrated at relatively low pressures, thereby minimizing the anomalies due to the compression of the test specimen.

2. Hexyl alcohol has a low vapor pressure so that the temperature of the liquid—and hence its surface tension—does not change appreciably during a test.

The apparatus used to collect the flow rate-pressure drop data in this study is shown diagrammatically in Fig. 10. A special gas-drive cell was used, and manometers M3 and M4 were used to measure the pressure drop across the specimen and the back pressure on the cell, respectively. In conducting a gas-drive test, valve V2 and pressure regulator PR2 were opened and micrometer needle valve MV3 was closed. The flow rate to the gas-drive cell was then controlled by means of micrometer needle valve MV1.

Photographs of the gas-drive cell used in this study are shown in Fig. 16 and 17. The cell was constructed primarily of brass and was mounted on a steel column. The upper cell plate (A) was attached to the 2-1/2-inch diameter steel column (B) while the lower cell plate (C) was attached to the ram of an air cylinder (D).

The lower cell plate was 5-3/4 inches in diameter and 1-1/2 inches thick at the top. The connecting rod was 1 inch in diameter and 2-1/2 inches long. The lower cell plate and the connecting rod were machined from a solid piece of brass. A carefully machined "land area" (E - see Fig. 17) on the top of the lower cell plate served as a bearing surface for the upper cell plate. A liquid reservoir 2-3/4 inches in diameter by about 1/4 inch deep was machined into the top of the lower cell plate, and this was tapered to meet a 3/8-inch diameter drain. The latter hole extended down into the connecting rod where it was connected with a 1/8-inch pipe tap. This arrangement allowed the liquid to be drawn from the cell through the liquid drain line (F) after the test was completed. Two 1/8-inch pipe taps were drilled into the tapered portion of the liquid reservoir. These served as a downstream pressure tap (G) and a gas inlet (H). A countersink in the bottom of the connecting rod was fitted over a 1/2-inch diameter steel ball in the "wobble" coupler.

The "wobble" coupler (I) was 2-1/2 inches long and was also machined from brass. The outside diameter of the coupler was 2 inches at the top and 1-1/2 inches at the bottom. A 1/2-inch hole was drilled into the bottom of the coupler to accept the shaft of the air cylinder, and a small Allen screw was used to hold the coupler in place. A 1-1/4-inch diameter hole was machined into the top of the coupler to a depth of about 1-1/4 inches. Three set screws (J), positioned 120° apart around the top of the coupler, were used to adjust the amount of wobble

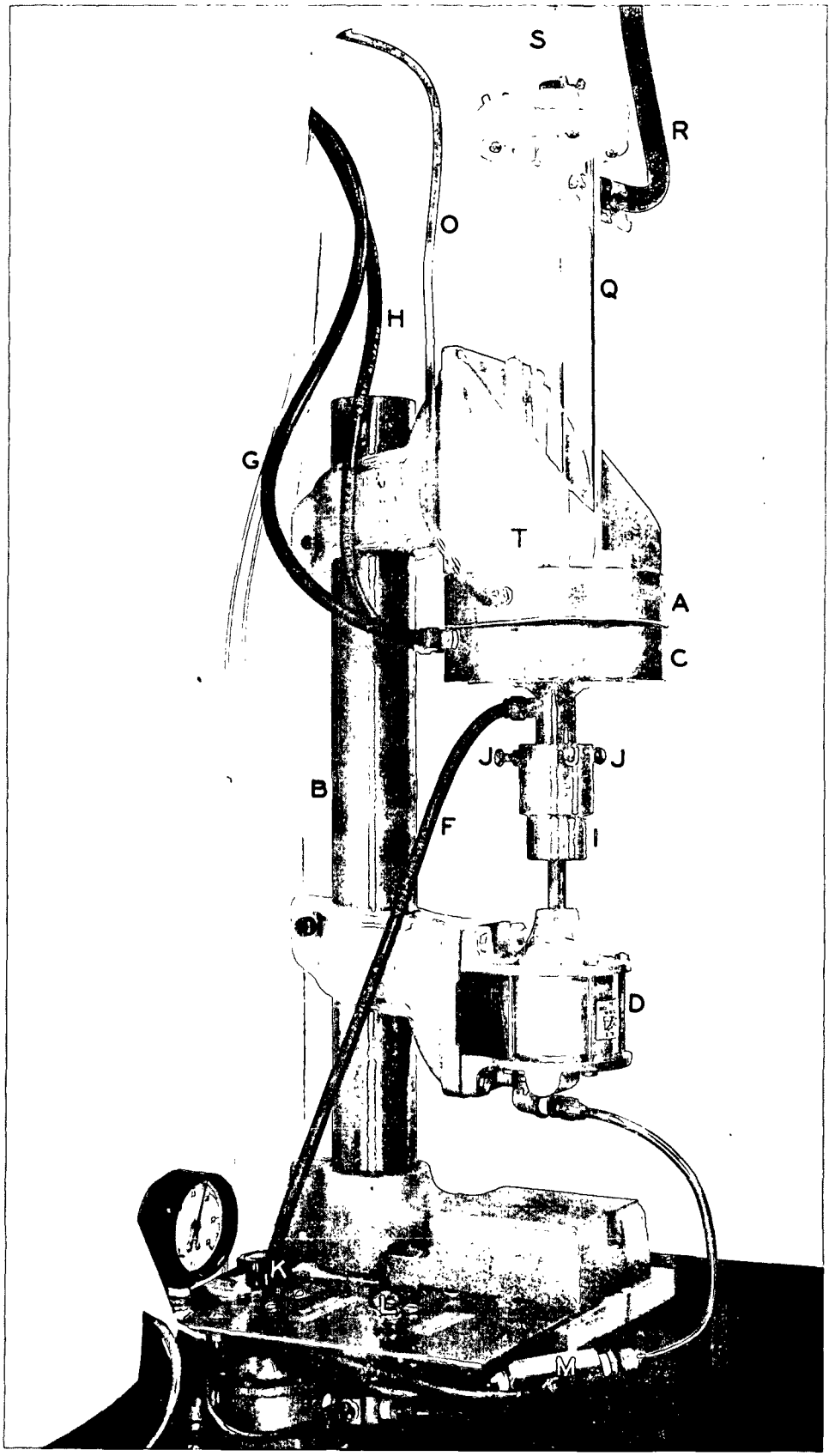

Figure 16. Gas-Drive Cell

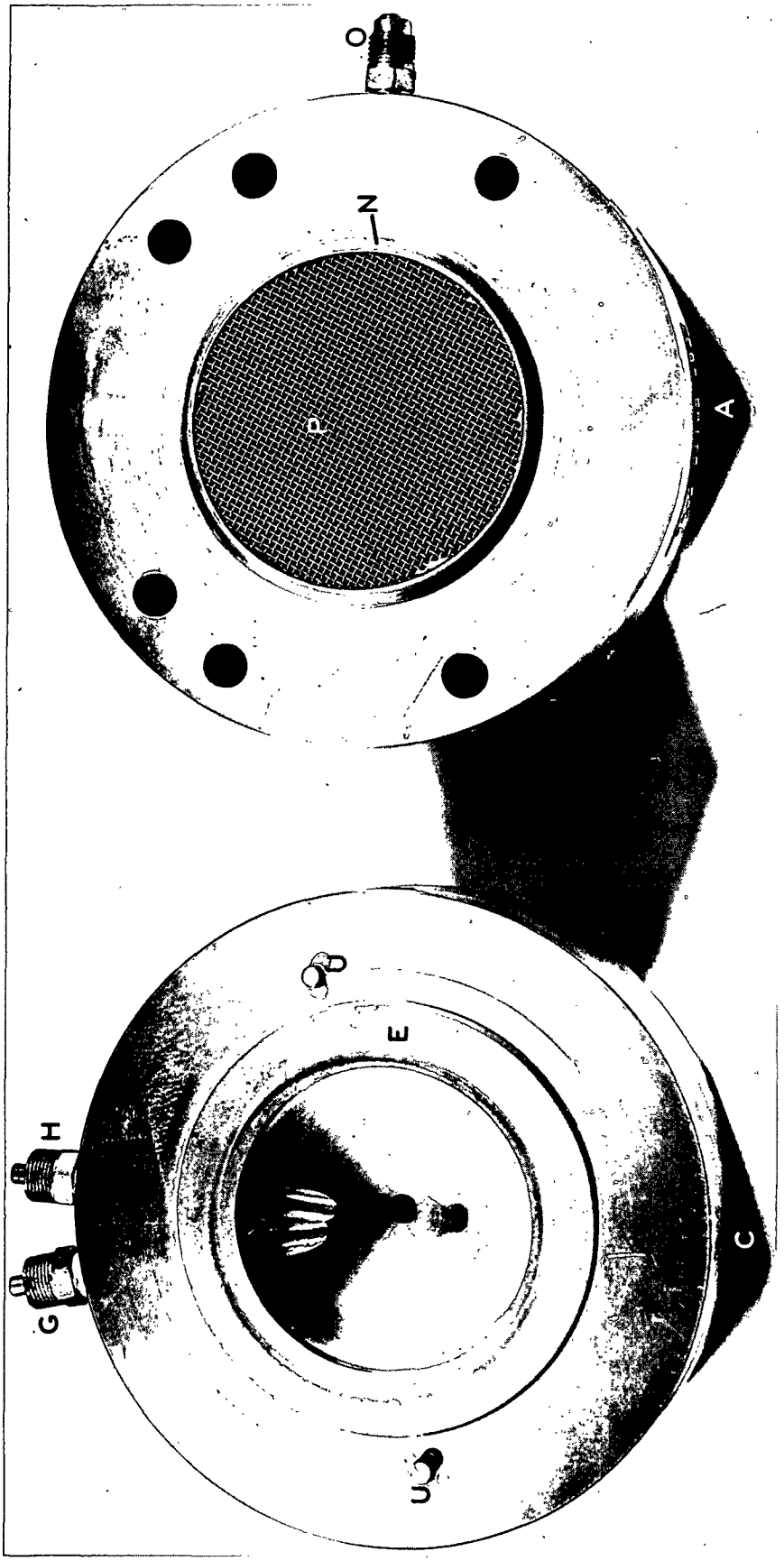

Figure 17. Clamping Arrangement of the Gas-Drive Cell

allowed in the connecting rod. The connecting rod from the lower cell plate was positioned over a 1/2-inch diameter steel ball which was recessed into the "wobble" coupler. With this arrangement, the lower cell plate was allowed to seek its own position against the upper cell plate.

The air cylinder (D) was an "Air-Mite" Model AP-7 and was clamped to the steel column by means of a special bracket. The supply air for the cylinder was passed through a filter-regulator (K) to a three-way valve (L). One side of the three-way valve was open to the atmosphere and the other side was led through a variable-orifice flow controller (M) to the air cylinder. The flow controller was required to prevent the two cell plates from slamming together. The air cylinder was equipped with a spring return to retract the ram when the air pressure was released.

The upper cell plate (A) was 5-3/4 inches in diameter and 1-1/4 inches thick and was machined from brass. A 1/4-inch half circle 3 inches in diameter was machined onto the bottom of this plate. Half of this radius was then machined away by a 3.000-inch diameter hole, 5/16 inch deep. In this way, a quarter-circle radius (N) was left, and this radius was allowed to bear on the "land area" of the lower cell plate (see Fig. 17). This clamping arrangement provided essentially a line clamp in which the test specimen served as its own gasket.

The air pressure to the air cylinder was controlled at 35 p.s.i. during a gas-drive test. This corresponded to a clamping "pressure" of about 25 pounds per inch of the line clamp.

The upstream pressure tap (O) was tapped into the upper cell plate just above the septum. The septum consisted of a 20-mesh stainless steel screen (P) which was carefully soldered to a thin bronze sleeve. A thin strip of brass

was soldered across the diameter of the bronze sleeve as a further support for the screen. This septum was pressed into the 3.000-inch diameter hole in the bottom of the upper cell plate (see Fig. 17). With the septum in place, the clearance between the screen and the clamping radius was approximately 1/32 inch.

A Lucite mist column (Q), 2 inches inside diameter by 12 inches long, was sealed to the top of the upper cell plate by a Teflon O-ring and was held in place by four brass screws. This mist column provided a space in which liquid entrained in the exit gas could be eliminated. A gas outlet (R) was located near the top of the mist column. The top cap of the mist column was held in place by four small brass bolts and was sealed by a second Teflon O-ring. An 18-inch mercury thermometer (0-50°C.) (S) was inserted through a rubber stopper in the top cap and was used to measure the temperature of the liquid during a test.

The upper cell plate (A) was attached to the steel column by means of a brace (T) and a clamping bracket. The upper cell plate was held to the brace by six Allen bolts (see Fig. 17).

The two 3/16-inch taper pins (U) in the lower cell plate were allowed to extend slightly above the "land area" and served to position the test specimen. These pins were placed in the same position, relative to the test area, as those on the mercury condenser and the handsheet permeability cell in order to insure that the same area was tested in all three tests.

Two Meriam U-type manometers were connected to the gas-drive cell, as shown in Fig. 10. Manometer M3 was filled with tetrabromoethane (density 2.964 g./cc.) and was used to measure the pressure drop across the cell. Manometer M4 was filled with octoil-s and was used to measure the back pressure on the cell.

It was found that at higher flow rates an appreciable back pressure was present, and all flow rates were corrected for this pressure.

The technique used in carrying out the gas-drive measurements was quite simple.

1. A specimen of known thickness was clamped in the cell and was conditioned with dry nitrogen.

2. The nitrogen flow was then shut off, and 100 cc. of technical-grade hexyl alcohol were introduced through the thermometer opening. The specimen was then allowed to stand several minutes to insure that the test specimen was in equilibrium with the hexyl alcohol.

3. The pressure beneath the specimen was increased slowly until the first bubbles of gas appeared in the liquid. At this point, the flow rate was measured on one of four calibrated rotameters, and the pressure drop across the cell was measured on Manometer M3 (see Fig. 10) using a cathetometer. The reading on the thermister unit, the liquid temperature, and the back pressure on the cell were also recorded.

4. The pressure beneath the specimen was then increased slightly, and the above data were again recorded. This procedure was repeated for 25 to 30 flow rates from 0 to 400 cc./sec.

5. When the gas-drive test was completed, the liquid was drawn off through the liquid outlet (see Fig. 16). The test specimen was removed from the cell, and the excess liquid was blotted off. The sheet was then dried overnight at 105°C. The ovendry weight was used to calculate the basis weight and the moisture content of the sheet.

The data gathered in the gas-drive test were used to calculate the pore size distribution of the test specimen using Equations (67) and (69). The mean and

variance of the data were then calculated, and the standard deviation of the data—a measure of the broadness of the pore size distribution—was computed as the square root of the variance.

The data were then fitted to a log normal distribution as suggested by Corte (46). It has been demonstrated by Hatch and Choate (53) that, for a log normal distribution, a plot of the measured property, e.g., pore size, versus the cumulative frequency should be linear when plotted on log-probability paper. Therefore, by plotting the pore size distribution data on a special log-probability paper* an estimate of the degree of fit of the data to the log normal distribution can be obtained.

A more quantitative measure of the degree of fit to a log normal distribution was obtained by fitting the experimental data to a straight line on a log-probability plot, using the methods developed by Jentzen (54). The pore size distribution data were also analyzed for skewness and kurtosis, using the Student "t" test described by Goulden (55).

An example of the pore size distribution calculated from the gas-drive data is shown in Fig. 17a. While there is some scatter of the data points, the distribution has the characteristic shape of a log normal distribution.

Through the use of the statistical tests described above, a great deal of information concerning the pore size distribution properties of paper was amassed during this thesis. A complete example of the calculation of the pore size distribution from the gas-drive data and the application of the above statistical tests to the data is presented in Appendix I.

*Logarithmic-probability graph paper was obtained from the Codex Book Company, Norwood, Mass.

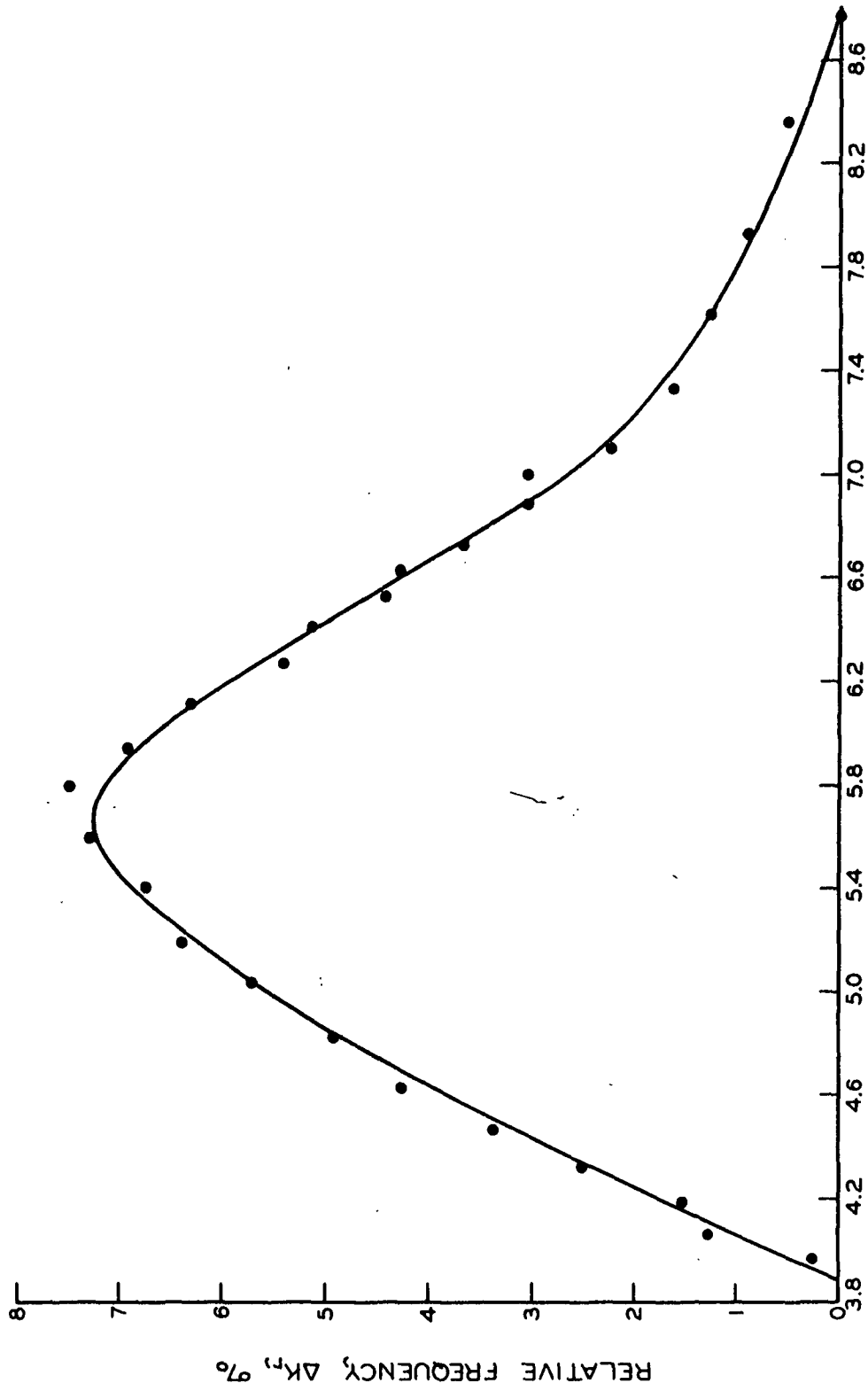

Figure 17a. Example of Pore Size Distribution from Gas-Drive Tests

WATER PERMEABILITY STUDIES ON SYNTHETIC FIBER BEDS

For reasons to be discussed later, it was considered advisable to study the effect of fiber shape on the Kozeny factor. Three different fiber shapes were used in this study. These included: (1) a 15-denier Du Pont nylon which had a circular cross section, (2) a 10-denier Du Pont orlon which had a "dog-bone" cross section, and (3) a flattened 15-denier nylon which was approximately elliptical in cross section. The flattened nylon fibers were prepared by passing the normal monofilament nylon (1) through the steel rolls of an Altor Model 37A rolling mill.* In preliminary tests it was found that severe splitting occurred in passing the filament through the steel rolls. This was overcome by plasticizing the fibers in boiling water before they were passed through the rolling mill.

The nylon fibers were obtained in the form of continuous filaments and were cut into the desired fiber length by means of gang razor blade cutters, as described by Arnold (56). The orlon fibers were obtained in the form of 3/4-inch staple, and in order to reduce the length of these fibers, the following procedure was adopted. Five grams of the staple were disintegrated for 150 counts in a British disintegrator and formed into a pad on a large Buchner funnel. This pad was cut into strips approximately 3/16 inch wide on a guillotine cutter. The fibers were then redispersed in 2 liters of water for 150 counts. This procedure was repeated six times. Four batches of 5 grams each were treated in this manner, and the resulting fibers were blended for 300 counts in a British disintegrator.

Samples of the three fibers were subjected to fiber length distribution measurements and photomicrographs of the cross sections of each fiber shape were

*Manufactured by the Altor Manufacturing Co., Brooklyn, N. Y.

prepared by Mr. Jack Hankey of the Institute Microscopy Section. These photomicrographs are shown in Fig. 18.

In an effort to establish the effect of fiber shape on the Kozeny factor, the synthetic fibers shown in Fig. 18 were subjected to permeability tests. Preliminary tests indicated that the mat air permeability cell previously described was not suitable for these tests due to the relatively high pressure drop across the sintered metal septums. As a result, water was selected as the permeating fluid. In order to cover a wide range of porosity, two different water permeability apparatus were used. For the higher porosities, the apparatus described by Ingmanson and Whitney (57) was used. The only modification was the installation of a differential manometer of water/chlorobenzene (effective density = 0.105 g./cc.). The lower porosity tests were conducted on the equipment described by Ingmanson, et al. (18). A differential manometer of water/carbon tetrachloride (effective density = 0.585 g./cc.) was installed on this apparatus to measure the pressure drop across the beds.

The fibers were formed into uniform beds from a dilute aqueous suspension using a constant-rate filtration procedure. The resulting beds were mechanically compressed to the desired porosity, and several flow rate-pressure drop readings were taken at each porosity.

The porosity at each level of compaction was calculated from Equation (16),

$$\epsilon = 1 - \rho_b/\rho_s \qquad (16)$$

where ρ_b is the density of the bed and ρ_s is the density of the fibers which compose the bed. In the case of the nylon fibers, ρ_s was corrected for a 3% swelling in water (18), while the value of ρ_s for the orlon fibers was taken as

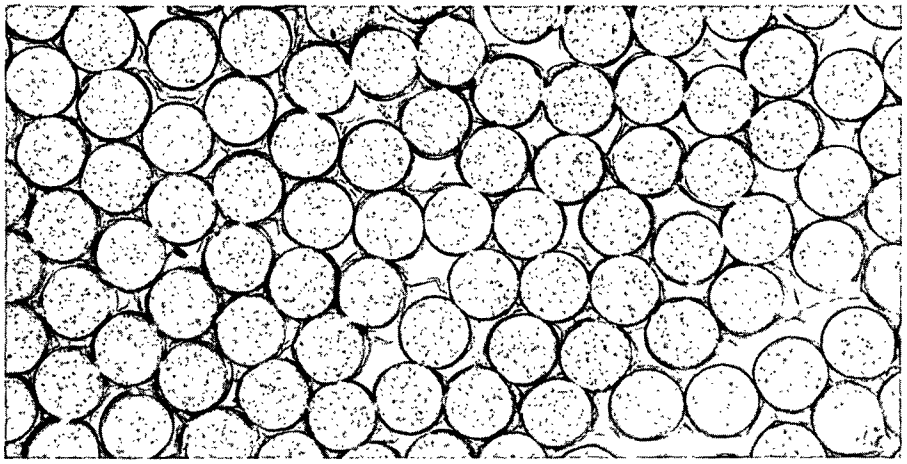

Round Nylon - 210X

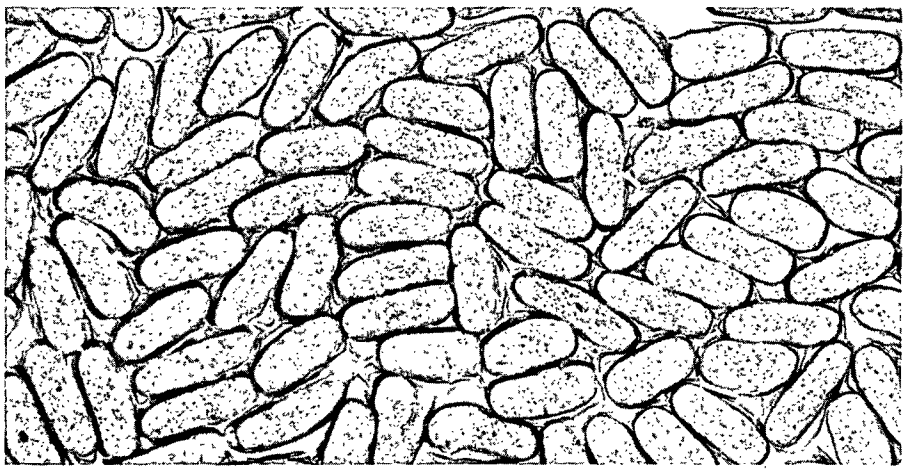

Flattened Nylon - 210X

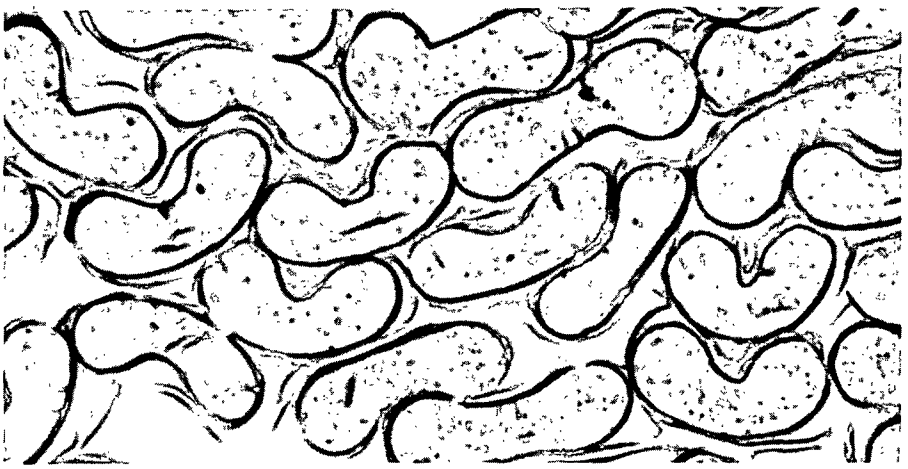

Orlon - 520X

Figure 18. Photomicrographs of Synthetic Fiber Cross Sections

the pycnometric density. Care was taken in these tests that the frictional pressure drop across the bed never exceeded about 2-3% of the compacting load in order to avoid the effects of a porosity gradient in the bed (18).

The Kozeny factors were calculated from the Kozeny-Carman equation [Equation (12)], using the surface areas measured from the photomicrographs of Fig. 18. It is apparent from these photomicrographs that the assumption of point contact between fibers is not a valid one for the orlon and flattened nylon fibers. As a result, it was necessary to correct the surface areas of these fibers for the area of contact between fibers. This was accomplished in the following manner.

The basic requirement for calculating the area of contact between the fibers of a fibrous bed is a value for the number of fiber-to-fiber contacts in the bed. An estimate of this number was obtained through the application of an equation derived by Onogi and Sasaguri (58) for the apparent density of a fibrous bed:

$$\rho_b = (\pi^3/16)(D\rho_s/b') \tag{80}$$

where b' is the length of the fiber segments between points of contact, ρ_s is the fiber density, and D is fiber diameter. Since the total number of contact points, N_c, is equal to the total fiber length L_f divided by the segment length, b',

See Errata - $N_c = \frac{L_f}{2b'}$ $\quad N_c = 8W^2/\pi^3 D A_f \rho_s^2 AL$

$$N_c = 16W^2/(\pi^3 DA_f\rho_s^2 AL) \tag{81}$$

In Equation (81), W is the mass of fibers in the bed, A_f is the cross-sectional area of the fibers, A is the area of the bed, and L is the bed thickness.

In order to apply Equation (81) to the flattened fibers tested in this study, it was necessary to introduce the additional assumption that N_c was not dependent on fiber shape. It was then possible to assign a meaningful value to the effective

fiber diameter, D, in Equation (81). This assumption appeared to be quite reasonable since, even though the number of fibers in a given x-y plane through the bed would be expected to be less for flattened fibers than for cylindrical fibers, one would expect a greater number of fibers in the z-direction for a given mat density. Thus, it seemed logical to suppose that at a given mat density the number of fiber-to-fiber contacts in the bed would be the same for flattened fibers as for cylindrical fibers. In view of these considerations, the effective value of D in Equation (81) was calculated from the cross-sectional area of the fibers.

The total area of contact in a fibrous bed was estimated by multiplying the total number of fiber-to-fiber contacts by the average area of each contact. It is easily shown (59) that for a bed in which the fibers are randomly oriented in the x-y plane, the average projected area of contact, A_c, is given by

$$A_c = (\pi/2)U^2 \tag{82}$$

where U is the average projected width of the fibers. The values of U were measured on the photomicrographs of Fig. 18.

Combining Equations (81) and (82), it is seen that the total area of contact in the bed is given by

$$\text{total area of contact} = 8W^2U^2/(\pi^2 D A_f \rho_s^2 AL) \tag{83}$$

The total area of the fibers in the bed is represented by

$$\text{total fiber area} = P'W/(\rho_s A_f) \tag{84}$$

where P' is the perimeter of the fibers estimated from the photomicrographs.

The effective area exposed to flow per unit volume of the fibers, $\underline{S_v}$, may be calculated by combining Equations (83) and (84). This results in

$$S_v = \left\{P'W/\rho_s A_f - [8W^2U^2/(\pi DA_f\rho_s{}^2AL)]\right\} /(W/\rho_s) \qquad (85)$$

where $\underline{W/\rho_s}$ represents the total volume of fiber in the bed.

Equation (85) was used to calculate the corrected surface area exposed to flow for the flattened nylon and orlon fibers, and this value of $\underline{S_v}$ was inserted in the Kozeny-Carman equation to calculate a corrected Kozeny factor for these beds. For the cylindrical nylon fibers, the assumption of point contact is valid and the value of $\underline{S_v}$ for these fibers was taken directly from measurements on the photomicrographs. The results of these experiments will be presented later.

EXPERIMENTAL DATA AND DISCUSSION OF RESULTS

POROUS PROPERTIES OF THICK MATS

The first step taken in studying the porous structure of paper was to establish the range of porosity over which the Kozeny-Carman equation could be expected to apply and to determine the specific volume of the fibers used in this study as a function of the apparent density of the sheets. These objectives were achieved by determining the permeability properties of thick mats as a function of the compacting pressure on the mat.

The data gathered on the thick mats were analyzed using Equation (19), which was originally proposed by Fowler and Hertel (12),

$$(KL)^{1/3} = [A^2/(kS_w^2 W^2)]^{1/3} (L - L_o) \qquad (19)$$

According to this equation, if the Kozeny-Carman theory applies, a plot of $(KL)^{1/3}$ versus L should be linear. The mat permeability data were plotted according to Equation (19), and the hydrodynamic specific surface area and the hydrodynamic specific volume were calculated from the slope and intercept, respectively, of the resulting plot. In calculating the hydrodynamic specific surface area, the Kozeny factor was assumed to have a value of 5.55 as suggested by Fowler and Hertel (12).

A typical example of the flow rate-pressure drop data obtained on the thick mats is presented in Fig. 19. These data are plotted according to Equation (25) in Fig. 20. The data presented in Fig. 19 and 20 were collected on a specimen with a basis weight of approximately 2300 g./sq. m. which was couched and wet pressed at 10 p.s.i. It can be seen from Fig. 19 that the permeability data are in excellent agreement with Darcy's law. Also, the data presented in Fig. 20

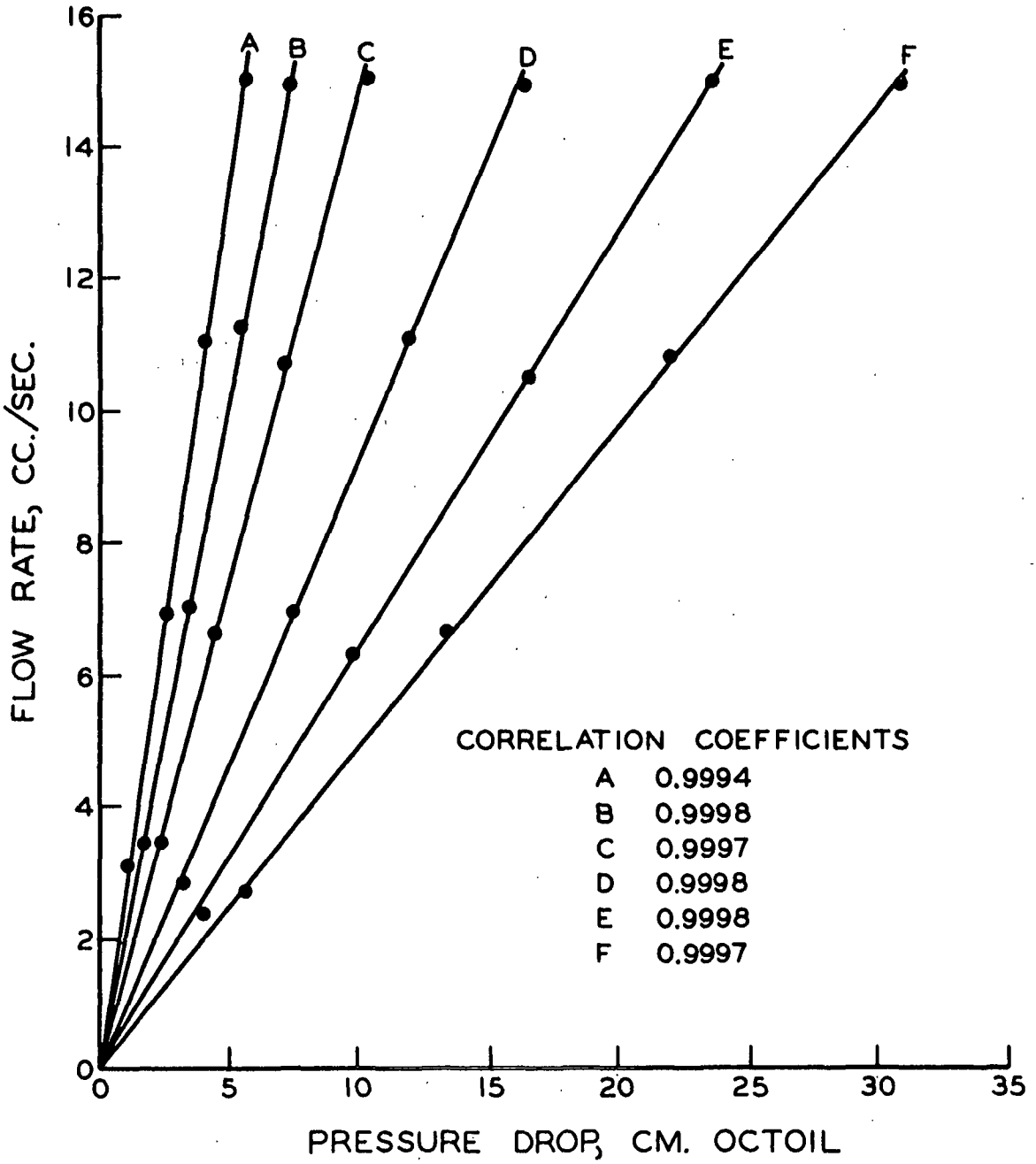

Figure 19. Typical Flow Rate-Pressure Drop Plots for Thick Mats

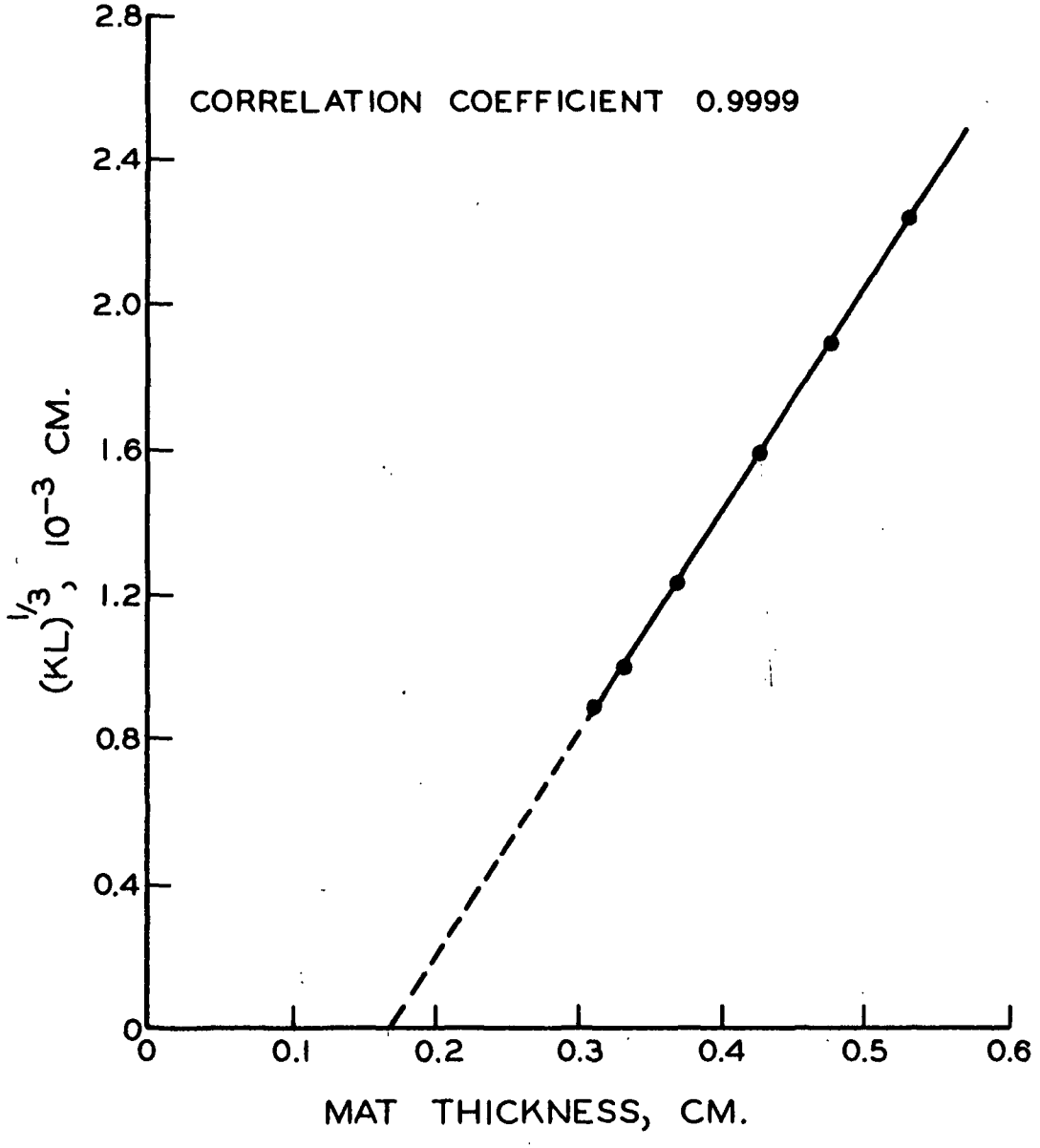

Figure 20. Typical Plot of Mat Permeability Data According to Equation (19)

agree quite well with Equation (19). These results are typical of those obtained in the mat permeability tests. In view of the excellent agreement of the data with Darcy's law, only the permeability coefficients and specimen thicknesses will be reported in this thesis. Appendix II contains all of the pertinent air permeability data collected on the thick mats tested during this study.

A number of preliminary tests were conducted to insure that the mat permeability cell was operating properly. In order to determine whether the guard ring arrangement in the mat permeability cell was functioning correctly, a number of tests were conducted in which the flow rates through both the guard-ring area and the test area were measured. If the guard ring was to function properly, it was necessary that the pressure gradient through the mat be the same in the test area and in the guard ring. If this condition was met and if the mat structure was homogeneous, the superficial velocity through the guard-ring area and the test area should be the same. The results of the preliminary tests indicated that this condition was met within $\pm$ 10%. These results led to the conclusions that (1) the compaction of the mat was uniform across the specimen surface, and (2) the leakage of the permeating fluid around the edges of the test specimen was not excessive.

Another way in which the guard ring could produce erroneous results is in the balance of the pressure between the guard ring and the test area. A series of tests were conducted in which the guard-ring pressure was purposely unbalanced to varying degrees. The results of these tests indicated that, within the accuracy with which these pressures could be controlled, the error in the measured pressure drop across the specimen was less than 2%.

In order to select a basis weight at which to conduct the mat permeability tests, three mats were prepared containing 15, 30, and 40 grams of pulp. These

mats were prepared in the usual manner and were couched and wet pressed at 10 p.s.i., using the procedures described earlier. Three specimens from each of these mats were then subjected to permeability tests. The results of these tests are presented in Table VIII.

TABLE VIII

EFFECT OF BASIS WEIGHT ON MAT PERMEABILITY COEFFICIENTS

Compacting Pressure, p.s.i.	Permeability Coefficient, K, 10^{-8} sq.cm.			
Test specimen	A	B	C	Average
Mat M-10(15)-1	(Average basis weight = 1200 g./sq. m.)			
215	1.743	1.635	2.089	1.822
340	1.265	1.136	1.402	1.268
500	0.871	0.830	0.986	0.896
780	0.528	0.505	0.591	0.541
1090	0.365	0.348	0.388	0.367
1405	0.260	0.248	0.285	0.268
Mat M-10(30)-4	(Average basis weight = 2350 g./sq. m.)			
215	2.250	2.141	2.119	2.162
340	1.413	1.442	1.491	1.449
465	0.971	0.948	1.018	0.979
780	0.514	0.509	0.553	0.525
1060	0.341	0.317	0.347	0.335
1395	0.232	0.227	0.222	0.227
Mat M-10(40)-4	(Average basis weight = 3200 g./sq. m.)			
215	1.788	2.499	2.086	2.124
340	1.117	1.692	1.442	1.417
465	0.873	1.073	0.957	0.968
780	0.466	0.582	0.499	0.519
1090	0.309	0.352	0.342	0.334
1375	0.209	0.225	0.218	0.217

The variations in permeability coefficients among the test specimens of a given mat make it difficult to draw any definite conclusions from the data of Table VIII. However, it does appear that there is no significant difference in the permeability coefficients of the 30- and 40-gram mats when compared at the same level of compacting pressure. The anomalous results obtained on the 15-gram

mat are attributed to errors in measuring the thickness of this thinner mat. On the basis of the results presented in Table VIII, 2300 g./sq. m. (30 grams of ovendry pulp in a 5-inch diameter mat) was selected as the basis weight at which to conduct the mat permeability tests.

Several additional thick mats were formed at a basis weight of approximately 2300 g./sq. m., and these mats were wet pressed at 25, 50, 75, and 100 p.s.i. Three specimens were cut from each mat, and these were subjected to permeability tests as previously described. The pertinent permeability properties calculated from the data collected in these tests are summarized in Table IX. The apparent densities and initial porosities recorded in Table IX were calculated from the initial specimen thickness, i.e., the thickness under a load of 0.1 p.s.i.

From the results recorded in Table IX, it is seen that the apparent density of the mats increased and the initial porosity and hydrodynamic specific volume decreased as the wet pressure applied to the mat was increased. These results were expected. However, the increase in the hydrodynamic specific surface area with increasing wet pressure is contrary to what one would expect. It would be anticipated that the surface area exposed to flow should decrease as the mat becomes more dense because of the increased bonding between the fibers in the structure.

As mentioned above, the results recorded in Table IX indicate a regular decrease in the hydrodynamic specific volume until, at a wet pressure of about 100 p.s.i., the calculated specific volume is nearly equal to the reciprocal of the pycnometric density of solid cellulose. These results suggest that a progressive collapse of the fibers occurs as the wet pressure is increased. This fiber collapse may also be responsible for the observed increase in the calculated hydrodynamic specific surface area as the wet pressure applied to the mat is increased.

TABLE IX

EFFECT OF WET PRESSURE ON MAT PERMEABILITY PROPERTIES

Specimen:	A	B	C	Average
		Mat M-10(30)-4		
$\underline{S_w}$, sq. cm./g.	3592	3761	3711	3688
$\underline{v}$, cc./g.	0.724	0.726	0.717	0.722
ρ_b, g./cc.	0.315	0.317	0.322	0.318
Initial porosity	0.772	0.769	0.769	0.770
		Mat M-25(30)-4		
$\underline{S_w}$, sq. cm./g.	3940	3843	4000	3928
$\underline{v}$, cc./g.	0.679	0.700	0.690	0.690
ρ_b, g./cc.	0.369	0.369	0.368	0.369
Initial porosity	0.739	0.741	0.746	0.742
		Mat M-50(30)-3		
$\underline{S_w}$, sq. cm./g.	4145	4321	4061	4176
$\underline{v}$, cc./g.	0.678	0.659	0.664	0.667
ρ_b, g./cc.	0.431	0.438	0.435	0.435
Initial porosity	0.708	0.712	0.711	0.710
		Mat M-75(30)-4		
$\underline{S_w}$, sq. cm./g.	4086	4122	4054	4091
$\underline{v}$, cc./g.	0.645	0.672	0.637	0.651
ρ_b, g./cc.	0.465	0.462	0.463	0.463
Initial porosity	0.700	0.689	0.705	0.698
		Mat M-100(30)-3		
$\underline{S_w}$, sq. cm./g.	4233	--	4268	4250
$\underline{v}$, cc./g.	0.640	--	0.643	0.641
ρ_b, g./cc.	0.506	--	0.514	0.510
Initial porosity	0.676	--	0.670	0.673

In the Kozeny-Carman equation, the resistance to flow is related directly to the square of the surface area exposed to flow if the Kozeny factor is assumed to be constant. As the fibers collapse, it is anticipated that the fiber cross section changes from a more or less circular shape to a flat, elliptical, or rectangular shape. An array of flat, ribbonlike fibers would probably offer more resistance to flow at a given porosity than an assemblage of cylinders. In terms of the Kozeny-Carman theory, these changes would be manifested in a higher value of the Kozeny factor. Conversely, if the Kozeny factor is assumed to remain constant as was the case in these studies, the calculated hydrodynamic surface area would increase as the fibers collapse more and more.

In order to test the validity of these assumptions, the effect of fiber shape on the Kozeny factor was investigated. The three fiber shapes used in this study were: (1) a 15-denier nylon which had a cylindrical cross section, (2) a 10-denier orlon which had a "dog-bone" cross section, and (3) a flattened 15-denier nylon which was approximately elliptical in cross section. The preparation and characterization of these synthetic fibers has been described earlier. The pycnometric densities and fiber length data of these fibers are recorded in Table X. The experimental values of fiber density on the nylon and orlon are in good agreement with those quoted by the manufacturer (1.14 and 1.16 g./cc., respectively). As expected, the fiber length distributions of the nylon fibers were very narrow, while that of the orlon fibers was quite broad. For purposes of comparison, the fiber length data obtained on the classified pulp used in this study is also presented in Table X.

Traces were prepared from the photomicrographs of Fig. 18 at a magnification of 750 diameters, and these were used to measure the surface areas of the fibers. The cross-sectional areas of the fibers were measured with a planimeter, and the

fiber perimeters were measured with a map reader. In addition, the axis ratio (ratio of maximum to minimum dimension) of the noncylindrical fibers and the diameter of the cylindrical fibers were recorded. Fifty sections were measured for each fiber shape. The results of these measurements, together with the calculated surface areas are summarized in Table XI.

TABLE X

FIBER LENGTH AND PYCNOMETRIC DENSITIES OF SYNTHETIC FIBERS

Fiber	Number of Fibers Measured	Fiber Lengths Arithmetic Av., mm.	Fiber Lengths Weighted Av., mm.	Pycnometric Density, g./cc.
Round nylon	339	4.12	4.13	1.145
Flattened nylon	341	4.37	4.38	1.141
Orlon	598	1.98	2.57	1.158
Bleached sulfite pulp	538	2.18	2.48	--

The data of Table XI may offer a logical, yet deceptively simple, effect which might influence the surface area of pulp fibers. An examination of the data on the nylon fibers reveals that while the cross-sectional area of the fiber did not change upon flattening, the perimeter increased by about 21%. This, of course, resulted in a corresponding increase in the surface area of the fiber as it was flattened. That the cross-sectional area of the fibers did not change is also shown by the equivalence of the pycnometric densities for the round and flattened nylon (see Table X).

These results are quite logical when it is recalled that a circular shape represents the minimum perimeter-to-area ratio of any geometrical shape. The magnitude of this effect is easily demonstrated by calculating the perimeter of an ellipse with unit cross-sectional area and varying axis ratios. The results of such a calculation are presented in Table XII.

TABLE XI

SURFACE AREAS OF SYNTHETIC FIBERS

Property	Arithmetic Av.	Surface Weighted Av.
Round Nylon		
Cross-sectional area, 10^{-5} sq. cm.	1.753 (0.081)[a]	1.757
Perimeter, 10^{-2} cm.	1.578 (0.046)	1.579
Surface area, sq. cm./cc.	900.9 (20.7)	901.2
Fiber diameter, μ	47.41	--
Flattened Nylon		
Cross-sectional area, 10^{-5} sq. cm.	1.742 (0.110)	1.749
Perimeter, 10^{-2} cm.	1.910 (0.087)	1.914
Surface area, sq. cm./cc.	1098 (43.7)	1100
Axis ratio	2.91	--
Orlon		
Cross-sectional area, 10^{-5} sq. cm.	1.039 (0.077)	1.044
Perimeter, 10^{-2} cm.	1.575 (0.073)	1.578
Surface area, sq. cm./cc.	1520 (59.0)	1522
Axis ratio	4.14	--

[a]The numbers in parentheses refer to the standard deviations of the measurements.

TABLE XII

FLATTENING OF AN ELLIPSE

Axis Ratio[a]	Perimeter of Ellipse	Perimeter Ratio[b]
1.0	3.554	1.00
1.2	3.567	1.01
1.4	3.620	1.02
1.6	3.691	1.04
1.8	3.774	1.06
2.0	3.865	1.09
2.4	4.056	1.14
2.8	4.254	1.20
3.2	4.452	1.26
3.6	4.667	1.31
4.0	4.839	1.37
4.5	5.073	1.43
5.0	5.301	1.50
6.0	5.735	1.62
7.0	6.144	1.73
8.0	6.531	1.84
9.0	6.899	1.95
10.0	7.250	2.05

[a]Ratio of major to minor axis of the ellipse.

[b]Ratio of the perimeter on an ellipse of the given axis ratio to that of a circle of the same cross-sectional area.

The results recorded in Table XII indicate that if a circular fiber is flattened into an elliptical shape with an axis ratio of approximately 9.5, while maintaining the cross-sectional area of the fiber constant, the surface area would be doubled. It is doubtful if the increase in surface area demonstrated in Table XII is of sufficient magnitude to account for the increase in the hydrodynamic specific surface area found in the permeability studies on thick mats for a number of reasons:

(1) It is probable that this effect would occur primarily, if not exclusively, in the summerwood fibers since it is generally felt that surface tension forces alone are sufficient to completely collapse a thin-walled springwood fiber.

(2) The data presented in Table XII are for a solid cross section, whereas pulp fibers contain a lumen, and therefore the increase in surface area would be correspondingly less for pulp fibers.

(3) The cross-sectional area of the pulp fibers did not remain constant as the wet pressure was increased, as shown by the decrease in the hydrodynamic specific volume of the pulp fibers.

In spite of these arguments, it is felt that the flattening of wood pulp fibers could produce an increase in surface area. Furthermore, this effect is probably of sufficient magnitude that it cannot be ignored altogether. For example, the data of Table XII indicate that for a solid cross section a change in the axis ratios from 4.5 to 7.0 results in an increase of about 21% in the surface area.

In an effort to establish the effect of fiber shape on the Kozeny factor, the synthetic fibers previously described were subjected to water permeability tests. The Kozeny factors were calculated from the Kozeny-Carman equation,

using the porosities calculated from Equation (16) and the surface-weighted average surface areas from Table XI. The surface areas of the flattened nylon and the orlon fibers were corrected for area in contact as described earlier. The results obtained for the round nylon, the flattened nylon, and the orlon fibers are presented in Tables XIII, XIV, and XV, respectively. These results are also plotted as a function of porosity in Fig. 21. For purposes of comparison, the empirical correlation of Ingmanson, et al. (18) [Equation (20)] for cylindrical fibers is also plotted in Fig. 21.

It can be seen from Fig. 21 that the data for the round nylon fibers fit the empirical correlation of Ingmanson, et al. (18) quite well. However, the data for the flattened nylon and the orlon fibers do not follow this relationship. For these fibers the corrected values of the Kozeny factor are significantly higher than those for cylindrical fibers, particularly at the lower porosities. Furthermore, the corrected Kozeny factors are higher for the orlon fibers than for the flattened nylon fibers at a given porosity. Since the orlon fibers had a higher axis ratio (i.e., they were flatter) than the flattened nylon fibers, these results are in qualitative agreement with the hypothesis proposed to explain the increase in calculated surface area found in the studies of thick mats of wood pulp fibers.

While the results recorded in Tables XIV and XV must be considered only approximate because of the assumptions made in correcting for the area of contact between fibers, the data obtained are not at all unreasonable. For example, several data reported in the literature (60, 61) for the relative bonded area of classified wood pulp fibers compare quite favorably with the percentage of area in contact calculated for the flattened nylon and the orlon fibers investigated in this study. It is felt that the data obtained in this study are

TABLE XIII

CALCULATED KOZENY FACTORS FOR ROUND NYLON FIBERS

Compacting Pressure,[a] cm. water	Porosity	Kozeny Factor
8.0	0.930	11.32
13.0	0.917	10.32
23.0	0.905	8.71
38.0	0.897	8.31
63.0	0.884	7.49
97.6	0.871	7.20
147.5	0.860	6.89
~~300~~ 350	0.846	6.41
575	0.829	6.15
1275	0.809	5.95
2100	0.785	5.74
3450	0.764	5.52
4700	0.748	5.36
6500	0.733	5.48

[a]These same mechanical compacting pressures were used in the permeability tests on the flattened nylon and the orlon fibers.

TABLE XIV

CALCULATED KOZENY FACTORS FOR FLATTENED NYLON FIBERS

Porosity	Percentage of Area in Contact	Corrected Area,[a] sq. cm./cc.	Kozeny Factors	
			Corrected[a]	Uncorrected[b]
0.885	6.6	1021	8.60	7.41
0.867	7.7	1009	7.95	6.69
0.849	8.8	997	7.57	6.22
0.834	9.7	988	7.35	5.93
0.805	11.3	970	6.90	5.36
0.782	12.7	955	6.87	5.18
0.761	13.9	942	6.83	5.01
0.748	14.6	934	6.88	4.96
0.705	17.1	906	7.10	4.82
0.676	18.9	887	7.18	4.63
0.643	20.8	867	7.28	4.52
0.615	22.4	848	7.27	4.33
0.593	23.7	835	7.34	4.23
0.571	24.9	821	7.36	4.10

[a]Corrected for area of fiber-to-fiber contact.

[b]Calculated assuming point contact between fibers.

TABLE XV

CALCULATED KOZENY FACTORS FOR ORLON FIBERS

Porosity	Percentage of Area in Contact	Corrected Area,[a] sq. cm./cc.	Kozeny Factors	
			Corrected[a]	Uncorrected[b]
0.930	5.4	1430	9.41	8.30
0.925	5.8	1424	9.09	7.95
0.917	6.4	1414	8.78	7.58
0.909	7.1	1404	8.59	7.32
0.899	7.8	1394	8.41	7.05
0.889	8.6	1382	8.22	6.77
0.876	9.6	1367	8.04	6.48
0.853	11.4	1340	7.78	6.03
0.828	13.3	1310	7.76	5.75
0.799	15.6	1276	7.93	5.57
0.768	18.0	1240	8.13	5.40
0.740	20.1	1207	8.27	5.21
0.718	21.8	1182	8.45	5.09
0.695	23.7	1154	8.65	4.97

[a]Corrected for area of fiber-to-fiber contact.

[b]Calculated assuming point contact between fibers.

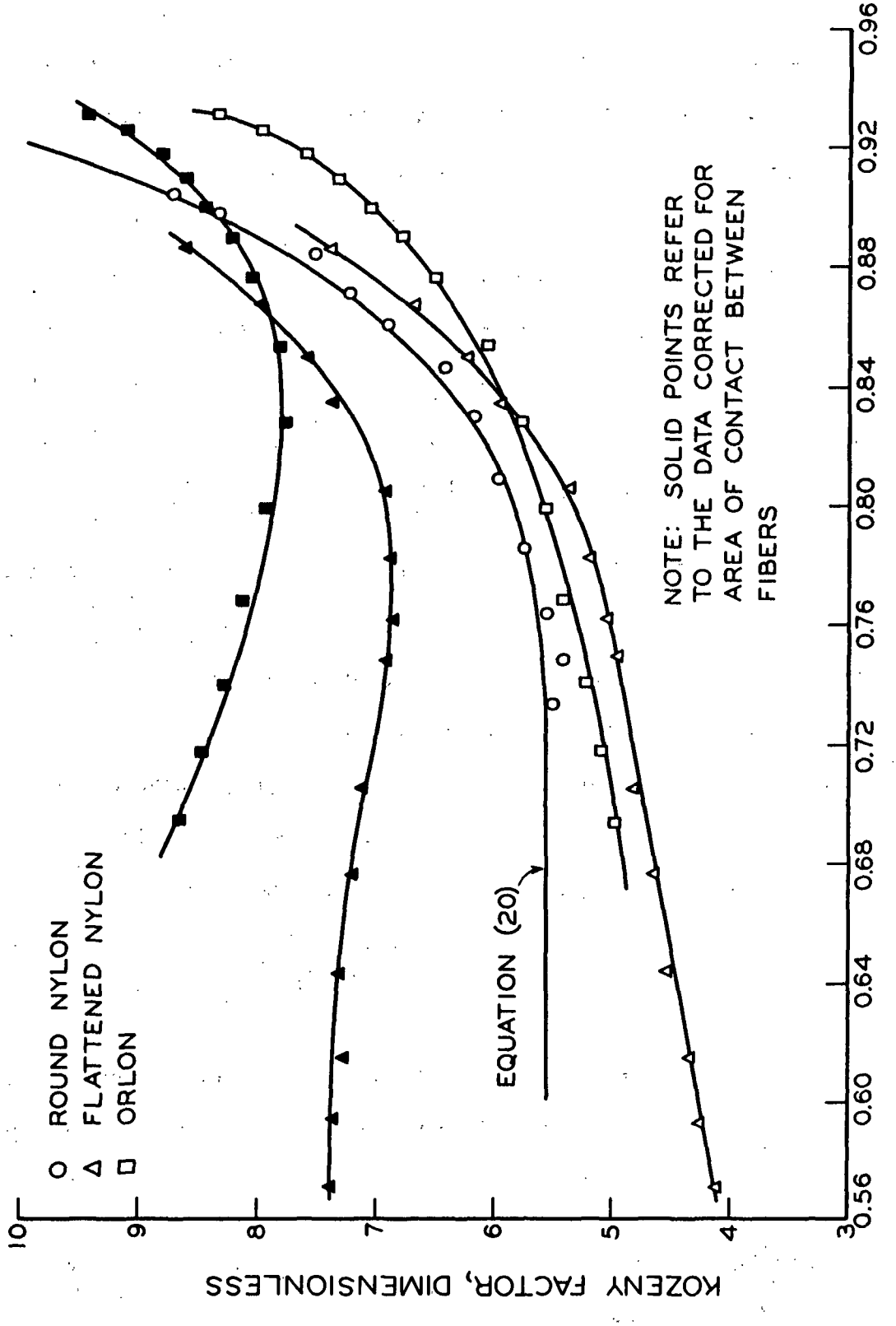

Figure 21. Variation of Kozeny Factor with Fiber Shape

sufficiently reliable to show that there is a definite effect of fiber shape on the Kozeny factor. The data of Wyllie and Gregory (11) recorded in Table II would also support this conclusion.

From the permeability studies on thick mats, it must be concluded that the Kozeny-Carman equation does apply to these structures over a porosity range from about 0.77 to 0.46.* This conclusion is based on the fact that the permeability data could be fitted to Equation (19) with a high degree of correlation. However, this method of analyzing the permeability data says nothing about the value of the Kozeny factor. From the water permeability tests on synthetic fibers, it is apparent that while a value of Kozeny factor of 5.55 may be realistic for flow through a bed of cylindrical fibers in the porosity range from 0.6 to 0.8, a much higher value is applicable to dried cellulose fibers.

In reality, the surface area exposed to flow in the thick mats tested is probably influenced by at least three effects:

(1) The actual exposed surface area is decreased by increased bonding as the mat is wet pressed at higher pressures,

(2) The actual surface area may be increased by a progressive collapse of the fibers as found in the tests on flattened nylon fibers, and

(3) The calculated surface area computed from a Kozeny-type equation is increased by some unknown amount because of the effect of fiber shape on the Kozeny factor.

It has not been possible in the present study to separate the contributions of the effects listed above, and the hydrodynamic specific surface areas reported in Table IX must be considered to be, at best, only a rough estimate of the actual

*The initial porosity of the mats wet pressed at 10 p.s.i. was approximately 0.77, while the lowest porosity reached during the compaction of the mats in the permeability tests was about 0.46.

area exposed to flow in the thick mats. However, the values of the hydrodynamic specific volume computed from Equation (19) are not dependent on the value selected for the Kozeny factor and, in view of the excellent agreement between the data and Equation (19), these results are considered to be quite reliable.

POROUS PROPERTIES OF HANDSHEETS

One of the objectives of this thesis was to measure the permeability characteristics and the pore size distribution on carefully prepared handsheets. The details of the experimental techniques used in this study have been presented earlier. A number of preliminary experiments were conducted in order to test the experimental methods used in this study. It will be recalled that a mercury head of 0.204 inch (compacting pressure of 0.1 p.s.i.) was arbitrarily selected as the conditions for measuring the handsheet thickness by the mercury capacitance method. Since it is well known that paper is a compressible material, it seemed advisable to determine the effect of the mercury head above the sheet on the calculated sheet thickness.

A handsheet (basis weight = 97 g./sq. m.) was formed and dried in the usual manner, and the sheet was placed in the mercury condenser (see Fig. 13 and 14). The capacitance of the condenser was then measured at several levels of mercury head above the test specimen. The results of these tests are recorded in Table XVI.

The data of Table XVI were fitted to an empirical equation of the form: thickness = $\underline{A}(\text{head})^{\underline{B}}$. The calculated exponent was -0.034, indicating only a slight dependence of sheet thickness on compacting pressure in the range of compacting pressures investigated. Examination of the data recorded in Table XVI indicated that doubling the mercury head (from 0.2 to 0.4 inch) decreased the

calculated sheet thickness by only 2%. These considerations and the data of Table XVI seemed to justify the use of an arbitrary mercury head of 0.204 inch in the handsheet thickness tests.

TABLE XVI

EFFECT OF MERCURY HEAD ON HANDSHEET THICKNESS

Mercury Head, in.	Compacting Pressure, p.s.i.	Capacitance, μμfarads	Thickness, 10^{-2} cm.
0.20	0.100	450	2.765
0.25	0.125	459	2.739
0.30	0.150	461	2.734
0.35	0.175	465	2.723
0.40	0.200	470	2.709
0.45	0.225	476	2.693
0.50	0.250	480	2.683

One of the basic assumptions which must be made in the use of the gas-drive technique for measuring pore size distribution is that only laminar flow is occurring during the test. The following experiments were conducted to check this assumption.

A relatively thick handsheet (basis weight = 142 g./sq. m.) was formed and dried in the usual manner. After the sheet thickness had been determined, the test specimen was clamped in the handsheet permeability cell. A normal handsheet permeability test was then conducted with the cell pressure maintained at 100 p.s.i. The sheet was then removed from the permeability test and was clamped in the gas-drive test cell, where a permeability test was conducted on the same area of the specimen. No hexyl alcohol was applied to the sheet for this test.

By using a thicker specimen and measuring the pressure drop across the gas-drive cell with a cathetometer, reasonable accuracy was achieved. The flow rate-pressure drop data obtained in these tests, together with the permeability coefficients from Darcy's law ($\underline{K}$), are recorded in Table XVII.

TABLE XVII

CHECK FOR LAMINAR FLOW IN THE GAS-DRIVE TEST

Permeability Cell		Gas-Drive Cell	
Flow Rate, cc./sec.	Pressure Drop, dynes/sq. cm.	Flow Rate, cc./sec.	Pressure Drop, dynes/sq. cm.
5.85	66.7	64.2	815
10.3	116	113	1340
15.2	172	114	1715
18.5	207	180	2180
21.6	242	216	2530
25.0	285	251	3025
28.4	327	280	3370
31.4	362	307	3690
35.0	404	345	4160
39.1	457	369	4450
$\underline{K} = 1.361 \times 10^{-8}$ sq. cm.		$\underline{K} = 1.392 \times 10^{-8}$ sq. cm.	

Since the above data plot as straight lines with quite high correlation coefficients, and since the calculated permeability coefficients differ by only 2.3%, it may be concluded that laminar flow occurred in both tests.

Another, though perhaps less desirable, method for testing for laminar flow is found by calculating a Reynolds number for flow through the sheet.

Collins (62) has suggested the following equation for the Reynolds number of porous materials,

$$Re = (Q\rho/\eta A\epsilon)\cdot(K/\epsilon)^{1/2} \qquad (86)$$

In the above equation, Re is the Reynolds number of a porous medium of area A, porosity ϵ, and permeability coefficient K. The flow rate, Q, density, ρ, and viscosity, η, all refer to the permeating fluid. A Reynolds number was calculated from Equation (86) using the following data, which were obtained on the specimen used in the previous tests:

$Q = 400$ cc./sec.

$\rho = 1.25 \times 10^{-3}$ g./cc.

$\eta = 1.763 \times 10^{-4}$ poises

$A = 45.6$ sq. cm.

$\epsilon = 0.762$

$K = 1.361 \times 10^{-8}$ sq. cm.

The calculated Reynolds number was 1.09×10^{-2}, and is well below the critical value of 1.0 (62). Since the flow rate used in the above calculation represents the maximum used in the gas-drive tests, it must again be concluded that the flow in the gas-drive test was laminar as required.

To calculate the pore size distribution from gas-drive data, it is necessary to know the surface tension of the wetting liquid used in the test. Since such data are not available in the literature for hexyl alcohol, the surface tension and density of technical-grade n-hexyl alcohol was determined as a function of temperature from 20 to 25°C. The surface tension was determined by the method of capillary rise, using two capillaries of unequal size as suggested by Glasstone (63). By using two capillaries in the liquid instead of just one,

the problems of measuring the liquid height in a large container is avoided, thereby improving the accuracy of the measurements. The heights of rise were carefully measured with a cathetometer and the densities were determined pycnometrically. The capillaries were calibrated with water which was prepared by distillation from an alkaline permanganate solution in a closed system to eliminate contamination by surface-active agents. The measurements were carried out with the hexyl alcohol contained in a large test tube which was suspended in a constant-temperature water bath. The temperature of the water bath was controlled within ± 0.02°C. by means of a mercury switch-electronic relay system. All tests were conducted in triplicate, and the results are summarized in Table XVIII.

TABLE XVIII

SURFACE TENSION AND DENSITY OF n-HEXYL ALCOHOL

Temperature, °C.	Surface Tension, dynes/cm.	Density, g./cc.
20.00	24.42	0.8182
21.00	24.23	0.8179
22.00	24.08	0.8176
23.00	23.91	0.8174
24.00	23.78	0.8169
25.00	23.64	0.8166

Since the surface tension values recorded in Table XVIII are somewhat higher than those reported by Sanborn (25), it was considered advisable to check the method used against known data. Accurate data are available in the literature (64) for benzene, and this liquid was chosen to check the experimental techniques. The data obtained on purified benzene corresponded to a

surface tension of 28.95 dynes/cm. and a pycnometric density of 0.878 g./cc. at a temperature of 20°C. The surface tension of benzene quoted in the literature (64) is 29.02 ± 0.03 dynes/cm. The lower surface tension found experimentally may be due, in part, to difficulties encountered in obtaining an accurate density because of the rapid evaporation of the benzene. If the literature value was taken for the density of benzene, the calculated surface tension of benzene was 29.00 dynes/cm. In any event, the experimental values compare quite favorably with the literature values and it was concluded that the surface tension data on hexyl alcohol are accurate.

The reproducibility of the handsheet permeability and pore size distribution tests was determined by conducting duplicate tests on a single specimen. A 100-g./sq. m. handsheet was formed, couched, and wet pressed at 25 p.s.i. in the usual manner and was subjected to a mercury capacitance test to determine the sheet thickness. The specimen was then clamped in the permeability cell, and a normal permeability test was conducted at a cell pressure of 100 p.s.i. The nitrogen flow was then shut off for a few minutes, and a second series of flow rate-pressure drop readings were taken without removing the specimen from the permeability cell. The same general procedure was used in testing the reproducibility of the gas-drive test. A summary of the calculated results from these tests is presented in Tables XIX and XX. For purposes of comparison, the hydrodynamic specific surface areas reported in Table XIX were calculated using a Kozeny factor of 5.55.

From the results presented in Table XIX, it can be seen that handsheet permeability tests were reproducible within less than 2%. Also, from the least squares fit of the data to a straight line, it is apparent that the agreement of data with Darcy's law was excellent. In view of this agreement, only the

permeability coefficients and the calculated porous properties of the handsheets will be reported in this thesis.

TABLE XIX

REPRODUCIBILITY OF HANDSHEET PERMEABILITY TEST

Property	Test 1	Test 2	Difference, %
Porosity[a]	0.763	0.763	--
Apparent density, g./cc.[a]	0.333	0.333	--
Thickness, cm.[a]	0.0306	0.0306	--
Exposed surface area, sq. cm./g.	7088.4	7142.4	0.76
Permeability coefficient, 10^{-8} sq. cm.	1.434	1.412	1.56
Least squares data:			
Slope	0.1211	0.1192	--
Intercept, cc./sec.	-0.125	0.289	--
Correlation coefficient	0.999	0.998	--

[a]The results reported for porosity, apparent density, and sheet thickness were calculated from the same data and are therefore the same for the two tests.

Several conclusions may be reached from the results presented in Table XX. The mean hydraulic radius and mean of the log normal distribution were reproducible within less than 1%, while the standard deviation of pore size and the standard deviation of the log normal distribution were reproducible within less than 3%. These results indicate that the sample was not damaged during the tests and that the surface tension of the n-hexyl alcohol was not changed by contact with the paper.

A slight increase in the third and fourth moments of the distribution was noted in the second test. However, the skewness and kurtosis are not statistically

significant in either case, as shown by the low Student "t" values. In view of the extreme sensitivity of these moments to a few outlying points, the agreement with the log normal distribution function is excellent. The high correlation coefficients obtained in the least squares fit of the gas-drive data to the log normal distribution also indicate a high degree of correlation.

TABLE XX

REPRODUCIBILITY OF GAS-DRIVE TEST

Property	Test 1	Test 2	Difference, %
Based on the Data:			
$\underline{\bar{m}}$, μ	4.726	4.744	0.38
$\sigma_{\underline{m}}$, μ	1.071	1.089	1.68
$\underline{\bar{X}}$, dimensionless	-7.6571	-7.6534	0.05
$\sigma_{\underline{x}}$, dimensionless	0.1590	0.1608	1.13
Based on Least Squares Fit to Log Normal Distribution:			
$\underline{\bar{m}}$, μ	4.805	4.824	0.37
$\underline{\bar{X}}$, dimensionless	-7.6405	-7.6367	0.05
$\sigma_{\underline{x}}$, dimensionless	0.1548	0.1593	2.90
Correlation coefficient	0.996	0.997	--
Moments of the Distribution About the Mean:			
Third	-0.064	-0.030	--
Fourth	2.558	2.643	--
Student "t" Test:			
Skewness	-0.149	-0.070	--
Kurtosis	-0.303	-0.186	--

The methods used in calculating the parameters of the pore size distribution from the gas-drive data and the method of fitting the pore size distribution data to the log normal curve are presented in detail in Appendix I. Because of the excellent fit of the pore size distribution data to the log normal distribution, only the properties of the distribution curve will be reported hereinafter.

The results reported in Tables XIX and XX are typical of those obtained in this study. For all specimens tested, the pore size distribution data agreed very well with the log normal distribution and in no case was the skewness or kurtosis statistically significant. The correlation coefficients from the least squares fit of data to the log normal distribution varied from 0.991 to 0.999.

In presenting the results obtained in the studies on thin handsheets, it is convenient to divide the study into two parts. The effect of basis weight on the permeability and pore size distribution properties of paper will be discussed first. This will be followed by the results obtained in the study on the effect of the wet pressure applied to sheets on these properties.

EFFECT OF BASIS WEIGHT ON THE POROUS PROPERTIES OF PAPER

It was not the purpose of this thesis to investigate all of the variables which might affect the porous properties of paper. However, rather than arbitrarily select a basis weight at which to conduct the tests, it was considered advisable to investigate the effect of basis weight on the permeability and pore size distribution properties of paper.

A series of handsheets were prepared in the normal manner covering a basis weight range from about 50 to 175 g./sq. m. These sheets were all couched at a

pressure of 10 p.s.i. and were wet pressed at a pressure of 25 p.s.i. After the usual capacitance tests for sheet thickness, the specimens were subjected to permeability and gas-drive tests. A number of specimens (usually three) were tested at each level of basis weight. The results of the permeability tests are recorded in Table XXI. The values recorded in Table XXI for the hydrodynamic specific surface area, $\underline{S}_w$, were calculated assuming a value of 5.55 for the Kozeny factor.

The porosities of these sheets were calculated from

$$\epsilon = 1 - v\rho_b \tag{87}$$

where $\underline{v}$ is the hydrodynamic specific volume of the fibers and ρ_b is the apparent density of the sheet. The specific volume was taken from a plot of $\underline{v}$ versus apparent density obtained in the mat permeability tests. This plot is shown in Fig. 22. The assumption was made that this relationship was also applicable to the thin handsheets prepared from the same pulp.

From the results presented in Table XXI, it can be seen that there is a considerable variation between test specimens at a given basis weight, particularly with respect to the permeability coefficient. Since the handsheet permeability test was found to be reproducible within less than 2%, it must be concluded that a real difference in porous structure exists between test specimens. Further analysis of the permeability data reveals that the permeability coefficients for the individual test specimens vary as much as 20% from the average of all tests. However, this variation may be accounted for, to a large extent, by the slight variations in the porosity of the specimens. Since the maximum variation in porosity between test specimens was only about 2%, this points up the importance which the porosity plays in determining the permeability of a sheet of paper.

TABLE XXI

EFFECT OF BASIS WEIGHT ON PERMEABILITY PROPERTIES OF HANDSHEETS

Property	Specimens A	B	C	Mean
H-25(50)-2 (Average basis weight = 52.4 g./sq. m.)				
$\underline{S}_w$, sq. cm./g.	7408	7165	7300	7291
ϵ, dimensionless	0.760	0.761	0.764	0.762
ρ_b, g./cc.	0.340	0.338	0.342	0.340
$\underline{K}$, 10^{-8} sq. cm.	1.254	1.355	1.361	1.323
H-25(75)-3 (Average basis weight = 67.8 g./sq. m.)				
$\underline{S}_w$, sq. cm./g.	7437	7205	7369	7337
ϵ, dimensionless	0.757	0.762	0.762	0.760
ρ_b, g./cc.	0.346	0.336	0.336	0.339
$\underline{K}$, 10^{-8} sq. cm.	1.186	1.374	1.325	1.295
H-25(75)-4 (Average basis weight = 79.2 g./sq. m.)				
$\underline{S}_w$, sqm. cm./g.	7400	7520	7559	7493
ϵ, dimensionless	0.756	0.757	0.758	0.757
ρ_b, g./cc.	0.347	0.344	0.342	0.344
$\underline{K}$, 10^{-8} sq. cm.	1.183	1.165	1.180	1.176
H-25(100)-6 (Average basis weight = 101.3 g./sq. m.)				
$\underline{S}_w$, sq. cm./g.	7111	7073	7088	7091
ϵ, dimensionless	0.764	0.756	0.763	0.761
ρ_b, g./cc.	0.331	0.346	0.331	0.337
$\underline{K}$, 10^{-8} sq. cm.	1.455	1.297	1.434	1.395

TABLE XXI (Continued)

EFFECT OF BASIS WEIGHT ON PERMEABILITY PROPERTIES OF HANDSHEETS

Property	Specimens A	B	C	Mean
H-25(100)-5 (Average basis weight = 118.5 g./sq. m.)				
$\underline{S}_w$, sq. cm./g.	7103	7174	7442	7240
ϵ, dimensionless	0.760	0.767	0.766	0.764
ρ_b, g./cc.	0.341	0.329	0.331	0.334
$\underline{K}$, 10^{-8} sq. cm.	1.356	1.479	1.366	1.400
H-25(150)-5 (Average basis weight = 147.8 g./sq. m.)				
$\underline{S}_w$, sq. cm./g.	7254	6923	--	7089
ϵ, dimensionless	0.766	0.759	--	0.763
ρ_b, g./cc.	0.326	0.341	--	0.333
$\underline{K}$, 10^{-8} sq. cm.	1.449	1.410	--	1.430
H-25(150)-3 (Average basis weight = 176.2 g./sq. m.)				
$\underline{S}_w$, sq. cm./g.	6993	7098	--	7030
ϵ, dimensionless	0.767	0.770	--	0.768
ρ_b, g./cc.	0.329	0.324	--	0.326
$\underline{K}$, 10^{-8} sq. cm.	1.572	1.591	--	1.582

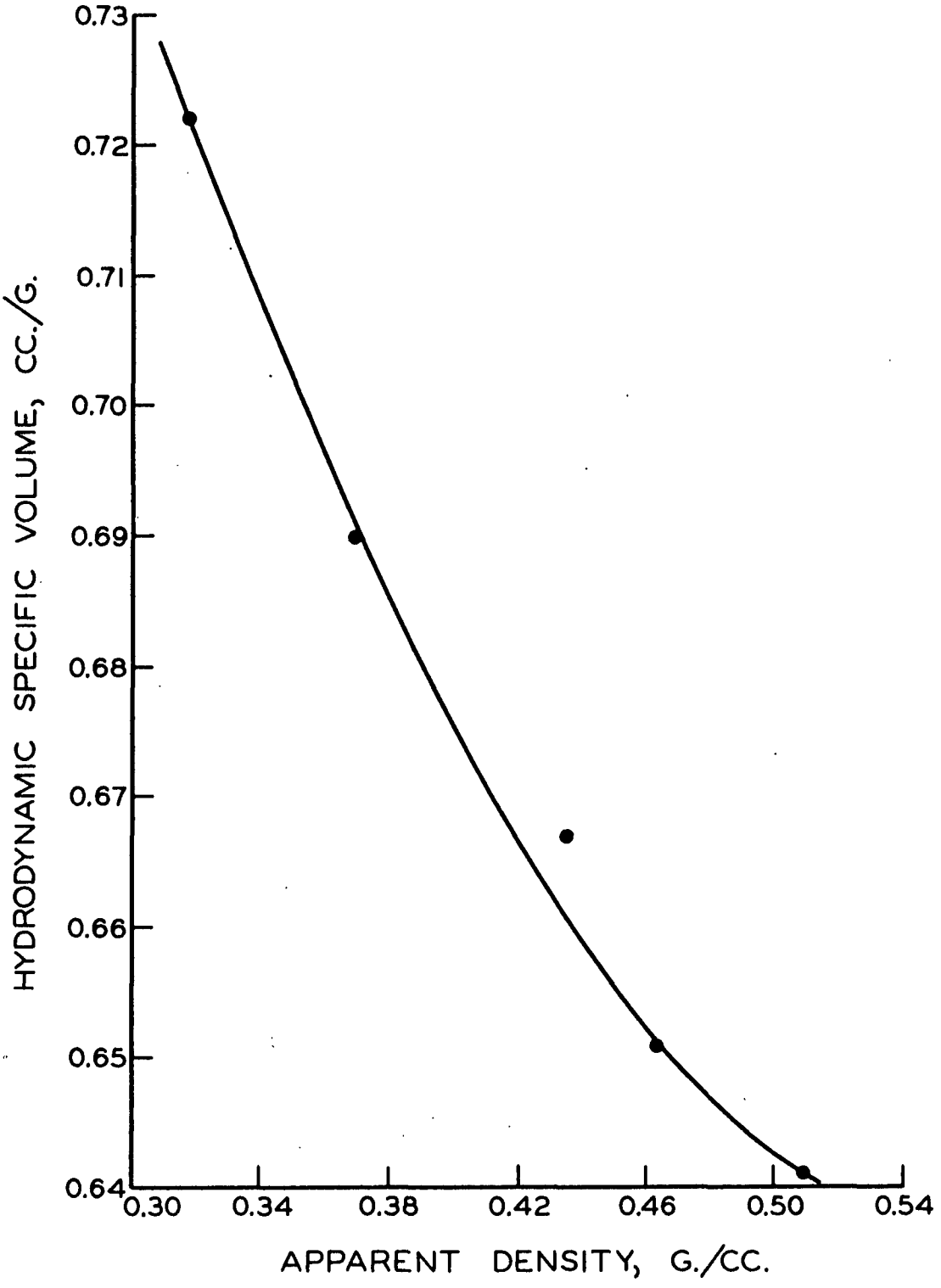

Figure 22. Relationship Between Hydrodynamic Specific Volume and Apparent Density (from Mat Permeability Study).

It is also apparent from the results presented in Table XXI that the hydrodynamic specific surface areas calculated by assuming a value of 5.55 for the Kozeny factor are much higher than those found in the studies on thick mats. These results support the contention of Sanborn (25) that the Kozeny-Carman equation is not applicable to thin handsheets of paper. While it is realized from the studies on flattened synthetic fibers that a Kozeny factor greater than 5.55 is applicable to these structures, it is seen that if k is assumed to have the same value for the mats and the thin handsheets, the calculated surface areas of the latter are higher by a factor of about 2.

The results of the gas-drive tests on these handsheets are summarized in Table XXII. In the interest of brevity, the computed moments of the distributions and the corresponding Student "t" values for skewness and kurtosis have been omitted from Table XXII. While there was some variation in these properties of the distributions, in no case did the pore size distribution curves exhibit statistically significant skewness or kurtosis.

An interesting result of the study on the effect of basis weight on the pore size distribution properties of paper is shown in Fig. 23. In this figure, it is seen that there is a definite relationship between the mean hydraulic radius determined from the gas-drive test and the standard deviation of the pore size distribution (expressed as a percentage of the mean). This indicates that, at a given wet pressure, the pores become smaller and the distribution of pore sizes becomes narrower as the basis weight is increased. Therefore, if the basis weight is increased to the levels used earlier in the permeability studies on thick mats, it is probable that the pore size distribution becomes quite narrow. In the thick mats, then, the concept of a mean hydraulic radius, upon which the Kozeny-Carman equation is based, is probably quite valid.

TABLE XXII

EFFECT OF BASIS WEIGHT ON PORE SIZE DISTRIBUTION PROPERTIES OF HANDSHEETS

Property	Specimens A	B	C	Mean
H-25(50)-2 (Average basis weight = 52.4 g./sq. m.)				
Based on the data:				
$\bar{m}$, μ	6.17	6.25	6.04	6.15
σ_m, μ	1.84	1.86	1.74	1.81
$\bar{X}$, dimensionless	-7.391	-7.378	-7.413	-7.394
σ_x, dimensionless	0.205	0.205	0.199	0.203
Based on least squares fit to log normal distribution:				
$\bar{m}$, μ	6.32	6.39	6.18	6.30
$\bar{X}$, dimensionless	-7.366	-7.355	-7.389	-7.370
σ_x, dimensionless	0.207	0.206	0.202	0.205
Correlation coefficient	0.998	0.999	0.997	--
H-25(75)-3 (Average basis weight = 67.8 g./sq. m.)				
Based on the data:				
$\bar{m}$, μ	5.24	5.35	5.36	5.32
σ_m, μ	1.37	1.40	1.41	1.39
$\bar{X}$, dimensionless	-7.555	-7.534	-7.531	-7.540
σ_x, dimensionless	0.181	0.182	0.182	0.182
Based on least squares fit to log normal distribution:				
$\bar{m}$, μ	5.37	5.44	5.49	5.43
$\bar{X}$, dimensionless	-7.529	-7.517	-7.508	-7.515
σ_x, dimensionless	0.177	0.184	0.180	0.180
Correlation coefficient	0.993	0.999	0.997	--

TABLE XXII (Continued)

EFFECT OF BASIS WEIGHT ON PORE SIZE DISTRIBUTION PROPERTIES OF HANDSHEETS

Property	Specimens A	B	C	Mean
H-25(75)-4 (Average basis weight = 79.2 g./sq. m.)				
Based on the data:				
$\bar{m}$, μ	4.81	4.81	4.92	4.85
σ_{m}, μ	1.20	1.18	1.25	1.21
$\bar{X}$, dimensionless	-7.640	-7.640	-7.616	-7.632
σ_{x}, dimensionless	0.174	0.171	0.176	0.174
Based on least squares fit to log normal distribution:				
$\bar{m}$, μ	4.90	4.88	5.02	4.93
$\bar{X}$, dimensionless	-7.622	-7.624	-7.598	-7.615
σ_{x}, dimensionless	0.174	0.174	0.181	0.178
Correlation coefficient	0.997	0.999	0.997	--
H-25(100)-6 (Average basis weight = 101.3 g./sq. m.)				
Based on the data:				
$\bar{m}$, μ	4.70	4.63	4.73	4.69
σ_{m}, μ	1.03	1.04	1.07	1.05
$\bar{X}$, dimensionless	-7.664	-7.679	-7.657	-7.667
σ_{x}, dimensionless	0.154	0.157	0.159	0.157
Based on least squares fit to log normal distribution:				
$\bar{m}$, μ	4.75	4.71	4.81	4.76
$\bar{X}$, dimensionless	-7.652	-7.662	-7.641	-7.651
σ_{x}, dimensionless	0.153	0.153	0.155	0.154
Correlation coefficient	0.998	0.997	0.996	--

TABLE XXII (Continued)

EFFECT OF BASIS WEIGHT ON PORE SIZE DISTRIBUTION PROPERTIES OF HANDSHEETS

Property	Specimens A	B	C	Mean
H-25(100)-5 (Average basis weight = 118.5 g./sq. m.)				
Based on the data:				
$\bar{m}$, μ	4.45	4.56	4.43	4.48
σ_{m}, μ	0.95	1.03	0.96	0.98
$\bar{X}$, dimensionless	-7.718	-7.694	-7.723	-7.712
σ_{x}, dimensionless	0.150	0.160	0.153	0.155
Based on least squares fit to log normal distribution:				
$\bar{m}$, μ	4.51	4.60	4.48	4.53
$\bar{X}$, dimensionless	-7.705	-7.685	-7.710	-7.700
σ_{x}, dimensionless	0.148	0.162	0.149	0.153
Correlation coefficient	0.998	0.997	0.997	--
H-25(150)-5 (Average basis weight = 147.8 g./sq. m.)				
Based on the data:				
$\bar{m}$, μ	4.37	4.30	--	4.33
σ_{m}, μ	0.95	0.88	--	0.91
$\bar{X}$, dimensionless	-7.734	-7.752	--	-7.743
σ_{x}, dimensionless	0.153	0.143	--	0.148
Based on least squares fit to log normal distribution:				
$\bar{m}$, μ	4.41	4.36	--	4.38
$\bar{X}$, dimensionless	-7.726	-7.738	--	-7.732
σ_{x}, dimensionless	0.149	0.140	--	0.144
Correlation coefficient	0.997	0.998	--	--

TABLE XXII (Continued)

EFFECT OF BASIS WEIGHT ON PORE SIZE DISTRIBUTION PROPERTIES OF HANDSHEETS

Property	Specimens A	B	C	Mean
H-25(150)-3 (Average basis weight = 176.2 g./sq. m.)				
Based on the data:				
$\bar{m}$, μ	4.28	4.34	--	4.31
σ_m, μ	0.88	0.88	--	0.88
$\bar{X}$, dimensionless	-7.755	-7.742	--	-7.749
σ_x, dimensionless	0.147	0.144	--	0.145
Based on least squares fit to log normal distribution:				
$\bar{m}$, μ	4.31	4.38	--	4.34
$\bar{X}$, dimensionless	-7.748	-7.733	--	-7.741
σ_x, dimensionless	0.142	0.137	--	0.139
Correlation coefficient	0.996	0.995	--	--

The results shown in Fig. 23 are in qualitative agreement with the arguments advanced by Corte (46). He suggested that a sheet of paper may be considered to be made up of a number of thin layers. He then presented evidence which indicated that, as the number of thin layers in the sheet is increased, the pore size distribution becomes narrower and shifts to smaller pore sizes.

The results presented in Tables XXI and XXII indicate that while the pore size distribution changes significantly as the basis weight is varied, the permeability properties of the sheets are not affected by changes in basis weight. As a result, it must be concluded that changes in pore size distribution have relatively little effect on the permeability properties of paper over the range of pore size distribution studied here. This conclusion is in qualitative agreement with the findings of Fatt (47).

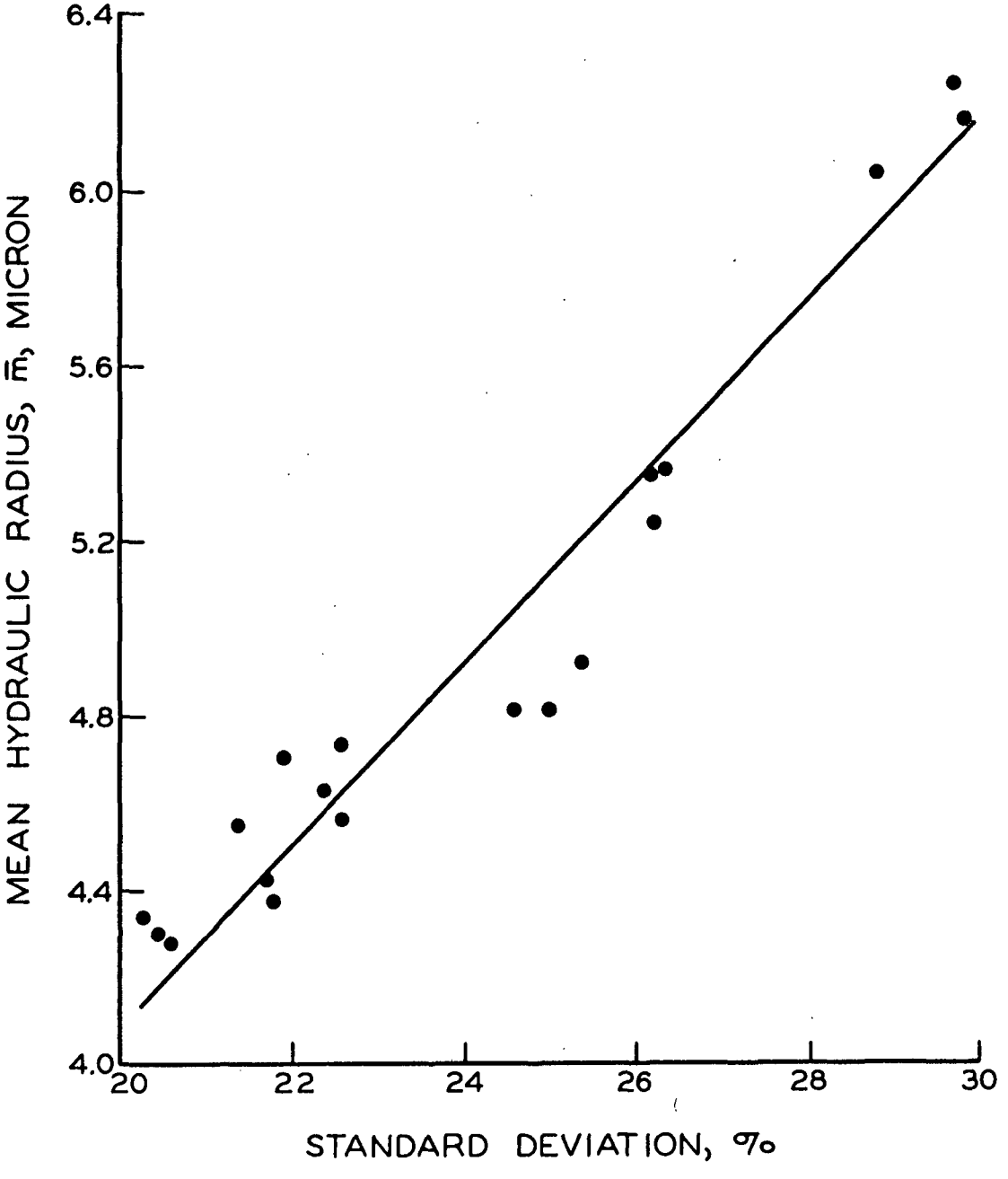

Figure 23. Relationship Between Mean and Standard Deviation of Pore Size Distribution (Basis Weight Study)

Corte and Kallmes (65) have recently presented the results of a study on the effect of basis weight on the pore sizes in a sheet of paper. These authors determined only the maximum pore size of the sheets, and it was shown that the maximum pore size was inversely proportional to the basis weight of the sheet.

The results of this study on the effect of basis weight on the mean hydraulic radius is shown graphically in Fig. 24. It can be seen from this figure that the mean hydraulic radius decreases regularly with increasing basis weight over the entire range of basis weights investigated. However, the relationship is not linear, and above a basis weight of about 100 g./sq. m., the curve appears to level off somewhat. On the basis of this observation, 100 g./sq. m. was selected as the basis weight to be used in the investigation on the effect of wet pressure on the permeability and pore size distribution properties of paper.

EFFECT OF WET PRESSURE ON THE POROUS PROPERTIES OF PAPER

Having selected a basis weight at which to conduct the tests, the porous structure of the specimens was varied by changing the wet pressure applied to the sheet. A series of handsheets were prepared in the usual manner at a basis weight of approximately 100 g./sq. m. These were couched at a pressure of 10 p.s.i. and were wet pressed at pressures of 10, 25, 50, 75, and 100 p.s.i. After the usual capacitance tests for sheet thickness, the specimens were subjected to air permeability and gas-drive tests. The results of the permeability tests are recorded in Table XXIII. For purposes of comparing the results, the hydrodynamic specific surface areas reported in Table XXIII were calculated by assuming a Kozeny factor of 5.55. The porosities recorded in this table were calculated in the same manner as those in the basis weight study.

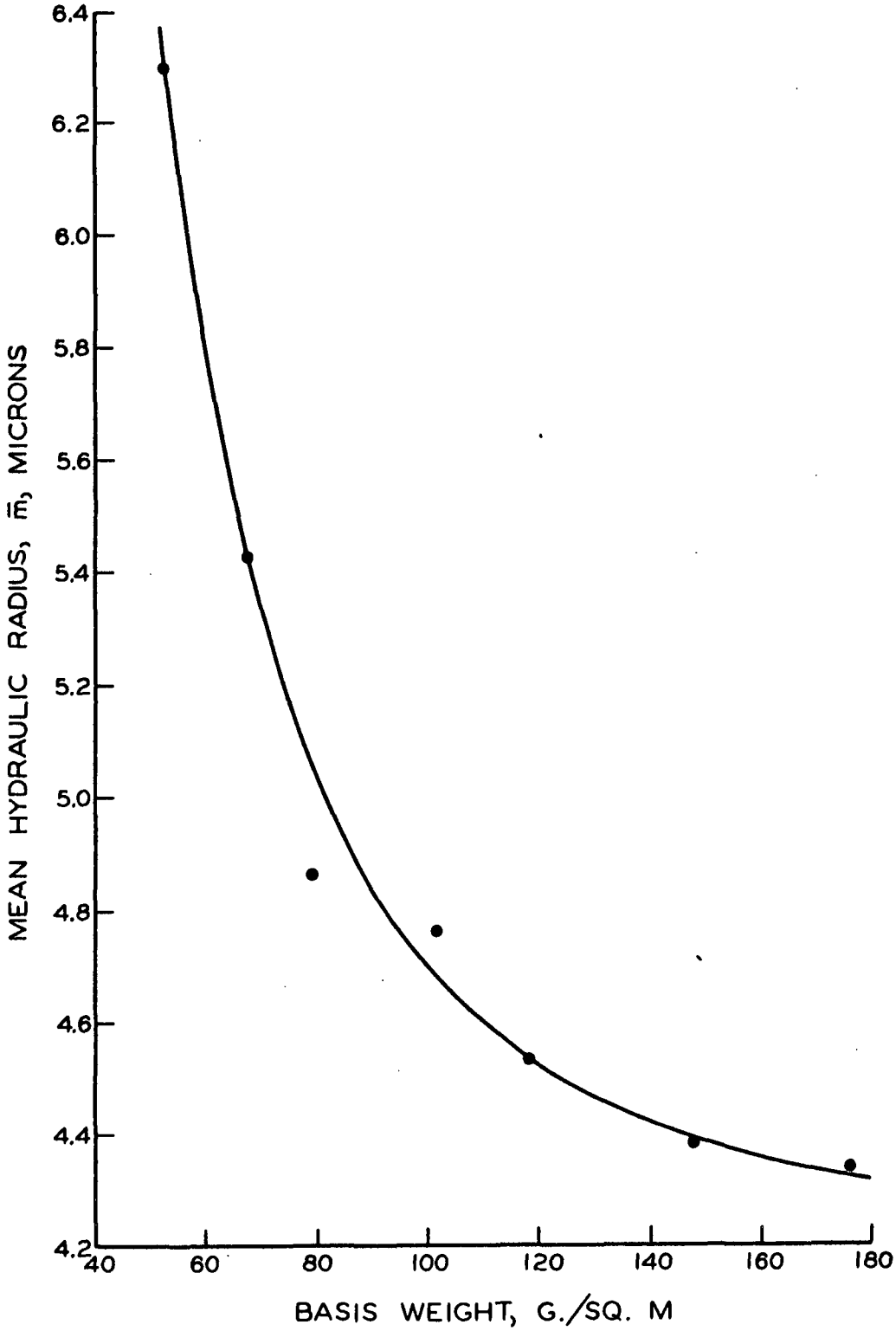

Figure 24. Variation of Mean Hydraulic Radius with Basis Weight

TABLE XXIII

EFFECT OF WET PRESSURE ON PERMEABILITY PROPERTIES OF HANDSHEETS

Property	Specimens A	B	C	Mean
H-10(100)-1	(Wet pressure = 10 p.s.i.)			
S_w, sq. cm./g.	6109	6120	6143	6124
ϵ, dimensionless	0.787	0.791	0.787	0.788
ρ_b, g./cc.	0.286	0.279	0.286	0.284
K, 10^{-8} sq. cm.	2.878	3.054	2.842	2.945
H-25(100)-6	(Wet pressure = 25 p.s.i.)			
S_w, sq. cm./g.	7111	7073	7088	7089
ϵ, dimensionless	0.764	0.756	0.763	0.761
ρ_b, g./cc.	0.331	0.346	0.333	0.337
K, 10^{-8} sq. cm.	1.455	1.297	1.434	1.395
H-50(100)-2	(Wet pressure = 50 p.s.i.)			
S_w, sq. cm./g.	9078	8721	9065	8955
ϵ, dimensionless	0.734	0.734	0.733	0.734
ρ_b, g./cc.	0.392	0.393	0.394	0.393
K, 10^{-8} sq. cm.	0.561	0.607	0.558	0.575
H-75(100)-1	(Wet pressure = 75 p.s.i.)			
S_w sq. cm./g.	10220	10100	10330	10217
ϵ, dimensionless	0.726	0.728	0.722	0.725
ρ_b, g./cc.	0.409	0.404	0.416	0.410
K, 10^{-8} sq. cm.	0.394	0.418	0.367	0.393
H-100(100)-1	(Wet pressure = 100 p.s.i.)			
S_w, sq. cm./g.	11650	11400	11540	11530
ϵ, dimensionless	0.710	0.716	0.715	0.714
ρ_b, g./cc.	0.440	0.428	0.430	0.433
K, 10^{-8} sq. cm.	0.245	0.277	0.268	0.267

The results reported in Table XXIII indicate that the porosity and permeability of the sheet decrease as the sheet becomes denser. These results were expected. However, the rapid increase in the calculated surface areas with increasing wet pressure was not anticipated. While a slight increase in the exposed surface area with increasing wet pressure was found in the permeability tests on thick mats, this effect is much more pronounced in the data of Table XXIII. These results will be discussed more fully later.

The effect of wet pressure on the pore size distribution properties is summarized in Table XXIV. The computed moments of the distributions along with the corresponding Student "t" values for skewness and kurtosis were omitted from Table XXIV. In no case was the calculated skewness or kurtosis of the pore size distribution data statistically significant.

The results of the study on the pore size distribution properties of paper as a function of the wet pressure applied to the sheets are difficult to interpret. The mean hydraulic radius of the sheet decreases regularly with increasing wet pressure as seen in the data of Table XXIV. In addition, these data indicate a decrease in the standard deviation of the pore size distribution as the wet pressure applied to the sheet is increased.

The following hypothesis is suggested as an explanation of these results. It is first supposed that at a given basis weight the porous structure of the sheet is determined when the sheet is formed. However, this structure may be altered in several ways—among which is the level of wet pressure applied to the sheet. Since the fibers are in a highly swollen state when the sheet is first formed, they are presumed to be quite mobile and are capable of being rearranged by applying a certain wet pressure to the sheet. As the pressure is applied to

TABLE XXIV

EFFECT OF WET PRESSURE ON PORE SIZE DISTRIBUTION PROPERTIES OF HANDSHEETS

Property	Specimens A	B	C	Mean
H-10(100)-1 (Wet pressure = 10 p.s.i.)				
Based on the data:				
$\bar{m}$, μ	5.78	5.86	5.76	5.80
$\sigma_{\bar{m}}$, μ	1.21	1.25	1.23	1.23
$\bar{X}$, dimensionless	-7.456	-7.443	-7.459	-7.452
$\sigma_{\bar{x}}$, dimensionless	0.149	0.151	0.151	0.150
Based on least squares fit to log normal distribution:				
$\bar{m}$, μ	5.84	5.92	5.82	5.86
$\bar{X}$, dimensionless	-7.446	-7.432	-7.448	-7.442
$\sigma_{\bar{x}}$, dimensionless	0.142	0.143	0.145	0.143
Correlation coefficient	0.995	0.995	0.996	--
H-25(100)-1 (Wet pressure = 25 p.s.i.)				
Based on the data:				
$\bar{m}$, μ	4.70	4.63	4.73	4.69
$\sigma_{\bar{m}}$, μ	1.03	1.04	1.07	1.05
$\bar{X}$, dimensionless	-7.664	-7.679	-7.657	-7.667
$\sigma_{\bar{x}}$, dimensionless	0.154	0.157	0.159	0.157
Based on least squares fit to log normal distribution:				
$\bar{m}$, μ	4.75	4.71	4.81	4.76
$\bar{X}$, dimensionless	-7.652	-7.662	-7.681	-7.652
$\sigma_{\bar{x}}$, dimensionless	0.153	0.153	0.155	0.153
Correlation coefficient	0.998	0.997	0.996	--

TABLE XXIV (Continued)

EFFECT OF WET PRESSURE ON PORE SIZE DISTRIBUTION PROPERTIES OF HANDSHEETS

Property	Specimens A	B	C	Mean
H-50(100)-2 (Wet pressure = 50 p.s.i.)				
Based on the data:				
$\bar{m}$, μ	3.57	3.70	3.59	3.62
$\sigma_{\bar{m}}$, μ	0.86	0.88	0.90	0.88
$\bar{X}$, dimensionless	-7.937	-7.901	-7.931	-7.923
$\sigma_{\bar{x}}$, dimensionless	0.166	0.165	0.173	0.168
Based on least squares fit to log normal distribution:				
$\bar{m}$, μ	3.64	3.79	3.68	3.70
$\bar{X}$, dimensionless	-7.917	-7.878	-7.908	-7.901
$\sigma_{\bar{x}}$, dimensionless	0.168	0.163	0.173	0.168
Correlation coefficient	0.996	0.993	0.995	--
H-75(100)-1 (Wet pressure = 75 p.s.i.)				
Based on the data:				
$\bar{m}$, μ	3.19	3.23	3.15	3.19
$\sigma_{\bar{m}}$, μ	0.83	0.84	0.85	0.84
$\bar{X}$, dimensionless	-8.052	-8.036	-8.062	-8.050
$\sigma_{\bar{x}}$, dimensionless	0.178	0.178	0.185	0.180
Based on least squares fit to log normal distribution:				
$\bar{m}$, μ	3.26	3.31	3.24	3.27
$\bar{X}$, dimensionless	-8.027	-8.012	-8.035	-8.025
$\sigma_{\bar{x}}$, dimensionless	0.181	0.182	0.187	0.183
Correlation coefficient	0.994	0.994	0.993	--

TABLE XXIV (Continued)

EFFECT OF WET PRESSURE ON PORE SIZE DISTRIBUTION PROPERTIES OF HANDSHEETS

Property	Specimens A	B	C	Mean
H-100(100)-1 (Wet pressure = 100 p.s.i.)				
Based on the data:				
$\bar{m}$, μ	2.72	2.83	2.81	2.79
$\sigma_{\underline{m}}$, μ	0.76	0.79	0.81	0.79
$\bar{X}$, dimensionless	-8.210	-8.170	-8.178	-8.186
$\sigma_{\underline{x}}$, dimensionless	0.189	0.191	0.195	0.192
Based on least squares fit to log normal distribution:				
$\bar{m}$, μ	2.79	2.91	2.89	2.86
$\bar{X}$, dimensionless	-8.184	-8.144	-8.148	-8.159
$\sigma_{\underline{x}}$, dimensionless	0.194	0.194	0.198	0.195
Correlation coefficient	0.994	0.994	0.991	--

the sheet, the fibers would tend to reorient and slide over one another in such a manner as to minimize the local compressive stresses in the structure. In doing so, the fibers would move from locally more dense areas into locally less dense areas, that is, into voids. The degree of fiber reorientation would probably be dependent on the total wet pressure applied to the sheet as well as the rate at which the pressure is applied.

In his study of the compression response of fiber mats, Jones (50) concluded, "During first compression, fiber slippage and repositioning are very important contributors to fiber bed deformations." While Jones's work was conducted on saturated mats, it is felt that fiber slippage could occur to an appreciable extent during the application of pressure to a wet, newly formed sheet of paper.

If fiber slippage did, in fact, occur during the wet pressing of the handsheets, it could easily account for the changes in pore size distribution observed in this study. As the fibers slipped into the void spaces in the sheet structure, the measured pore sizes would be decreased, and if the fiber slippage occurred more or less randomly throughout the sheet, the broadness of the pore size distribution could also be affected. While it is not suggested that the data of Table XXIII prove this hypothesis, it is felt that the hypothesis does offer a plausible explanation of the results obtained in this study.

In examining the permeability results of Table XXIII, it is found that the porosities and apparent densities follow the expected trends. The porosities decrease while the apparent density of the sheets increases with increasing wet pressure. The surface areas calculated from the Kozeny-Carman equation, however, are not only too high, but they increase with increasing wet pressure. The calculated surface areas obtained in earlier studies on thick mats increased from about 3700 to 4250 sq. cm./g. as the wet pressure was changed from 10 to 100 p.s.i. The calculated surface areas of the handsheets (using the ordinary form of the Kozeny-Carman equation with $\underline{k} = 5.55$) varied from about 6000 to 11500 sq. cm./g. over the same range of applied wet pressure. Thus, it must be concluded that the ordinary form of the Kozeny-Carman equation is not applicable to the thin handsheets of paper. The failure of the Kozeny-Carman approach may be attributed to the wide distribution of pore sizes in the handsheets and to the fact that the Kozeny factor changes with the wet pressure applied to the sheet. The latter effect was shown by the studies on the permeability of synthetic fiber beds.

ESTIMATION OF THE EXPOSED SURFACE AREA OF THE HANDSHEETS FROM PORE SIZE DISTRIBUTION DATA

One of the important objectives of this thesis was to relate the pore size distribution properties of paper to such properties as the permeability and exposed surface area of the sheet. An attempt to apply a model of parallel cylindrical capillaries to this problem was grossly unsuccessful. The development of the equations describing the permeability properties of the parallel capillary model, together with the results obtained in applying this model to the data obtained in this study, are presented in Appendix III.

In an effort to overcome the inadequacy of the parallel capillary model, the modified hydraulic radius theory described earlier was developed. The flow parameter, ψ, involved in this theory is represented by

$$\psi = (\epsilon \gamma^2/K) \int_0^1 dK_r/(\Delta P)^2 \qquad (74)$$

The empirical parameter, ψ, includes the effects of pore shape, tortuosity, pore branching, etc. In short, ψ incorporates all of the immeasurable quantities which influence the flow of fluids through a sheet of paper. However, for a given test specimen, ψ is a constant and may be calculated from experimentally measurable quantities using Equation (74).

As mentioned earlier, the modified hydraulic radius theory leads to the consequence that the hydrodynamic specific surface area, S_w, is given by

$$S_w = \left\{v\epsilon/[(1 - \epsilon)\gamma]\right\} \sqrt{\frac{1}{\int_0^1 dK_r/(\Delta P)^2}} \qquad (78)$$

In analyzing the data gathered in this study using Equations (74) and (78), the integral was evaluated from the gas-drive data using the trapezoidal rule and $\underline{K}$ was taken from the handsheet permeability tests.

The results of applying Equations (74) and (78) to the data obtained in the study of the effect of wet pressure on the porous properties of paper, together with the porosity of the specimens, are recorded in Table XXV. The calculated hydrodynamic specific surface areas are plotted as a function of the wet pressure applied to the sheet in Fig. 25. For comparative purposes, the values of $\underline{S}_{\underline{w}}$ calculated from the Kozeny-Carman equation (assuming $\underline{k} = 5.55$) are also plotted in this figure.

Two facts are immediately apparent from Fig. 25. First, the exposed surface areas calculated from the modified hydraulic radius theory are much lower than those computed from the permeability data using 5.55 as the value of the Kozeny factor. Secondly, the increase in the calculated surface areas with increasing wet pressure is much less pronounced when the modified hydraulic radius theory is used to estimate the surface area. The modified hydraulic radius theory therefore appears to offer a significant improvement over the usual form of the Kozeny-Carman equation in which a constant value is used for the Kozeny factor.

A rapid increase in the values of the flow parameter, ψ, with increasing wet pressure is shown in the data of Table XXV. As mentioned earlier, this empirical parameter incorporates the effects of pore shape, tortuosity, particle shape, and all of the inadequacies of the modified hydraulic radius theory. Any or all of these factors could influence the calculated value of ψ. It would certainly be expected that the average tortuous path through the specimen (if such a property is definable) would increase as the sheet becomes denser. In addition, one might also expect that the effects of pore constrictions and pore branching would become more severe as the apparent density of the sheet increases.

TABLE XXV

SURFACE AREAS FROM MODIFIED HYDRAULIC RADIUS THEORY

Property	Specimens A	B	C	Mean
H-10(100)-1	(Wet pressure = 10 p.s.i.)			
S_w, sq. cm./g.	4592	4664	4600	4619
ψ, dimensionless	9.82	9.55	9.90	9.76
ϵ, dimensionless	0.787	0.791	0.787	0.788
H-25(100)-6	(Wet pressure = 25 p.s.i.)			
S_w, sq. cm./g.	4741	4536	4652	4643
ψ, dimensionless	12.49	13.50	12.88	12.96
ϵ, dimensionless	0.764	0.756	0.763	0.761
H-50(100)-2	(Wet pressure = 50 p.s.i.)			
S_w, sq. cm./g.	5008	4828	4943	4926
ψ, dimensionless	18.24	18.11	18.67	18.34
ϵ, dimensionless	0.734	0.734	0.733	0.734
H-75(100)-1	(Wet pressure = 75 p.s.i.)			
S_w, sq. cm./g.	5297	5302	5216	5272
ψ, dimensionless	20.67	20.16	21.78	20.87
ϵ, dimensionless	0.726	0.728	0.722	0.725
H-100(100)-1	(Wet pressure = 100 p.s.i.)			
S_w, sq. cm./g.	5606	5580	5584	5590
ψ, dimensionless	23.98	23.17	23.72	23.62
ϵ, dimensionless	0.710	0.716	0.715	0.714

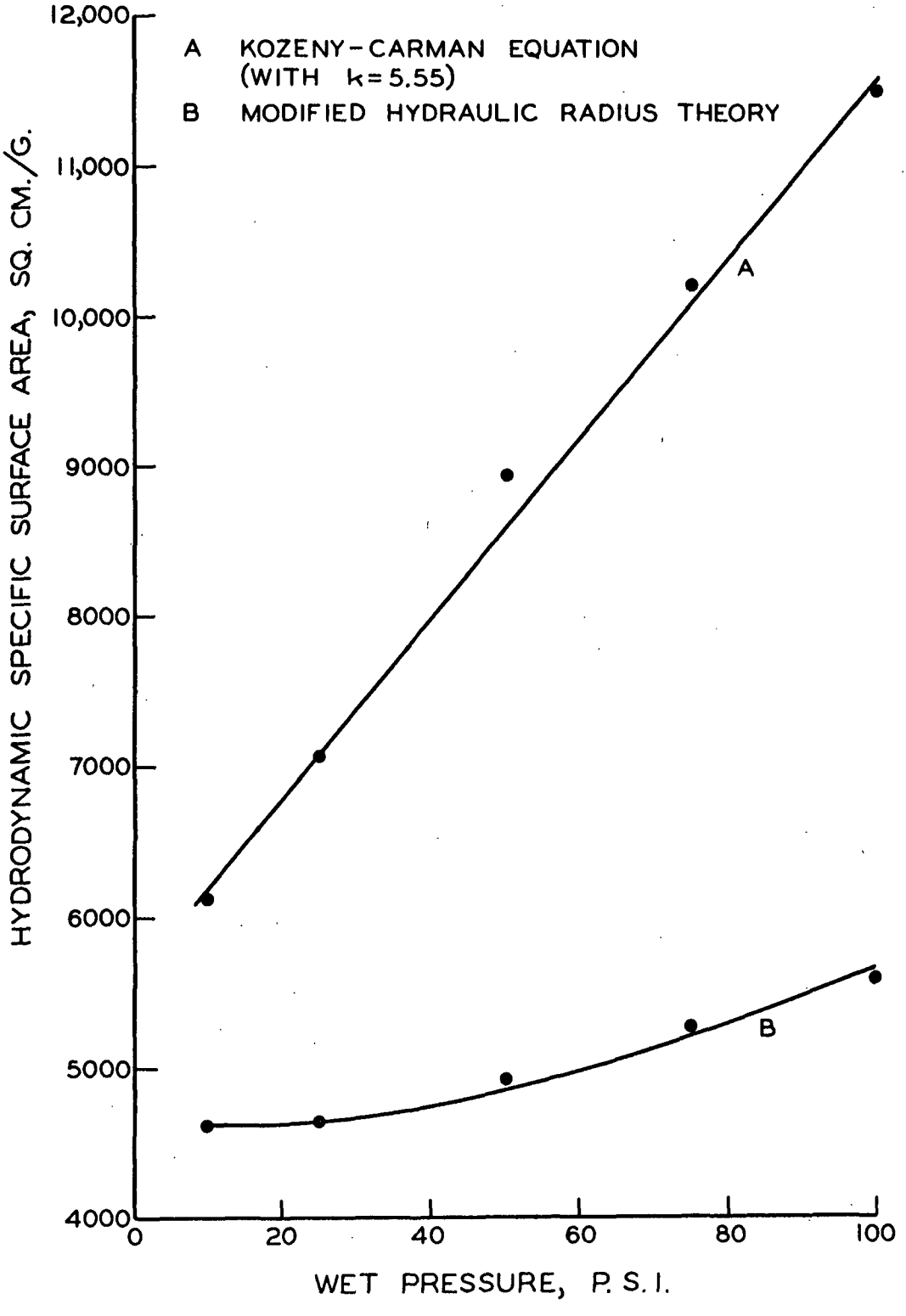

Figure 25. Effect of Wet Pressure on Surface Area

The effect of pore constrictions on the computed values of exposed surface area may be seen by considering Equation (7),

$$m = \epsilon/S_o \qquad (7)$$

Assuming the porosity to be constant (as was the case in the basis weight study) the effect of pore constrictions would be to reduce the value of m, as measured in the gas-drive test, and therefore the calculated surface area must increase.

It will be recalled that in developing the modified hydraulic radius theory it was necessary to introduce the assumption that flow through pores of a given size is possible without interference from pores of different sizes. This assumption, in effect, ignores the possibility of branched and interconnected pores in the sheet and is one of the most obvious deficiencies of the theory. It seems probable that this assumption would become less and less valid as the sheet becomes more dense.

A convenient method of determining the importance of pore constrictions and pore interconnections is found in applying the modified hydraulic radius theory to the data gathered in the study of the effect of basis weight on the porous structure of paper. In this study the porosity, apparent density, and permeability of the specimens were constant, and therefore the surface area exposed to flow should also be independent of basis weight. On the other hand, one might expect that the possibility of pore constrictions and pore interconnections should increase as the sheet becomes thicker. In terms of the modified hydraulic radius theory, it would be anticipated that these changes should influence the computed values of the surface area exposed to flow. The results of applying Equations (74) and (78) to the data obtained in the basis weight study are summarized in Table XXVI.

TABLE XXVI

EFFECT OF BASIS WEIGHT ON COMPUTED SURFACE AREAS

Property	Specimens A	B	C	Mean
H-25(50)-2	(Average basis weight = 52.4 g./sq. m.)			
S_w, sq. cm./g.	3408	3383	3576	3456
ψ, dimensionless	26.23	24.89	23.13	24.75
ϵ, dimensionless	0.760	0.761	0.764	0.762
H-25(75)-3	(Average basis weight = 67.8 g./sq. m.)			
S_w, sq. cm./g.	3975	4050	4051	4025
ψ, dimensionless	19.42	17.56	18.36	18.45
ϵ, dimensionless	0.757	0.762	0.762	0.760
H-25(75)-4	(Average basis weight = 79.2 g./sq. m.)			
S_w, sq. cm./g.	4325	4364	4298	4329
ψ, dimensionless	16.25	16.48	17.17	16.63
ϵ, dimensionless	0.756	0.757	0.759	0.757
H-25(100)-6	(Average basis weight = 101.3 g./sq. m.)			
S_w, sq. cm./g.	4741	4536	4652	4643
ψ, dimensionless	12.49	13.50	12.88	12.96
ϵ, dimensionless	0.764	0.756	0.763	0.761
H-25(100)-5	(Average basis weight = 118.5 g./sq. m.)			
S_w, sq. cm./g.	4852	4950	5091	4964
ψ, dimensionless	11.90	11.66	11.86	11.81
ϵ, dimensionless	0.760	0.767	0.766	0.764
H-25(150)-5	(Average basis weight = 147.8 g./sq. m.)			
S_w, sq. cm./g.	5179	4977	--	5078
ψ, dimensionless	10.89	10.65	--	10.77
ϵ, dimensionless	0.766	0.759	--	0.763

TABLE XXVI (Continued)

EFFECT OF BASIS WEIGHT ON COMPUTED SURFACE AREAS

Property	Specimens A	B	C	Mean
H-25(150)-3	(Average basis weight = 176.2 g./sq. m.)			
$\underline{S}_w$, sq. cm./g.	5320	5356	--	5338
ψ, dimensionless	9.59	9.75	--	9.67
ϵ, dimensionless	0.767	0.770	--	0.768

The results recorded in Table XXVI reveal a significant increase in $\underline{S}_w$ with basis weight. These anomalies are again attributed to the effects of pore constrictions and pore interconnections. Consider briefly what happens in a sheet of paper as the basis weight is increased at a given level of wet pressure. For the extreme case of very thin sheets only a few fibers thick, the pores must pass directly through the sheet. In this case, the branching and interconnecting of pores is at a minimum. However, as the basis weight is increased, the possibility of branched and interconnected pores must also increase. As a result, as the basis weight is increased to the levels used in this study, the assumption of noninterference between flow components from different sized pores, which is involved in the development of the modified hydraulic radius theory, becomes less and less valid. In addition, one might also expect that the constrictions in the pores might become more severe at higher basis weights.

CONCLUSIONS

The experimental observations made in this study have led to the following conclusions:

1. The Kozeny-Carman equation applied very well to the thick mats tested in this study. This was shown by the high correlation coefficients obtained on the rectified plots of the permeability data.

2. A progressive collapse of the fibers occurred as the wet pressure applied to the thick mats was increased. This conclusion was supported by the observation that the hydrodynamic specific volume of the fibers decreased as the structure became denser.

3. The Kozeny factor is affected by fiber shape, becoming larger as the fibers become more and more flattened. The increase in the calculated surface area exposed to flow as the wet pressure applied to the mat was increased and the results of the permeability tests on synthetic fiber beds support this conclusion.

4. The pore size distribution of paper can be fitted to a log normal distribution with a high degree of correlation. This was demonstrated by the high correlation coefficients obtained on the log probability plots of the pore size distribution data as well as by the fact that no evidence of a statistically significant skewness or kurtosis was found in the pore size distribution data.

5. As the basis weight of the sheet was increased, the pore size distribution shifted toward smaller pore sizes and became narrower. Therefore, at higher basis weights the concept of a mean hydraulic radius, upon which the Kozeny-Carman equation is based, is probably a valid one.

6. From the results obtained in the basis weight study, it was concluded that the pore size distribution of a sheet of paper (as measured by the gas-drive technique) has relatively little effect on the permeability properties of the sheet over the range of pore size distribution studied.

7. As the wet pressure applied to the sheet was increased, the pore size distribution (determined by the gas-drive method) became narrower and shifted to smaller pore sizes. These changes were attributed to the rearrangement of fibers in the sheet.

8. The ordinary form of the Kozeny-Carman equation does not apply to thin handsheets of paper. Attempts to employ this equation resulted in a calculated surface area which was too high by a factor of about 2 to 3.

9. The modified hydraulic radius theory, in which the pore size distribution is taken into account, represents a significant improvement over the normal form of the Kozeny-Carman equation. However, when this theory was used to analyze the data, an increase in the hydrodynamic specific surface area with basis weight and with wet pressure was found. This result was believed to be due primarily to the failure of the theory to take account of the interconnection of pores and to the effects of constrictions in the pores within the sheet.

SUGGESTIONS FOR FUTURE WORK

In the field of flow through porous media in general, there is a need for more work on both the theoretical and experimental fronts. In the theoretical area, the major stumbling block is the lack of a workable model with which to describe the structure of porous media. While the network models suggested by Fatt (47) and Rose (48) represent an interesting possibility, these models are not yet amenable to mathematical treatment with any reasonable amount of labor.

The several statistical techniques offer a promising area of approach, but these will probably have to be modified extensively before they are applicable to fibrous sheets.

In the area of experimental work, it would be desirable to conduct a more systematic study of the effect of fiber shape on the Kozeny factor than was possible in this thesis. It would be particularly useful to establish a means of determining the Kozeny factor as a function of porosity for wood pulp fibers. The results obtained in this study indicate that while a value of k of about 5.55 is applicable to cylindrical fibers in the porosity range from 0.6 to 0.8, a much higher value is probably applicable to flatter fibers such as those in wood pulp. As a result of this observation, one must conclude that the hydrodynamic specific surface areas of wood pulp fibers reported in the literature (where the Kozeny factor is taken from correlations based on cylindrical fibers) are too high.

The gas-drive test and the permeability test offer a combination which may prove useful in establishing the relationship between the Kozeny factor and porosity for wood pulp fibers. By measuring the mean hydraulic radius of very thick mats (which should have a narrow range of pore sizes) using the gas-drive technique and relating these data to the permeability coefficients of the same

mats, the relationship between $\underline{k}$ and porosity might be studied. While there remains some doubt as to the equivalence of the mean hydraulic radius from the gas-drive test and the hydraulic radius effective in offering resistance to flow, the experimental techniques could be calibrated easily using cylindrical, synthetic fibers. Even though such an approach is quite empirical in nature, it is felt that some useful information could be obtained from such a study.

ACKNOWLEDGMENTS

It would be difficult to list all of the people who have contributed in many different ways to the successful completion of this thesis. However, a number of people deserve special mention.

In particular, the author would like to express his sincere appreciation to Dr. W. L. Ingmanson, the chairman of his thesis advisory committee, and to Dr. G. R. Sears and Mr. S. T. Han, the members of his advisory committee. The advice and encouragement of the members of this committee have contributed greatly to the completion of this work.

The aid of the following is also gratefully acknowledged:

Mr. Jack Hankey and Mrs. M. Davis of the Institute Microscopy Section for preparing the photomicrographs of the synthetic fiber cross sections and for determining the length distribution of these fibers.

Mr. Bruce Andrews of the Engineering and Technology Section of The Institute of Paper Chemistry for his assistance in determining the permeability properties of the synthetic fiber beds.

Messrs. H. Marx and M. Filz of the Machine Shop of The Institute of Paper Chemistry for their aid in the design and construction of the equipment used in this study.

NOMENCLATURE

(In consistent c.g.s. units)

A = cross-sectional area of a test specimen perpendicular to the direction of macroscopic flow, sq. cm.

A_c = average projected area of contact between fibers in a bed, sq. cm.

A_f = cross-sectional area of a fiber, sq. cm.

a = radius of a cylinder, cm.

b = radius of a unit cell in the free surface model, cm.

b' = free segment length between contact points in a fibrous bed, cm.

C = number of times a pin dropped randomly onto a porous medium crosses the perimeter of a void, dimensionless

C' = capacitance of a mercury-paper-mercury condenser, micromicrofarads

C_o = a dimensional constant, $\text{sec.}^7/\text{g.}^3$

D = effective fiber diameter, cm.

d = diameter of a cylinder, cm.

e = base of Naperian logarithms

F = "formation resistivity factor," dimensionless

F_d = drag force on a unit length of a cylinder, dynes

F_t = total drag force on an assemblage of particles, dynes

f_i = frequency of occurrence of pores of size, m_i, dimensionless

g = the acceleration due to gravity, cm./sec.^2

$g(\vec{r})$ = a function of the vector $\vec{r}$, dimensionless

$g(x)$ = a distribution function, dimensionless

H = number of times that the head of a pin dropped randomly onto a porous medium falls within a void, dimensionless

h = height of capillary rise, cm.

h' = a distance, cm.

$h(R)$ = a distribution function, dimensionless

K = permeability coefficient, sq. cm.

K' = dielectric constant of a sheet of paper, dimensionless

K_a = apparent permeability coefficient, sq. cm.

K_i = permeability coefficient of an idealized medium, sq. cm.

K_o = proportionality factor in Equation (7), cc. sec./g.

K_r = relative permeability, dimensionless

ΔK_r = the increase in relative permeability coefficient which results when a given idealized medium is opened to flow, dimensionless

k = Kozeny factor, dimensionless

k_c = Kozeny factor corrected for area of contact between particles in the bed, dimensionless

k_o = shape factor, dimensionless

L = thickness of a test specimen, cm.

L_c = length of a cylinder, cm.

L_e = average tortuous length of the flow path through a bed of thickness, L, cm.

L_i = "initial" thickness of a thick fibrous mat, cm.

L_o = thickness of a fibrous bed at zero porosity, cm.

ℓ = length of a capillary, cm.

M_3 = third moment of a distribution about the mean, dimensionless

M_4 = fourth moment of a distribution about the mean, dimensionless

$M(X^j)$ = jth moment of a distribution about the origin, dimensionless

m = a hydraulic radius, cm.

$\bar{m}$ = mean hydraulic radius, cm.

N = number of cylinders in a unit volume, dimensionless

N_c = total number of contact points in a fibrous bed, dimensionless

N_i = number of pores opened to flow at a pressure drop, ΔP_i, dimensionless

N_t = total number of cylindrical tubes in a capillary model, dimensionless

$\underline{P}$ = a probability, dimensionless

$\Delta\underline{P}$ = over-all pressure drop across a test specimen, dynes/sq. cm.

$\underline{P'}$ = perimeter of a fiber, cm.

$\Delta\underline{P}_{\underline{i}}$ = the pressure drop required to open a given idealized medium to flow, dynes/sq. cm.

$\underline{P}_{\underline{D}}$ = probability that the ends of a line thrown randomly onto a porous medium will land with its ends in different environments, dimensionless

$\underline{P}_{\underline{p}}$ = probability that an incremental change in the length of a line thrown randomly onto a porous medium will allow the line to penetrate across a solid boundary, dimensionless

$\underline{p}$ = local pressure, dynes/sq. cm.

$\underline{Q}$ = volumetric flow rate, cc./sec.

$\Delta\underline{Q}$ = change in volumetric flow rate when a given idealized medium is opened to flow, cc./sec.

$\underline{R}$ = radius of a cylindrical capillary, cm.

$\underline{R}_1, \underline{R}_2$ = principal radii of curvature of a meniscus confined within a pore space, cm.

$\underline{Re}$ = Reynolds number of a porous medium, dimensionless

$\underline{R}_o$ = electrical resistance of a porous medium saturated with an electrolyte, ohms

$\underline{R}_w$ = electrical resistance of a free electrolyte, ohms

$\underline{r}$ = a radius, cm.

$\vec{\underline{r}}$ = a position vector, cm.

$\underline{S}_c$ = total surface area of the capillaries in a capillary model, sq. cm.

$\underline{S}(\vec{\delta})$ = a correlation function, dimensionless

$\underline{S}_o$ = surface area of a bed per unit volume of the bed, sq. cm./cc.

$\underline{S}_v$ = surface area of a bed per unit volume of the particles which compose the bed, sq. cm./cc.

$\underline{S}_w$ = hydrodynamic specific surface area of a bed, sq. cm./g.

$\underline{U}$ = projected width of a fiber, cm.

$\underline{u}$ = superficial linear velocity or a local velocity, cm./sec.

$\underline{u_e}$ = superficial linear velocity within a pore space, cm./sec.

$\underline{V'}$ = an approach velocity, cm./sec.

$\underline{V_c}$ = total capillary volume in a capillary model, cc.

$\underline{v}$ = hydrodynamic specific volume of the fibers in a bed, cc./g.

$\underline{v_r}$ = velocity component in the $\underline{r}$ direction, cm./sec.

$\underline{v_\alpha}$ = velocity component in the α direction, cm./sec.

$\underline{W}$ = mass of fibers in a test specimen, g.

$\underline{X}$ = natural logarithm of the hydraulic radius, dimensionless

$\underline{\bar{X}}$ = mean of a log normal pore size distribution, dimensionless

$\underline{x}$ = $\underline{x}$ co-ordinate

$\underline{y}$ = $\underline{y}$ co-ordinate

$\underline{Z}$ = "standardized variable" in Equation (93), dimensionless

$\underline{z}$ = $\underline{z}$ co-ordinate

α = an angle, radians

β = β-factor, number of tubes connected to a given tube in a network model, dimensionless

γ = surface tension, dynes/cm.

$\vec{\delta}$ = length vector, cm.

$\Delta\delta$ = an incremental length, cm.

ϵ = porosity or fractional void volume of a porous medium, dimensionless

η = fluid viscosity, g./(cm.sec.)

θ = an angle, radians

μ = microns - 10^{-4} cm.

ρ = fluid density, g./cc.

$\underline{\rho_b}$ = apparent density of a fibrous bed, g./cc.

$\underline{\rho_s}$ = fiber density, g./cc.

$\sigma_{\underline{m}}$ = standard deviation of hydraulic radii, cm.

$\sigma_{\underline{x}}$ = standard deviation of a log normal distribution, dimensionless

ϕ = angle between the normal to a surface and the length vector $\vec{\delta}$, radians

ϕ' = a constant, dimensionless

ψ = the "flow parameter" in the modified hydraulic radius theory, dimensionless

∇^2 = Laplacian operator $\equiv (\partial^2/\partial\underline{x}^2) + (\partial^2/\partial\underline{y}^2) + (\partial^2/\partial\underline{z}^2)$

LITERATURE CITED

1. Muskat, M. The flow of homogeneous fluids through porous media. New York, McGraw-Hill, 1937. 763 p.

2. Lamb, H. Hydrodynamics. 6th ed. London, Cambridge University Press, 1932. 738 p.

3. Mokadam, R. G., J. Appl. Mech. 28:208-12(1961).

4. Carson, F. T., J. Res. Natl. Bur. Standards 12:587-608(1934).

5. Bublitz, W. J., Jr. A study of the air permeability of paper at high pressures. Master's Dissertation. Appleton, Wis., The Institute of Paper Chemistry, 1947. 89 p.

6. Coupe, R. R., Proc. Tech. Sect. British Paper & Board Makers' Assoc. 31, no. 2:383-457(1950).

7. Kozeny, J., Akad. Wiss. Wien, Math.-naturw. Kl. 36(abt IIa):271-306(1927).

8. Carman, P. C., Trans. Inst. Chem. Engr. (London) 15:150-66(1937).

9. Scheidegger, A. E. The physics of flow through porous media. Rev. ed. New York, Macmillan, 1960. 313 p.

10. Carman, P. C. Flow of gases through porous media. New York, Academic Press, 1956. 182 p.

11. Wyllie, M. R. J., and Gregory, A. R., Ind. Eng. Chem. 47, no. 7:1379-88 (1955).

12. Fowler, J. L., and Hertel, K. L., J. Appl. Phys. 11:496-502(1940).

13. Sullivan, R. R., and Hertel, K. L., J. Appl. Phys. 11:761-5(1940).

14. Sullivan, R. R., J. Appl. Phys. 12:503-8(1941).

15. Sullivan, R. R., J. Appl. Phys. 13:725-30(1942).

16. Brown, J. C., Jr. Determination of the exposed surface area of pulp fibers from air permeability measurements, using a modified Kozeny equation. Doctor's Dissertation. Appleton, Wis., The Institute of Paper Chemistry, 1949. 146 p.

17. Hirsch, E. H., J. Appl. Phys. 32:977-82(1961).

18. Ingmanson, W. L., Andrews, B. D., and Johnson, R. C., Tappi 42, no. 10:840-9 (1959).

19. Macklem, J. E. A study of the resistance of woven wool felts to liquid flow. Doctor's Dissertation. Appleton, Wis., The Institute of Paper Chemistry, 1960. 156 p.

20. Wyllie, M. R. J., and Rose, W. D., Nature 165:972(1950).

21. Wyllie, M. R. J., and Spangler, M. B., Bull. Am. Assoc. Petrol. Geol. 36, no. 2:359-403(1952).

22. Archie, G. E., Trans. A.I.M.E. 146:54-62(1942).

23. Bikerman, J. J., J. Phys. Chem. 46:724-30(1942).

24. Goring, D. A. I., and Mason, S. G., Can. J. Res. 28B:307-22(1950).

25. Sanborn, I. B. A study of the irreversible, stress-induced changes in the macrostructure of paper. Doctor's Dissertation. Appleton, Wis., The Institute of Paper Chemistry, 1961. 105 p.

26. McDonald, T. D., Jr. Unpublished work, 1961.

27. Childs, E. C., and Collis-George, N., Proc. Royal Soc. (London) 201A:392-405(1950).

28. Fatt, I., and Dykstra, H., Petrol. Trans., A.I.M.E. 192:249-56(1951).

29. Tollenaar, D., and Blokhuis, G., Appl. Sci. Res. A2:125-41(1950).

30. Burdine, N. T., Gournay, L. S., and Reichertz, P. P., Trans. A.I.M.E. 189:195-204(1950).

31. Iberall, A. S., J. Res. Natl. Bur. Standards 45:398-406(1950).

32. Emersleben, O., Phys. Z. 26:601(1925).

32a. Han, S. T. Personal communication, 1963.

33. Happel, J., A.I.Ch.E. Journal 5, no. 2:174-7(1959).

34. Debye, P., Anderson, H. R., Jr., and Brumberger, H., J. Appl. Phys. 28, no. 6:679-83(1957).

35. Prager, S., Phys. of Fluids 4, no. 12:1477-82(1961).

36. Cornfield, J., and Chalkeley, H. W., J. Washington Acad. Sci. 41, no. 7:226-9(1951).

37. Chalkeley, H. W., Cornfield, J., and Park, H., Science 110:295-7(1949).

38. Banacki, W. J., Jr., and Bowers, R. L., Tappi 45, no. 10:805-7(Oct., 1962).

38a. Schultze, K., Kolloid-Z. 36:65-78 and 37:10-17(1925).

39. Ritter, H. L., and Drake, L. C., Ind. Eng. Chem. (Anal. Ed.) 17:782-6(1945).

40. Grace, H. P., A.I.Ch.E. Journal 2, no. 3:307-36(1956).

41. McKnight, T. S., Marchessault, R. H., and Mason, S. G., Pulp Paper Mag. Can. 59, no. 2:81-8(1958).

42. Pierce, C., J. Phys. Chem. 57:149-52(1953).

43. Wyllie, M. R. J., and Gardner, G. H. F., World Oil 146, no. 4:121-37(1958).

44. Parker, J. D. An investigation of the permeability to water of partially saturated beds of glass fibers. Doctor's Dissertation. Appleton, Wis., The Institute of Paper Chemistry, 1958. 203 p.

45. White, R. E., and Marceau, W. E., Tappi 45, no. 4:279-84(1962).

46. Corte, H. The porous structure of paper. In Bolam's Fundamentals of paper-making fibers. p. 301-31. Kenley, England, Tech. Sect. British Paper & Board Makers' Assoc., 1958.

47. Fatt, I. The network model in the study of porous media. Doctor's Dissertation. Los Angeles, Cal., University of Southern California, 1955. 246 p.

48. Rose, W., Illinois State Geol. Survey Circ. 237, 1957. 31 p.

49. Institute Method 415, 1951.

50. Jones, R. L. An investigation of the effect of fiber structural properties on the compression response of fibrous beds. Doctor's Dissertation. Appleton, Wis., The Institute of Paper Chemistry, 1962. 150 p.

51. Carson, F. T., J. Res. Natl. Bur. Standards 12:567-85(1934).

52. Pouradier, J., and Chateau, H., Assoc. tech. ind. papetière, Bull. no. 1: 8-10(1954).

53. Hatch, T., and Choate, S. P., J. Franklin Inst. 207:369-87(1928).

54. Jentzen, C. A. Personal communication, 1963.

55. Goulden, C. H. Methods of statistical analysis. p. 34-6. New York, John Wiley and Sons, 1952.

56. Arnold, E. W. Light scattering in fibrous sheets. Doctor's Dissertation. Appleton, Wis., The Institute of Paper Chemistry, 1962. 139 p.

57. Ingmanson, W. L., and Whitney, R. P., Tappi 37, no. 11:523-34(1954).

58. Onogi, S., and Sasaguri, K., Tappi 44, no. 12:874-80(1961).

59. Van den Akker, J. A. In Bolam's The formation and structure of paper. Vol. I. p. 205-41. London, England, Tech. Sect. British Paper & Board Makers' Assoc., 1962.

60. Swanson, J. W., and Steber, A. J., Tappi 42, no. 12:986-94(1959).

61. Ingmanson, W. L., and Thode, E. F., Tappi 42, no. 1:83-93(1959).

62. Collins, R. E. Flow of fluids through porous materials. p. 52. New York, Reinhold, 1961.

63. Glasstone, S. Textbook of physical chemistry. 2d ed. p. 488. New York, D. Van Nostrand, 1946.

64. International Critical Tables. Vol. IV. p. 454. New York, McGraw-Hill, 1928.

65. Corte, H., and Kallmes, O. J. In Bolam's The formation and structure of paper. Vol. I. p. 351-68. London, England, Tech. Sect. British Paper & Board Makers' Assoc., 1962.

66. Crow, E. L., Davis, F. A., and Maxfield, M. W. Statistics manual. New York, Dover Publications, 1960. 288 p.

67. Spiegel, M. R. Theory and problems of statistics. p. 91. New York, Schaum Publishing Co., 1961.

68. Hastings, C., Jr. Approximations for digital computers. p. 169. Princeton, N. J., Princeton University Press, 1955.

69. Aitchison, J., and Brown, J. A. C. The log normal distribution. London, England, Cambridge University Press, 1957. 176 p.

APPENDIX I

SAMPLE CALCULATION OF PORE SIZE DISTRIBUTION FROM GAS-DRIVE DATA

The general methods used to calculate the pore size distribution of the handsheets from the gas-drive data have been described earlier. The purpose of this presentation is to present an example of these calculations using the data gathered on one of the specimens tested. The gas-drive data were gathered by covering the specimen with technical-grade hexyl alcohol and then making flow rate-pressure drop measurements on it. Some typical flow rate-pressure drop data obtained on Specimen H-25(100)-6B are presented in Fig. 26. The pore size distributions of all specimens were calculated from such plots. The additional pertinent data on Specimen H-25(100)-6B are presented in Table XXVII.

TABLE XXVII

ADDITIONAL DATA FOR SPECIMEN H-25(100)-6B

Property	Value
Specimen weight, g. (ovendry)	1.2850
Moisture content, %	1.86
Specimen thickness, 10^{-2} cm.	2.986
Gas viscosity, 10^{-4} poises	1.765
Surface tension, dynes/cm.	23.90

The first step in calculating the pore size distribution from the flow rate-pressure drop plots was to convert each data point to an apparent permeability coefficient defined by

$$K_a = Q\eta L/(A\Delta P) \qquad (68)$$

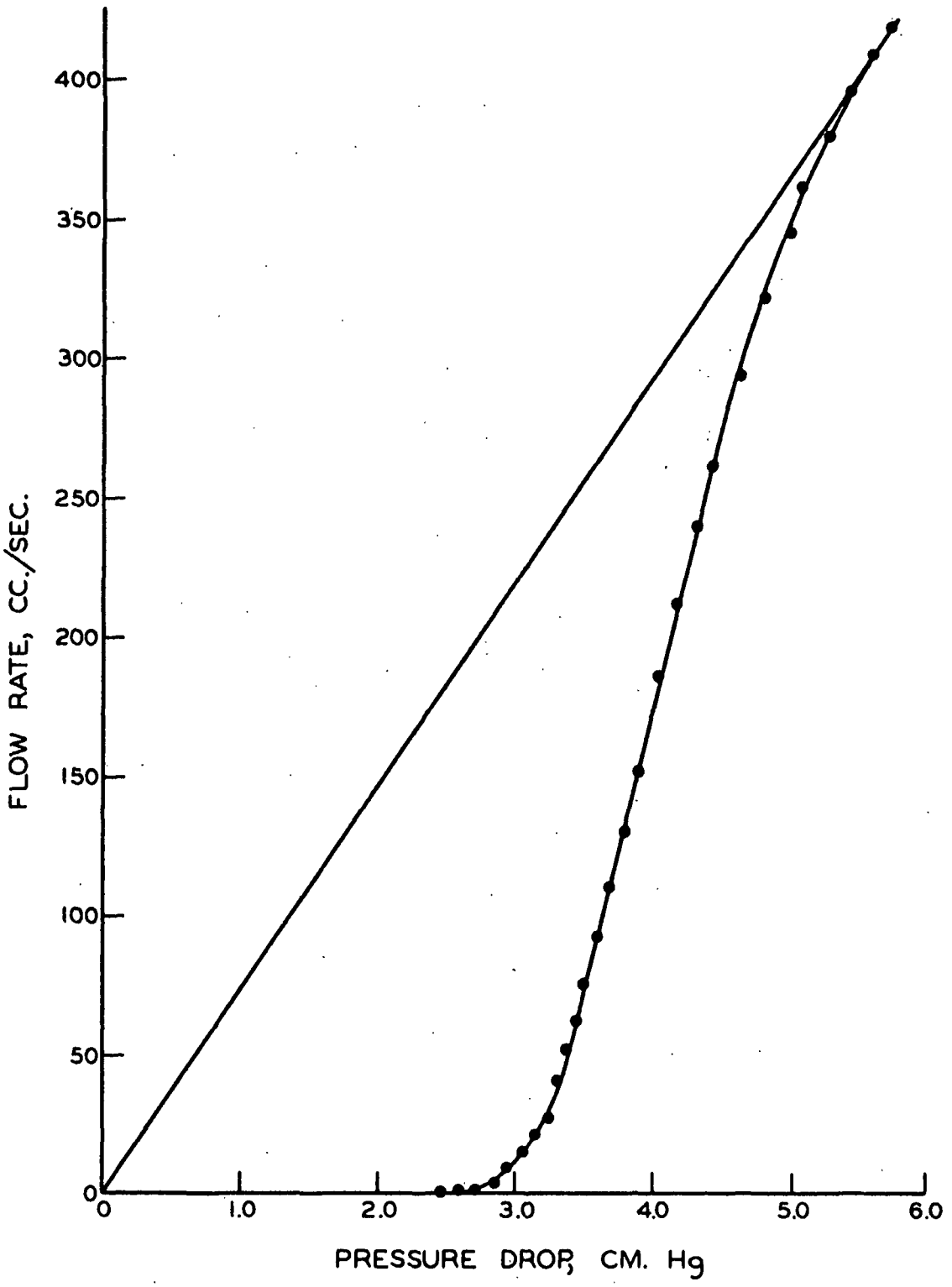

Figure 26. Gas-Drive Data for Specimen H-25(100)-6B

The values of $\underline{K}_a$ were then converted to relative permeability values, $\underline{K}_r$, by dividing through by the limiting value of $\underline{K}_a$, that is, by $(\underline{K}_a)_{max.}$. The frequency of occurrence of each pore size, $\Delta\underline{K}_r$, was then calculated by subtracting the preceding value of $\underline{K}_r$ from the value at the data point under consideration. The hydraulic radii at each measured pressure drop were calculated from Equation (67),

$$m = \gamma/\Delta P \tag{67}$$

where γ is the surface tension of the hexyl alcohol and $\Delta\underline{P}$ is the measured pressure drop. A summary of these data for Specimen H-25(100)-6B is presented in Table XXVIII.

A plot of the hydraulic radii versus $\underline{K}_r$ represents the pore size distribution of the specimen. The next step is to fit the pore size distribution data to the log normal distribution. This can be done in a semiquantitative manner by plotting log $\underline{m}$ against $\underline{K}_r$ on log probability paper. As shown by Hatch and Choate (53), such a plot should be linear if the data fit the log normal distribution. A plot of these data for Specimen H-25(100)-6B is given in Fig. 27. It can be seen from this figure that the data fit the log normal distribution quite well.

The mean and variance of the pore size distribution were calculated from Equations (88) and (89), respectively,

$$\bar{m} = \sum_{i=1}^{n} f_i m_i \tag{88}$$

$$\sigma_m^2 = \sum_{i=1}^{n} (f_i m_i^2) - \bar{m}^2 \tag{89}$$

TABLE XXVIII

DERIVED DATA FOR SPECIMEN H-25(100)-6B

$\underline{m}$, 10^{-4} cm.	ln $\underline{m}$, dimensionless	$\underline{K}_r$, dimensionless	$\Delta\underline{K}_r$, %
7.33	-7.219	0.000	0.0
6.95	-7.272	0.007	0.7
6.62	-7.320	0.015	0.8
6.31	-7.367	0.028	1.3
6.11	-7.401	0.044	1.6
5.91	-7.434	0.064	2.0
5.72	-7.466	0.093	2.8
5.57	-7.493	0.125	3.2
5.45	-7.515	0.161	3.6
5.34	-7.535	0.202	4.1
5.24	-7.554	0.245	4.3
5.14	-7.573	0.295	5.0
5.02	-7.597	0.351	5.5
4.90	-7.620	0.408	5.8
4.76	-7.649	0.482	7.4
4.64	-7.675	0.549	6.7
4.49	-7.709	0.627	7.9
4.33	-7.745	0.692	6.4
4.19	-7.778	0.758	6.7
4.06	-7.810	0.814	5.6
3.90	-7.850	0.864	5.0
3.75	-7.890	0.908	4.4
3.61	-7.926	0.943	3.5
3.54	-7.945	0.968	2.6
3.42	-7.980	0.982	1.4
3.33	-8.007	0.996	1.4
3.23	-8.038	1.000	0.4

In these equations, f_i is the frequency of occurrence of pores of size m_i, $\bar{m}$ is the mean hydraulic radius, and σ_m^2 is the variance of m. The frequency, f_i, is simply the values of ΔK_r listed in Table XXVIII. The standard deviation of the data was calculated as the square root of the variance. The mean and standard deviation of the log normal distribution were also calculated from Equations (88) and (89) by substituting $X = \ln m$ for m in these equations.

The third and fourth moments of the logarithms of the hydraulic radii (about the mean) were then computed from the following equations:

$$M_3 = \sum_{i=1}^{n} (X - \bar{X})^3/n \qquad (90)$$

$$M_4 = \sum_{i=1}^{n} (X - \bar{X})^4/n \qquad (91)$$

These moments of the distribution were then used to test the data for skewness and kurtosis as described by Goulden (55).

Two other ways in which a distribution curve may differ from normal involve the above-mentioned moments of the distribution about the mean. For a normal distribution, the third moment is zero, and the fourth moment is 3.0 (66). The third moment is a measure of a property known as skewness. A distribution is said to have a positive skewness if there are more values greater than the mean than there are less than the mean. The opposite condition is known as a negative skewness.

The fourth moment of the distribution is related to a property known as kurtosis. The kurtosis is a measure of the peakedness of the distribution curve. A positive kurtosis exists if the distribution curve is more peaked than normal.

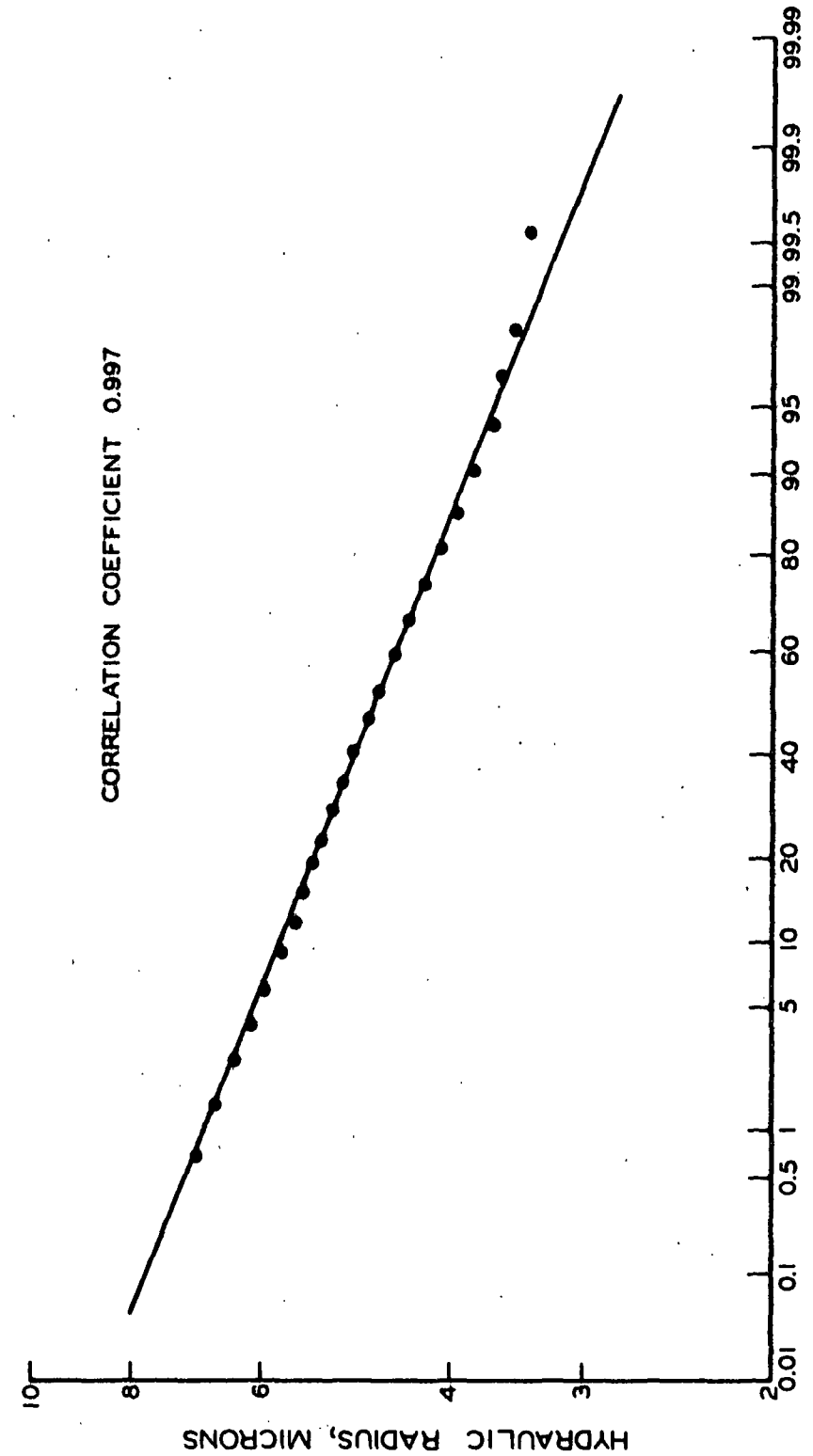

Figure 27. Plot of Pore Size Distribution Data for Specimen H-25(100)-6B on Log-Probability Paper

This condition is referred to as leptokurtosis (67). A negative kurtosis (platykurtosis) indicates a distribution which is flatter than normal. A distribution which is normal or very nearly normal is referred to as mesokurtic.

A convenient method for testing the data for skewness and kurtosis, utilizing the Student "t" test, has been described by Goulden (55). This method was used to test the pore size distribution data for skewness and kurtosis, and the third and fourth moments together with the corresponding Student "t" values were computed for all of the specimens tested in this study. The Student "t" values were compared with the tabular values at infinite degrees of freedom (1.960 at the 5% significance level) to determine whether or not the skewness and kurtosis of the data were statistically significant when compared with the log normal distribution. The results of these calculations for Specimen H-25(100)-6B are presented in Table XXIX.

In order to obtain a quantitative measure of the degree to which the data fitted the log normal distribution, the X versus K_r data were fitted to a straight line using the method of least squares developed by Jentzen (54). The following transformation of variables was employed to convert the nonlinear normal probability scale to a linear scale,

$$Z = (X - \bar{X})/\sigma_x \qquad (92)$$

The "standardized variable," Z, is normally distributed with a zero mean and unit standard deviation (66), and, as shown by Equation (103), Z is linear with X. A trial-and-error procedure was used to convert the values of K_r to the values of Z expected from the normal distribution. This was accomplished by repeatedly comparing the value of K_r with the integral of the normal probability distribution estimated from a Hasting's approximation (68). The value of X from

the data and $\underline{Z}$ from the approximation of the normal distribution were fitted to a straight line by least squares, and the least squares mean and standard deviation of the log normal distribution were then calculated from the intercept and slope, respectively, of the fitted line. At the same time, an over-all correlation coefficient was calculated from the data. These calculations were carried out with the aid of an IBM 1620 computer. The calculated pore size distribution properties of Specimen H-25(100)-6B are summarized in Table XXIX.

TABLE XXIX

PORE SIZE DISTRIBUTION PROPERTIES OF SPECIMEN H-25(100)-6B

Based on the data:	
$\bar{\underline{m}}$, μ	4.63
$\sigma_{\underline{m}}$, μ	1.04
$\bar{\underline{X}}$, dimensionless	-7.679
$\sigma_{\underline{x}}$, dimensionless	0.157
Moments of the log normal distribution about the mean:	
Third moment, dimensionless	-0.030
Fourth moment, dimensionless	2.537
Student "t" test:	
Skewness	-0.07
Kurtosis	-0.33
Based on least squares fit to log normal distribution:	
$\bar{\underline{m}}$, μ	4.71
$\bar{\underline{X}}$, dimensionless	-7.662
$\sigma_{\underline{x}}$, dimensionless	0.153
Correlation coefficient	0.997

APPENDIX II

MAT PERMEABILITY DATA

The results obtained in the air permeability studies on thick mats are summarized in Tables VIII and IX. The data from which these results were calculated are presented in Table XXX. The experimental data collected on the thick mats fitted Darcy's law extremely well, as shown in Fig. 19; therefore, only the permeability coefficient–thickness data are presented in Table XXX. The values of $\underline{W}$ recorded in this table are the specimen weights after being conditioned with dry nitrogen. The moisture content of these specimens varied from 0.50 to 1.25% above oven dry. The values recorded in Table XXX for the initial mat thickness, $\underline{L}_i$, are the thicknesses extrapolated to a compacting pressure of 0.1 p.s.i.

TABLE XXX

MAT PERMEABILITY DATA

Specimen A		Specimen B		Specimen C	
$\underline{K}$, 10^{-8} sq. cm.	$\underline{L}$, cm.	$\underline{K}$, 10^{-8} sq. cm.	$\underline{L}$, cm.	$\underline{K}$, 10^{-8} sq. cm.	$\underline{L}$, cm.
Mat M-10(15)-1					
$\underline{W}$ = 2.449 g. $\underline{L}_i$ = 0.370 cm.		$\underline{W}$ = 2.458 g. $\underline{L}_i$ = 0.372 cm.		$\underline{W}$ = 2.445 g. $\underline{L}_i$ = 0.382 cm.	
1.743	0.255	1.635	0.250	2.089	0.267
1.265	0.231	1.136	0.225	1.402	0.238
0.871	0.208	0.830	0.206	0.986	0.216
0.528	0.185	0.505	0.182	0.591	0.188
0.365	0.170	0.348	0.167	0.398	0.170
0.260	0.157	0.248	0.155	0.285	0.160

TABLE XXX (Continued)

MAT PERMEABILITY DATA

Specimen A		Specimen B		Specimen C	
K, 10^{-8} sq. cm.	L, cm.	K, 10^{-8} sq. cm.	L, cm.	K, 10^{-8} sq. cm.	L, cm.
Mat M-10(40)-4					
W = 6.744 g. L_i = 0.991 cm.		W = 6.578 g. L_i = 1.034 cm.		W = 6.511 g. L_i = 1.010 cm.	
1.788	0.673	2.449	0.759	2.086	0.717
1.117	0.592	1.692	0.677	1.442	0.644
0.873	0.558	1.073	0.600	0.957	0.579
0.466	0.479	0.582	0.521	0.499	0.497
0.309	0.439	0.352	0.468	0.342	0.459
0.209	0.406	0.225	0.428	0.218	0.419
Mat M-10(30)-4					
W = 4.913 g. L_i = 0.750 cm.		W = 4.708 g. L_i = 0.724 cm.		W = 4.913 g. L_i = 0.746 cm.	
2.250	0.543	2.141	0.526	2.119	0.542
1.413	0.473	1.442	0.473	1.491	0.490
0.971	0.427	0.948	0.424	1.018	0.443
0.514	0.365	0.509	0.366	0.553	0.384
0.341	0.333	0.317	0.330	0.347	0.346
0.232	0.307	0.227	0.309	0.222	0.318
Mat M-25(30)-4					
W = 4.822 g. L_i = 0.639 cm.		W = 4.842 g. L_i = 0.640 cm.		W = 4.858 g. L_i = 0.646 cm.	
1.420	0.479	1.536	0.493	1.339	0.483
1.028	0.437	1.137	0.453	0.976	0.442
0.759	0.406	0.812	0.412	0.732	0.411
0.452	0.357	0.478	0.368	0.453	0.367
0.316	0.332	0.296	0.332	0.295	0.334
0.211	0.305	0.205	0.307	0.222	0.316

TABLE XXX (Continued)

MAT PERMEABILITY DATA

Specimen A		Specimen B		Specimen C	
K, 10^{-8} sq. cm.	L, cm.	K, 10^{-8} sq. cm.	L, cm.	K, 10^{-8} sq. cm.	L, cm.
Mat M-50(30)-3					
W = 4.758 g. L_i = 0.539 cm.		W = 4.815 g. L_i = 0.537 cm.		W = 4.839 g. L_i = 0.543 cm.	
0.951	0.435	0.680	0.407	0.813	0.417
0.743	0.408	0.563	0.387	0.633	0.390
0.589	0.384	0.465	0.369	0.519	0.369
0.391	0.349	0.340	0.344	0.351	0.340
0.272	0.324	0.245	0.320	0.255	0.318
0.206	0.306	0.188	0.304	0.183	0.297
Mat M-75(30)-4					
W = 5.008 g. L_i = 0.526 cm.		W = 5.035 g. L_i = 0.532 cm.		W = 5.046 g. L_i = 0.532 cm.	
0.803	0.424	0.707	0.422	0.853	0.431
0.619	0.397	0.452	0.379	0.679	0.404
0.495	0.377	0.314	0.351	0.531	0.382
0.346	0.347	0.217	0.325	--	--
0.235	0.319	0.189	0.316	0.237	0.319
0.182	0.302	0.156	0.304	0.176	0.299
Mat M-100(30)-3					
W = 4.494 g. L_i = 0.434 cm.		Specimen B was delaminated during the cutting operation.		W = 4.501 g. L_i = 0.428 cm.	
0.618	0.361			0.614	0.364
0.509	0.343			0.513	0.347
0.402	0.326			0.410	0.329
0.293	0.305			--	--
0.215	0.282			0.212	0.285
0.158	0.267			0.175	0.274

APPENDIX III

APPLICATION OF A PARALLEL CAPILLARY MODEL TO PAPER

As mentioned earlier, a number of authors (27-30) have suggested the use of cylindrical capillary models to describe the structure of porous media. Such a model was applied to the data gathered in this study. Specifically, a model of parallel, cylindrical capillaries in which the radii of the capillaries were distributed according to the log normal distribution was employed. The equations describing the permeability properties of this model may be developed as follows.

For a system of N_t uniform capillary tubes of radius R and length ℓ,

$$\text{capillary volume, } V_c = \pi R^2 \ell N_t$$

$$\text{capillary surface area, } S_c = 2\pi R \ell N_t$$

Now, consider a system of N_t capillaries of equal length, ℓ, whose radii are distributed according to some distribution function, $h(R)$:

$$V_c = \pi \ell N_t \int_0^\infty R^2 h(R) dR \tag{93}$$

$$S_c = 2\pi \ell N_t \int_0^\infty R h(R) dR \tag{94}$$

If the function $h(R)$ is assumed to be log normal, the distribution of the logarithms of the capillary radii (to the Naperian base) is given by

$$g(X) = (1/\sigma_x)\sqrt{2\pi}\exp[-(X - \bar{X})^2/(2\sigma_x^2)] \tag{95}$$

where $X = \ln R$ and $g(X)$ is the log normal distribution function with a mean of $\bar{X}$ and variance σ_x^2. Or, in terms of the distribution function $h(R)$ (69),

$$h(R) = g(X)\, e^{-X} = (1/\sigma_x)\sqrt{2\pi}\, \exp[-(X - \bar{X})^2/(2\sigma_x{}^2)]\, \exp(-X) \qquad (96)$$

Combining Equations (93) and (96) and noting that since $\underline{R} = \underline{e^{X}}$, $\underline{R^2} = \underline{e^{2X}}$ and $\underline{dR} = \underline{e^{X} dX}$,

$$V_c = \pi \ell\, N_t \int_{-\infty}^{+\infty} (1/2\sigma_x)\, \sqrt{2\pi}\, \exp[-(X - \bar{X})^2/(2\sigma_x{}^2)]\, \exp(2X)dX \qquad (97)$$

[Note: When $\underline{R} = 0$, $\underline{X} = -\infty$, and when $\underline{R} = \infty$, $\underline{X} = +\infty$; hence the change of the limits of integration in Equation (97).]

The integral in Equation (97) is simply the second moment of the distribution about the origin. It can be shown (69) that these moments of the log normal distribution are represented by

$$M(X^j) = \exp(jX + j^2\, \sigma_x{}^2/2) \qquad (98)$$

where $\underline{M(X^j)}$ represents the $\underline{j}$th moment about the origin.

If $\underline{j}$ is set equal to 2 in Equation (98) and the result is substituted into Equation (97),

$$V_c = \pi\, \ell\, N_t\, \exp[2\bar{X} + 2\sigma_x{}^2] \qquad (99)$$

The above equation represents the total void volume of the capillary system. The porosity of the system is then

$$\epsilon = V_c/AL = (\pi\, \ell\, N_t/AL)\, \exp[2\bar{X} + 2\sigma_x{}^2] \qquad (100)$$

where $\underline{A}$ and $\underline{L}$ are the bulk area and thickness of the model.

From Equation (94), substituting for $\underline{R}$ and $\underline{dR}$ as before,

$$S_c = 2\pi\, \ell\, N_t \int_{-\infty}^{+\infty} (1/\sigma_x)\, \sqrt{2\pi}\, \exp[-(X - \bar{X})^2/(2\sigma_x{}^2)]\, \exp(X)dX \qquad (101)$$

The integral in Equation (101) represents the first moment about the origin. Applying Equation (98) with $\underline{j} = 1$,

$$S_c = (2\pi \ell N_t) \exp[X + \sigma_x^2/2] \qquad (102)$$

This equation represents the total surface area of the capillary system.

Equations (100) and (102) were used to estimate the porosity and exposed surface area, respectively, of the thin handsheets tested in this study. However, in order to apply these equations, the following assumptions must be made:

1. The flow channels through the sheet are assumed to be uniform cylinders of constant length where effective radii (as determined in the gas-drive test) are distributed according to the log normal distribution.
2. The model is assumed to have the physical dimensions of the test specimen in the gas-drive test.

In addition, it is necessary to analyze the gas-drive data using a method which is consistent with the model of parallel, cylindrical capillaries. Such an analysis is presented below.

In the gas-drive test, the additional increase in flow rate, above that expected from Poiseuille's equation, is proportional to the number of pores opened to flow. This can be stated mathematically as

$$\Delta Q_i = N_i Q_p \qquad (103)$$

where $\Delta\underline{Q_i}$ is the increase in flow rate due to the opening of $\underline{N_i}$ pores and $\underline{Q_p}$ is the flow rate through each new pore opened to flow. If the pores are assumed to be cylindrical, the effective radius can be calculated from the Kelvin equation

(assuming a contact angle of zero),

$$R = 2\gamma/\Delta P \tag{65}$$

In Equation (65), ΔP is the measured pressure drop, γ is the surface tension of the liquid, and R is the effective radius of the pores.

For cylindrical pores, the flow rate through each pore at a given pressure drop can be calculated from Poiseuille's equation,

$$Q_p = \pi R^4 \Delta P/(8\eta \ell) \tag{104}$$

where η is the viscosity of the permeating fluid and ℓ is the length of the pores (assumed to be constant in this case).

Combining Equations (65), (103), and (104), one obtains

$$\Delta Q_i = N_i[2\pi \gamma^4/(\eta \ell \Delta P^3)] \tag{105}$$

Assuming that the surface tension, pore length, and viscosity are constant, the number of pores opened to flow at each pressure increment is

$$N_i = [\eta \ell/(2\pi \gamma^4)](\Delta Q_i)(\Delta P)^3 = C_o(\Delta Q_i)(\Delta P)^3 \tag{106}$$

where C_o is a constant.

The pore size distribution (based on a capillary model) can be calculated from Equation (106) since

$$N_i/\Sigma N_i = (\Delta Q_i)(\Delta P)^3/\Sigma[(\Delta Q_i)(\Delta P)^3] \tag{107}$$

represents the fraction of the total number of pores at a given pore size.

The gas-drive data gathered in the study on the effect of wet pressure on the porous properties of paper were evaluated using the parallel capillary model described above. A summary of these results are presented in Table XXXI. In the interest of brevity, only the average of three specimens tested at each level of wet pressure are recorded in this table.

TABLE XXXI

APPLICATION OF A PARALLEL CAPILLARY MODEL TO PAPER

Wet Pressure, p.s.i.	$\bar{R}_{\mu}$,	$\sigma_{\bar{R}_{\mu}}'$,	Number of Capillaries[a]	ϵ, dimensionless	$\bar{S}_w$, sq. cm./g.
10	10.90	1.65	7.09×10^4	0.0059	37.1
25	8.78	1.33	1.16×10^5	0.0064	42.5
50	6.71	1.05	2.16×10^5	0.0069	50.5
75	5.86	0.95	3.06×10^5	0.0074	59.7
100	5.06	0.86	4.38×10^5	0.0079	67.8

[a]The total number of capillaries in the model was calculated by summing the number of capillaries opened to flow at each pressure increment, using Equation (106).

It is quite apparent from the results recorded in Table XXXI that the model of parallel capillaries does not even approximately describe the porous properties of these sheets. Both the calculated porosities and the calculated surface areas are much too low. In addition, the parallel capillary model predicts an increase in porosity and surface area with increasing wet pressure applied to the sheet. Neither of these predictions is logical.